GEOMETRIC AND MATERIAL NONLINEAR ANALYSIS OF LAMINATED COMPOSITE PLATES AND SHELLS

by

K. Chandrashekhara

Dissertation submitted to the Faculty of the
Virginia Polytechnic Institute and State University
in partial fulfillment of the requirements
for the degree of

DOCTOR OF PHILOSOPHY

in

Engineering Mechanics

APPROVED:

J. N. Reddy, Chairman

D. Frederick

C. W. Smith

E. G. Henneke, II

R. H. Plaut

November 1985

Blacksburg, Virginia

ACKNOWLEDGEMENTS

The author is indebted to Professor J. N. Reddy for his constant guidance, support and encouragement. Professor Reddy's keen interest and vast professional knowledge has truly been a great inspiration to the author. I would also like to thank Professors D. Frederick, C. W. Smith, E. G. Henneke and R. H. Plaut for serving as members of the thesis committee. A special thanks to Professor H. Sword for his help in computer funds.

The work reported in this thesis was supported by the Structural Mechanics Divisions of AFOSR, NASA, and Office of Naval Research. The support is gratefully acknowledged.

In looking back over the years, I can discern the influences of many people to whom I owe a debt of gratitude which I can never repay. Among these are my parents, who instilled in me a love of knowledge, and my teachers, who created the inspiration and encouragement.

Finally, infinite thanks are due to my friends who made my stay a pleasant and memorable one.

TABLE OF CONTENTS

TABLE OF CONTENTS (CONTINUED)

CHAPTER 1

INTRODUCTION

1.1 Movivation

Fiber reinforced composites are increasingly being introduced into a variety of structures in aeronautical, mechanical, nuclear and marine engineering applications where high ratios of stiffness and strength to weight are of paramount importance. However, the engineering community is faced with many challenging problems associated with the use of these new materials. Of these, the nonlinear response of laminated plates and shells is of major interest in their design.

The nonlinearity in structural problems can be of two types: (i) the geometric nonlinearity, which is associated with the changing geometry of a structure, and (ii) the material nonlinearity which is associated with the nonlinear material behavior (stress-strain relations). Often a combination of the two is present when materials are loaded to their ultimate loads. The phenomena of plasticity, creep or other complex constitutive relations come under the class of material nonlinearity. The geometric nonlinearity enters the equations of equilibrium via the strain-displacement relations and the governing equations. Both classes of problems have their own field of application and each covers a wide area of mechanics.

Since the finite element method has proved to be a very powerful tool for analyzing elastic structural problems, involving complex geometries, variety of loading and boundary conditions, it is quite natural to extend this technique to the solution of nonlinear problems. Also, due to the complexity involved in the nonlinear

problems, it is a good practice that a nonlinear analysis is always preceded by a linear analysis, so that the nonlinear analysis is considered as an extension of the complete analysis process beyond the assumptions of linear analysis. Based on the linear solution response, the analyst is able to predict which nonlinearities will be significant and how to account for these nonlinearities most appropriately.

The nonlinear solution is reached by a combined incremental and iterative procedure as exact solutions are not tractable for nonlinear problems. The present study has the objective of developing a finite-element analysis that can handle efficiently geometric and material nonlinearity acting separately or in combination. The main thrust of the present research is on the development of suitable material models, finite-element formulations and choice of elements. The following literature survey provides the background for the present study.

1.2 Literature Review

For isotropic materials, the finite element codes are well established for both types of nonlinearities. While in the case of composite materials, though considerable investigations have been done in the area of geometric nonlinearity, the work on material nonlinearity is limited.

1.2.1 Geometric Nonlinearity

The use of classical shell theories, which are based on the Kirchhoff-Love kinematic hypothesis, namely, straight lines normal to the undeformed midsurface remain straight and normal to the midsurface after deformation and undergo no thickness stretching, results in the

underprediction of energy in the laminated shells. This is due to the neglect of transverse shear strains in the classical shell theories.

Refinements of the classical shell theories (e.g., Love's first approximation theory [1]) for shells to include transverse shear deformation have been presented by Reissner [2-4]. Sanders [5] presented modified first and second approximation theories that removed an inconsistency (nonvanishing of small rigid-body rotations of the shell) that existed in Love's first approximation theory.

The first thin shell theory of laminated orthrotropic shells was due to Ambartsumyan [6,7]. In these works Ambartsumyan assumed that the individual orthotropic layers were oriented such that the principal axes of material symmetry coincided with the principal coordinates of the shell reference surface. Dong, Pister, Taylor [8] presented an extension of Donnell's shallow shell theory [9] to thin laminated shells. Using the asymptotic integration of the elasticity equations, Widera and Chung [10] derived a first-approximation theory for the unsymmetric deformation of nonhomogeneous, anisotropic, cylindrical shells. This theory, when specialized to isotropic materials, reduces to Donnell's shell theory.

The effects of transverse shear deformation and thermal expansion through the shell thickness were considered by Zukas and Vinson [11]. Dong and Tso [12] constructed a laminated orthotropic shell theory that includes transverse shear deformation. This theory can be regarded as an extension of Love's first-approximation theory [1] for homogeneous isotropic shells. Other refined theories, specialized to anisotropic

cylindrical shells, were presented by Whitney and Sun [13], and Widera and Logan [14,15].

Finite element analyses of layered anisotropic shells, all of which are concerned with bending, stability, vibration of shells, can be found in the works of Schmit and Monforton [16], Panda and Natarajan [17], Shivakumar and Krishna Murty [18], Rao [19], Seide and Chang [20], Hsu, Reddy, and Bert [21], Reddy [22], and Venkatesh and Rao [23,24]. Recently, Reddy [25] extended Sanders shell theory to account for simply supported cross-ply laminated shells. All of these studies are limited to small displacement theories and static analysis.

Most of the structures, whether they are used in land, sea or air, are subjected to dynamic loads during their operation. Therefore, there exists a need for assessing the transient response of composite structures. Compared to static analysis, little progress has been made in the analysis of nonlinear dynamic behavior of laminated composite plates and shells through the finite element approach. Moon [26] investigated the response of infinite laminated plates subjected to transverse impact loads at the center of the plate, while Chow [27] employed the Laplace transform technique to investigate the dynamic response of orthotropic laminated plates, and Whang, Chou and Rose [28] applied themethod of characteristics to unsymmetrical orthotropic laminated plates. Dobyns [29] analyzed simply-supported orthotropic plates subject to static and dynamic loads. However, these developments were confined to plates only.

In the present work, an extension of the Sanders shell theory that accounts for the shear deformation and the von Karman strains is used

for the geometrically nonlinear static and dynamic analysis of laminated composite plates and shells.

1.2.2 Material Nonlinearity

While considering the geometric nonlinear analysis, it is assumed that the relationship between stress and strain is linear. But it is a common knowledge that the elastic analysis is unduly conservative because it fails to take advantage of the ability of many materials to carry stresses above the yield surface. Plasticity effects must then be included to gain additional insight into the physical response of the structure to additional loading.

The two major plasticity theories that are usually considered are the total deformation theory and the flow theory. Flow theory is presumably a better model of material behavior than the deformation theory since certain conditions requird by thermodynamic principles are accounted for and path dependent behavior is predicted.

Most of the previous investigations on the elasto-plastic analysis is based on the isotropic material in which the material is assumed to obey the von Mises yield criterion and the Prandtl-Reuss flow rule. The finite element method has proved to be a powerful method also for solving elasto-plastic problems. References [30] through [35] are representative of the investigations concerned with incorporating the effect of plastic behavior in finite element analysis. Among the previous investigations, the ones by Armen et al. [34] and Popov et al. [31,32] deserve mentioning.

Though considerable progress has been made in the elasto-plastic analysis of isotropic materials, the work on laminated composite plates and shells is limited due to the complexity involved in anisotropic plasticity. The elasto-plastic behavior of laminated composites can be accounted for using a macroscopic approach in which the laminate is treated as an equivalent single anisotropic layer. Hills [36] anisotropic yield criterion is based on this approach, which is a generalization of Huber-Mises yield criterion. Hill's theory was extended by Hu [37] and Jensen et al. [38] for strain hardening materials. Whang [39] considered the elasto-plastic analysis of orthotropic plates and shells using finite element analysis. Also, Valliappan [40] and Owen and Figueras [41] presented results for anisotropic materials. But Hill's formulation entirely neglects the micromechanical effects, in which different mechanical properties of the filament and matrix are considered.

At the other extreme, micromechanical finite element models can be used to study the complex fiber-matrix interaction. Initial yield surface behvaior [42] and, to some extent, post-yield behavior [43] have been studied by this method. This micromechanics analysis provides an understanding of the behavior of unidirectional composites. However, for general loading cases, this method becomes too complex, and as such, has only a limited applicability. For most general loading cases, it seems more practical to employ a simplified model that averages out local stress variations yet still retains the essential mechanisms of fiber-matrix interaction. Notable efforts in this area have been made

by, among others, Sawicki [44], Bahei-El-Din et al. [45], Aboudi and Benvenist [46], Dvorak and Bahei-El-Din [4>].

It is apparent from the cited references that there do not exist general theories for anisotorpic plasticity. In the present work, the material model is based on the modified version of Hill's anisotropic yield criterion is utilized in which anisotropic parameters of plasticity are introduced. The method accounts for the fact that these parameters vary as the material strain strain hardens.

The above studies are confined to the staic regime only. Considerable attention has been given to the elasto-plastic dynamic analysis ofisotropic plates and shells. Notable efforts in this area have been made by, among others, Levine et al. [48], Nagarajan and Popov [49], Bathe and Bolourechi [50], and Liu and Lin [51]. However, no work has been reported to date for elasto-plastic dynamic response of laminated composite plates and shells to the author's knowledge.

1.2.3 Combined Geometric and Material Nonlinearity

Many advances have been made in the finite element analysis of isotropic materials considering both geometrically and materially nonlinear problems. Among the papers dealing with the static analysis of plates and shells taking into account both plasticity and geometric nonlinearity, the ones by Javaherian et al. [52], Herting and Narayan Swami [53], Parish [54], and Dvorkin and Bathe [55] should be noted. The dynamic responses of structures that cause large displacement and plastic deformations were determined by Nagarajan and Popov [49], Bathe et al. [56], and Mondkar and Powell [57]. No work has been reported, to

the author's knowledge, that handles the simultaneous treatment of plasticity and geometric nonlinearity for fiber-reinforced composites.

1.3 Present Study

A review of the literature indicates that for isotropic materials, several authors have applied the finite element method to structures exhibiting only geometric nonlinearity, whereas others have considered only material nonlinearity. The literature on combined effects of geometric and material nonlinearities is also extensive. Most of the applications have been to structures subjected to static loading, and relatively few applications of dynamic behavior have been reported. In the case of the nonlinear analysis of fiber-reinforced composites, though much progress has been made in the geometric nonlinear analysis, the advances in the area of material and/or combined nonlinearity is still at its infancy due to the complexity involved in anisotropic plasticity.

In the present work, consideration is given to geometric and material nonlinearity of laminated composite plates and shells acting separately or in combination. The material model is based on the Huber-Mises yield criterion and the Prandtl-Reuss flow rule in accordance with the theory of strain hardening yield function, which is generalized for anisotropic materials by introducing the parameters of anisotropy. The method accounts for the fact that the parameters vary as the material strain hardens. Geometric nonlinearity is incorporated using the von Karman strains. The element is based on an extension of the Sanders

shell theory and accounts for transverse shear strains. Through the thickness plastification is introduced using a layered model.

The methodology resulting from the current investigation is capable of treating the nonlinear response of a broad spectrum of plate and shell problems, under a variety of loads and boundary conditions.

CHAPTER 2

GEOMETRIC NONLINEAR DESCRIPTION

It is a common knowledge that during continuously increasing load application, all real structures, sooner or later, start behaving in a nonlinear fashion. Geometric nonlinearity accounts for the fact that the shape of the structure changes during deformation which in turn results in relative change of the force pattern.

2.1 First Order Shear Deformation Theory

Due to the high ratio of inplane modulus to transverse shear modulus, the shear deformation effects are more pronounced in the composite laminates subjected to transverse loads than in the isotropic case under similar loading. The thin shell theory is based on the Kirchhoff-Love hypothesis in which the straight lines normal to the undeformed midsurface remain straight and normal to the midsurface and undergo no thickness stretching. These theories, known as the Love's first approximation theories [1], are expected to yield sufficiently accurate results when the radius-to-thickness ratio is large and the material anisotropy is not severe. However, the application of such theories to layered anisotropic composite shells could lead to as much as 30% or more errors in deflections and stresses.

The present formulation is based on the first order shear deformation theory in which transverse normal stress is neglected and the transverse shear stresses are assumed to be constant through the thickness. To account for the parabolic distribution of the transverse stresses, shear correction factors are used. The displacement finite

element model is developed using an extension of Sanders shell theory [5] and the geometric nonlinearity is incorporated using the von Karman [58] strains.

2.2 Strain-Displacement Relations

Consider a laminated shell constructed of a finite number of uniform thickness orthotropic layers, oriented arbitrarily with respect to the shell coordinates (ξ_1,ξ_2,ζ). The orthogonal curvilinear coordinate system (ξ_1,ξ_2,ζ) is chosen such that the ξ_1- and ξ_2-curves are lines of curvature on the midsurface $\zeta = 0$, and ζ-curves are straight lines perpendicular to the surface $\zeta = 0$ (see Fig. 2.1). An element of the shell is given by (see Reddy [25])

$$(ds)^2 = [(1 + \zeta/R_1)\alpha_1 d\xi_1]^2 + [(1 + \zeta/R_2)\alpha_2 d\xi_2]^2 + (d\zeta)^2 \quad (2.1)$$

where α_i and R_i $(i = 1,2)$ are the surface metrics and radii of curvature, respectively. In general, α_i and R_i are functions of ξ_i only. For the doubly curved shells considered in the present theory, α_i and R_i are constant.

The strain-displacement equations of the shear deformable theory of doubly-curved shells are given by

$$\begin{aligned} \varepsilon_1 &= \varepsilon_1^0 + \zeta\kappa_1 \\ \varepsilon_2 &= \varepsilon_2^0 + \zeta\kappa_2 \\ \varepsilon_4 &= \varepsilon_4^0 \\ \varepsilon_5 &= \varepsilon_5^0 \\ \varepsilon_6 &= \varepsilon_6^0 + \zeta\kappa_6 \end{aligned} \quad (2.2)$$

where

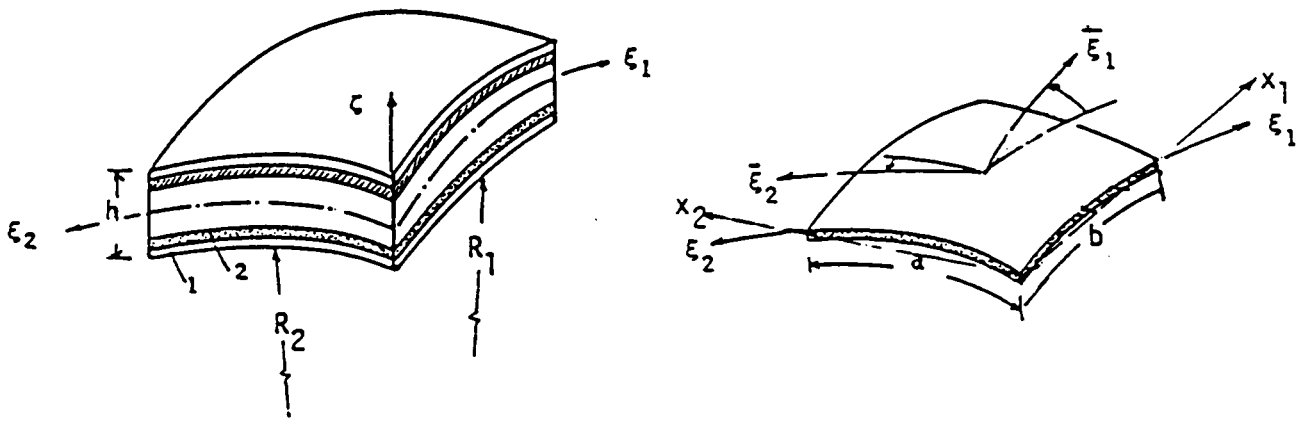

Figure 2.1 Laminated shell geometry and lamina details

$$\varepsilon_1^o = \frac{\partial u_1}{\partial x_1} + \frac{u_3}{R_1} + \underline{\frac{1}{2}\left(\frac{\partial u_3}{\partial x_1}\right)^2} \quad ; \quad \kappa_1 = \frac{\partial \phi_1}{\partial x_1}$$

$$\varepsilon_2^o = \frac{\partial u_2}{\partial x_2} + \frac{u_3}{R_2} + \underline{\frac{1}{2}\left(\frac{\partial u_3}{\partial x_2}\right)^2} \quad ; \quad \kappa_2 = \frac{\partial \phi_2}{\partial x_2}$$

$$\varepsilon_6^o = \frac{\partial u_1}{\partial x_2} + \frac{\partial u_2}{\partial x_1} + \underline{\frac{\partial u_3}{\partial x_1}\frac{\partial u_3}{\partial x_2}} \quad ; \quad \kappa_6 = \frac{\partial \phi_1}{\partial x_2} + \frac{\partial \phi_2}{\partial x_1} - C_o\left(\frac{\partial u_2}{\partial x_1} - \frac{\partial u_1}{\partial x_2}\right)$$

$$\varepsilon_4^o = \phi_2 + \frac{\partial u_3}{\partial x_2} - \frac{u_2}{R_2}$$

$$\varepsilon_5^o = \phi_1 + \frac{\partial u_3}{\partial x_1} - \frac{u_1}{R_1}$$

$$C_o = \frac{1}{2}\left(\frac{1}{R_1} - \frac{1}{R_2}\right) \quad ; \quad dx_i = \alpha_i d\xi_i \quad (i = 1,2)$$

Here u_i are the displacements of the reference surface along ξ_i ($\xi_3 = \zeta$) axes, and ϕ_1 and ϕ_2 are the rotations of transverse normals about the ξ_2- and ξ_1-axes respectively. The underscored terms account for geometric nonlinearity and the C_o term is due to Sanders theory which accounts for the condition of zero strain for rigid body motion.

It is informative to note that the strains of the von Karman theory are infinitesimal; it is only the rotations that are finite quantities. However, as will be demonstrated by a wide range of examples, later, the accuracy of these strain terms is sufficient for almost all practical applications to nonlinear problems. Consequently, the von Karman theory represents a reasonable approximation of plates and shells undergoing moderately large displacements but small strains.

Any two-dimensional theory of shells would not be valid for shell problems that involve large strains and rotations. We exclude such problems from our consideration in the present study.

CHAPTER 3

MATERIAL NONLINEAR DESCRIPTION

Because of the complexity associated with the anisotropic plastic deformation, the laws governing the behavior of materials in the plastic range have not, as yet, reached a level of general acceptance. Thus, any attempt to predict analytically the behavior of structures in the plastic range must begin with a choice, among the available plasticity theories, of one which successfully combines mathematical simplicity with a proper representation of experimentally observed material behavior.

3.1 Material Model

In the present work, the elasto-plastic analysis is based on the Huber-Mises yield criterion extended by Hill for anisotropic materials. The yield function is generalized by introducing anisotropic parameters of plasticity which are updated during the material strain hardening history.

3.2 Hill's Anisotropic Yield Criterion

The criterion that approximately describs the yielding of an isotropic material is due to von Mises [59]. The simplest yield criterion for anisotropic material is therefore one which reduces to the von Mises law when anisotropy is vanishingly small. Hill's [36] initial yield criterion is based on this approach and has the form

$$f(\sigma_{ij}) = F(\sigma_2 - \sigma_3)^2 + G(\sigma_3 - \sigma_1)^2 + H(\sigma_1 - \sigma_2)^2 + 2L\sigma_{23}^2 + 2M\sigma_{13}^2 + 2N\sigma_{12}^2 = 1 \qquad (3.1)$$

where F, G, H, L, M, N are parameters that characterize the current

state of anisotropy

$$2F = \frac{1}{Y^2} + \frac{1}{Z^2} - \frac{1}{X^2} \quad ; \quad 2L = \frac{1}{R^2}$$

$$2G = \frac{1}{Z^2} + \frac{1}{X^2} - \frac{1}{Y^2} \quad ; \quad 2M = \frac{1}{S^2}$$

$$2H = \frac{1}{X^2} + \frac{1}{Y^2} - \frac{1}{Z^2} \quad ; \quad 2N = \frac{1}{T^2}$$

and X, Y, Z are the tensile yield stresses in the principal direction of anisotropy and R, S, T are the yield stresses in shear with respect to the principal axes of anisotropy. Hill's yield criterion assumes a relatively simple case of orthotropic anisotropy, that is, there are three mutually orthogonal planes of symmetry at every point and the intersections of these planes are considered as the principal axes of anisotropy. Fiber reinforced composite structures almost invariably possess this kind of symmetry. Also, the yield criterion has this form when the principal axes of anisotropy are the axes of reference.

For a plane stress state in the 1-2 plane with transverse shear, Eq. (3.1) reduces to

$$f = (G + H)\sigma_1^2 + (F + H)\sigma_2^2 - 2H\sigma_1\sigma_2 + 2L\sigma_{23}^2 + 2M\sigma_{13}^2 + 2N\sigma_{12}^2 = 1 \qquad (3.2)$$

For an isotropic material, according to the von Mises yield criterion [60], we have

$$X = Y = Z = \sigma_o$$

and

$$R = S = T = \frac{\sigma_o}{\sqrt{3}}$$

where σ_o is the yield stress in uniaxial tension. Therefore, F = G = H

$= \frac{1}{2\sigma_o^2}$ and $2L = 2M = 2N = \frac{3}{2}$ and Eq. (3.2) becomes

$$\sigma_1^2 + \sigma_2^2 - \sigma_1\sigma_2 + 3(\sigma_{23}^2 + \sigma_{13}^2 + \sigma_{12}^2) = \sigma_o^2 \qquad (3.3)$$

which is the familiar von Mises yield criterion.

For a three-dimensional state of stress the yield stresses X, Y, Z, R, S, T are determined by means of a total of six directional stress-strain tests, where, alternatively, all stress components are equal to zero except the one under consideration. But the two dimensional version is based on the assumption that the yield stress in the thickness direction is the same as that of the longitudinal or transverse directions. In the present work, as will be shown in the next section, this restriction has been removed with a systematic derivation of the parameters of anisotropy. Also, Hill's criterion is limited to elastic-perfectly plastic material inwhich the yield surface remains fixed (see Fig. 3.1a). In the present formulation the incremental theory of plasticity is considered with strain hardening.

3.3 Modified Hill's Yield Criterion

Hill's theory was extended to consider strain hardening behavior by Hu [37] and Jensen et al. [38]. The present work is based ona modified version of Hill's initial yield criterion in which the derivation of the anisotropic parameters depends on the initial yield surface and subsequently on the histories of the plastic deformation. The strain hardening is assumed to be isotropic, which at progressively higher stresses exhibits uniform expansion of the initial yield surface (see Fig. 3.1b). This rule, however, does not account for the Bauschinger effect (which, in the case of uniaxial stress is characterized by a

reduction in compressive yield stress due to prior yielding in tension and vice versa). One attempt at including this was made by Prager [64] who suggested kinematic hardening in which the yield surface is translated without rotation (see Fig. 3.1c). Because cyclic loading is not of interest here, the isotropic hardening approach is considered adequate and is adopted inthe following derivations.

The plstic potential or the effective stress $\bar{\sigma}$ for the von Mises yield function is given by

$$\bar{\sigma}^2 = \sigma_1^2 - \sigma_1\sigma_2 + \sigma_2^2 + 3(\sigma_{23}^2 + \sigma_{13}^2 + \sigma_{12}^2) \tag{3.4}$$

In a similar manner, the anisotropic yield criterion takes the form (see [37,38])

$$\bar{\sigma}^2 = \beta_{11}\sigma_1^2 - \beta_{12}\sigma_1\sigma_2 + \beta_{22}\sigma_2^2 + 3\beta_{44}\sigma_{23}^2 + 3\beta_{55}\sigma_{13}^2 + 3\beta_{66}\sigma_{12}^2 \tag{3.5}$$

The six independent parameters of anisotropy β_{11}, β_{22}, β_{44}, β_{55}, β_{66} and β_{12} in Eq. (3.5) has to be determined by experiment; β_{11} and β_{22} are determined using tensile tests in the orthotropic directions while β_{44}, β_{55} and β_{66} are obtained using the shear tests. For the parameter β_{12}, which is the coefficient of the product of σ_1 and σ_2, a tensile test with a specimen cut at 45° from one of the orthotropic directions is proposed (see [39]).

3.3.1 Initial Parameters of Anisotropy

These parameters depend on the initial yield stress in various directions. For a tensile test in one direction, Eq. (3.5) gives

$$\beta_{11}^{o} = \frac{\bar{\sigma}_o^2}{\sigma_{o1}^2}$$

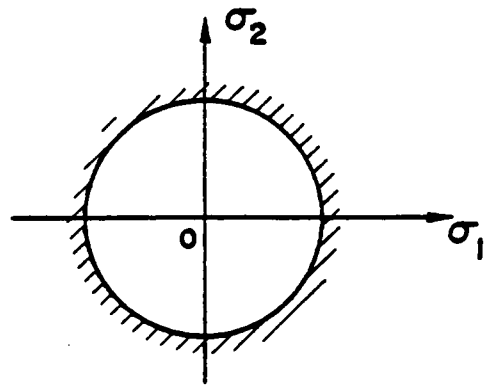

(a) Perfectly Plastic

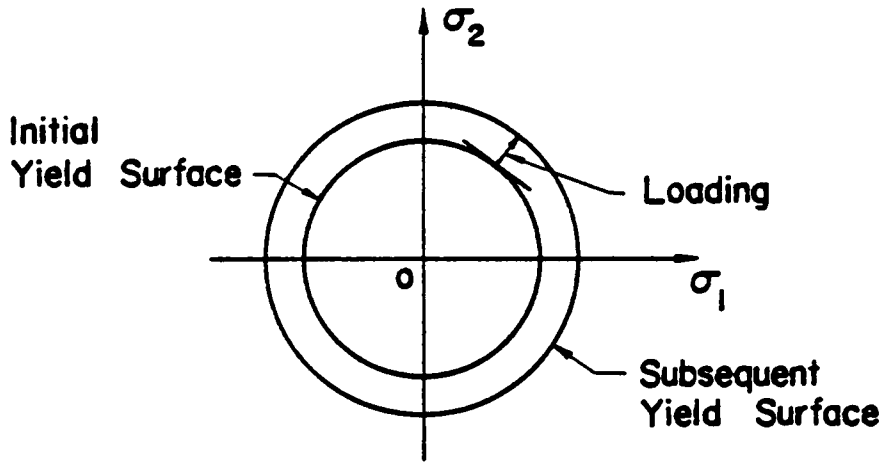

(b) Isotropic Strain Hardening

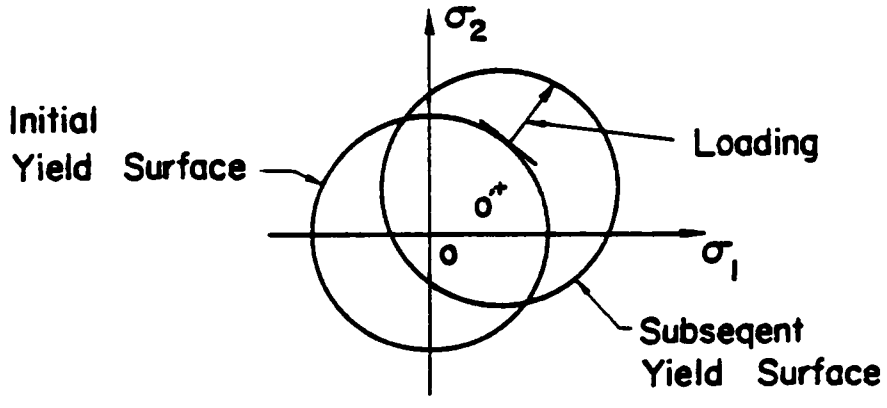

(c) Kinematic Strain Hardening

Fig. 3-1 Mathematical Models for Strain Hardening Behavior

where $\bar{\sigma}_o$ is the equivalent initial yield stress in the reference direction σ_{o1} is the initial uniaxial yield stress in the 1-direction (the superscript 'o' denotes values before hardening commences).

Taking 1-direction as the reference direction, we have

$$\beta_{11}^o = 1.0$$

Similarly,

$$\beta_{22}^o = \left(\frac{\bar{\sigma}_o}{\sigma_{o2}}\right)^2 \quad ; \quad \beta_{55}^o = \frac{1}{3}\left(\frac{\bar{\sigma}_o}{\sigma_{o13}}\right)^2$$

$$\beta_{44}^o = \frac{1}{3}\left(\frac{\bar{\sigma}_o}{\sigma_{o23}}\right)^2 \quad ; \quad \beta_{66}^o = \frac{1}{3}\left(\frac{\bar{\sigma}_o}{\sigma_{o12}}\right)^2 \tag{3.6}$$

To find β_{12}^o, consider a tensile test in the plane of the plate at an angle θ from one of the orthotropic axes, say x-axis, as shown in Fig. 3.2. Then the stresses are transformed as

$$\begin{aligned} \sigma_1 &= \sigma_{\theta o} \cos^2\theta \\ \sigma_2 &= \sigma_{\theta o} \sin^2\theta \\ \sigma_{12} &= \sigma_{\theta o} \sin\theta \cos\theta \end{aligned} \tag{3.7}$$

and

$$\sigma_{23} = \sigma_{13} = 0$$

where $\sigma_{\theta o}$ is the initial yield stress in the θ-direction. Substituting Eq. (3.7) into Eq. (3.5) we obtain

$$\begin{aligned} \bar{\sigma}_o^2 = \sigma_{\theta o}^2 [\beta_{11}^o \cos^4\theta &- \beta_{12}^o \sin^2\theta \cos^2\theta + \beta_{22}^o \sin^4\theta \\ &+ 3\beta_{66}^o \sin^2\theta \cos^2\theta] \end{aligned}$$

Now, letting $\theta = 45°$,

$$\bar{\sigma}_o^2 = \frac{\sigma_{\theta o}^2}{4} [\beta_{11}^o - \beta_{12}^o + \beta_{22}^o + 3\beta_{66}^o]$$

or

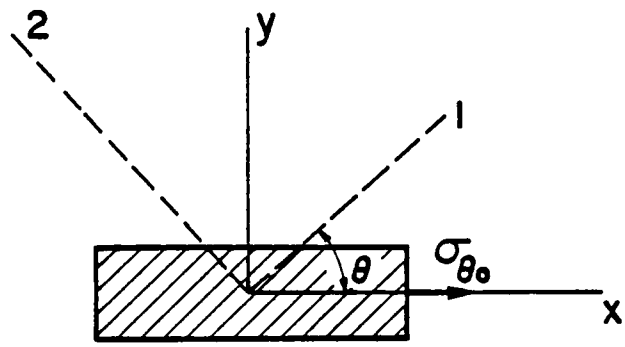

Fig. 3·2 Tensile Test with Fibers Oriented at an Angle θ to the X-axis

$$\beta_{12}^{o} = [\beta_{11}^{o} + \beta_{22}^{o} + 3\beta_{66}^{o}] - 4\frac{\bar{\sigma}_o^2}{\sigma_{\theta o}^2} \qquad (3.8)$$

Now substituting the values of β_{11}^{o}, β_{22}^{o} and β_{66}^{o} into Eq. (3.8), we get,

$$\beta_{12}^{o} = 1 + (\frac{\bar{\sigma}_o}{\sigma_{o2}})^2 + (\frac{\bar{\sigma}_o}{\sigma_{o12}})^2 - (\frac{2\bar{\sigma}_o}{\sigma_{\theta o}})^2$$

3.3.2 Subsequent Parameters of Anisotropy

Due to the strain hardening characteristic of the material, the structure is capable of carrying load beyond first yield. As mentioned in the preceding section, in the present development isotropic strain hardening is incorporated inwhich the subsequent yield surface retains the same shape as the initial yield surface but merely increases in size following any loading path.

For a strain hardening material, the uniaxial yield stress varies with increasing plastic deformation, and therefore the anisotropic parameters should vary, as pointed out by Jensen et al. [38], since they are functions of current yield stresses. The change inyield stress in any direction depends on the total amount of plastic work done in that direction. For an equivalent change in effective stress, the total work done in each direction should be the same.

For a tensile specimen in 1-direction, the plastic work done is (see Fig. 3.3a)

$$W^P = \int \sigma_1 d\varepsilon_1^P = \int \bar{\sigma} d\bar{\varepsilon}^P$$

Similarly, in the 2-direction,

$$W^P = \int \sigma_2 d\varepsilon_2^P$$

Let σ_1^H = uniaxial yield stress in 1-direction including hardening effects

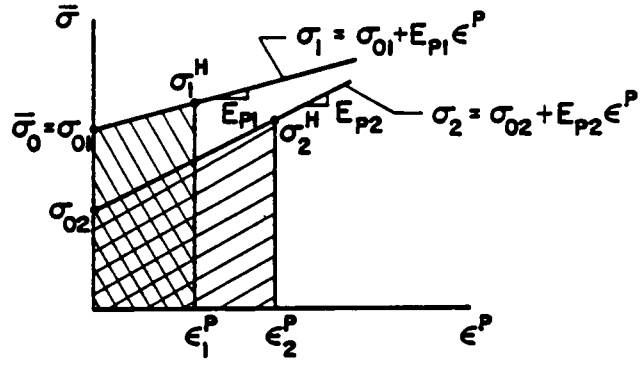

(a)

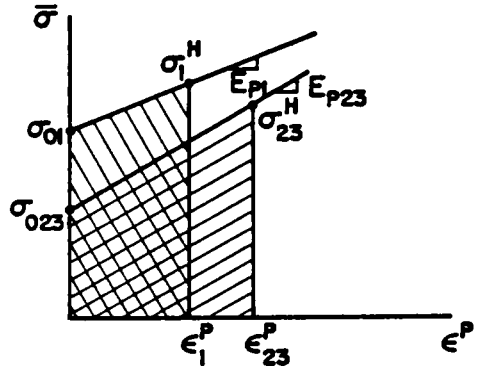

(b)

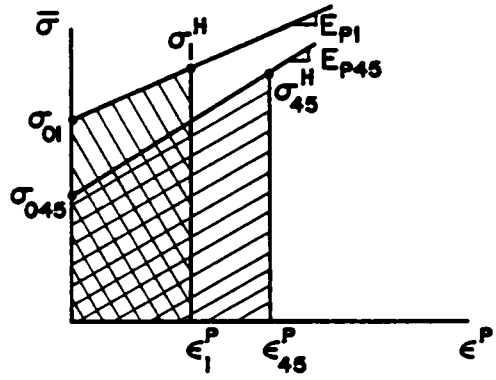

(c)

Fig. 3-3 Stress-Plastic Strain Curves

$\bar{\sigma}$ = corresponding effective stress,

ε_1^P = plastic strain in 1-direction, and

E_{P1} = slope of the stress-plastic strain curve in the 1-direction

For σ_1^H and σ_2^H to correspond to the same effective stress $\bar{\sigma}$, the work done should be the same. Equating the shaded areas in Fig. 3.3a, we obtain

$$\sigma_{o1}\varepsilon_1^P + \frac{1}{2}\varepsilon_1^P(\sigma_1^H - \sigma_{o1}) = \sigma_{o2}\varepsilon_2^P + \frac{1}{2}\varepsilon_2^P(\sigma_2^H - \sigma_{o2}) \qquad (3.9)$$

But

$$\varepsilon_1^P = \frac{1}{E_{P1}}(\sigma_1^H - \sigma_{o1})$$

and

$$\varepsilon_2^P = \frac{1}{E_{P2}}(\sigma_2^H - \sigma_{o2}) \qquad (3.10)$$

Substituting Eq. (3.10) in Eq. (3.9) results in

$$\frac{\sigma_{o1}}{E_{P1}}(\sigma_1^H - \sigma_{o1}) + \frac{1}{2E_{P2}}(\sigma_1^H - \sigma_{o1})^2 = \frac{\sigma_{o2}}{E_{P1}}(\sigma_2^H - \sigma_{o2}) + \frac{1}{2E_{P2}}(\sigma_2^H - \sigma_{o2})^2$$

$$-\frac{\sigma_{o1}^2}{2E_{P1}} + \frac{(\sigma_1 H)^2}{2E_{P1}} = -\frac{\sigma_{o2}^2}{2E_{P2}} + \frac{(\sigma_2 H)^2}{2E_{P2}}$$

$$(\sigma_2 H)^2 = \frac{E_{P2}}{E_{P1}}[(\sigma_1 H)^2 - \sigma_{o1}]^2 + \sigma_{o2}^2 \qquad (3.11)$$

By definition, $\beta_{11} = 1.0$ and $\sigma_1^H = \bar{\sigma}$. Now, using Eqs. (3.5) and (3.6), we get

$$\beta_{22} = \frac{\bar{\sigma}^2}{(\sigma_2 H)^2} \qquad (3.12)$$

Substituting Eq. (3.11) into Eq. (3.12) gives

$$\beta_{22} = \frac{\bar{\sigma}^2}{\frac{E_{P2}}{E_{P1}}(\bar{\sigma}^2 - \sigma_{o1}^2) + \sigma_{o2}^2}$$

Similarly, using Eq. (3.5) and Eq. (3.6) (see Fig. 3.3b)

$$\beta_{44} = \frac{\bar{\sigma}^2}{3(\sigma_{23}^H)^2} = \frac{\bar{\sigma}^2}{3[\frac{G_{P23}}{E_{P1}}(\bar{\sigma}^2 - \sigma_{o1}^2) + \sigma_{o23}^2]}$$

and

$$\beta_{55} = \frac{\bar{\sigma}^2}{3(\sigma_{13}^H)^2} = \frac{\bar{\sigma}^2}{3[\frac{G_{P13}}{E_{P1}}(\bar{\sigma}^2 - \sigma_{o1}^2) + \sigma_{o13}^2]}$$

$$\beta_{66} = \frac{\bar{\sigma}^2}{3(\sigma_{12}^H)^2} = \frac{\bar{\sigma}^2}{3[\frac{G_{P12}}{E_{P1}}(\bar{\sigma}^2 - \sigma_{o1}^2) + \sigma_{o12}^2]}$$

To find β_{12}, consider Fig. (3.3c) and using Eqs. (3.5) and (3.8)

$$\beta_{12} = \beta_{11} + \beta_{22} + 3\beta_{66} - 4\frac{\bar{\sigma}^2}{\sigma_{o45}^2}$$

$$= \beta_{11} + \beta_{22} + 3\beta_{66} - 4\frac{\bar{\sigma}^2}{\frac{E_{P45}}{E_{P1}}(\bar{\sigma}^2 - \sigma_{o1}^2) + \sigma_{o45}^2}$$

Thus, we have the modified yield criterion which is valid for both elastic-perfectly plastic and strain hardening material. The method accounts for the fact that the parameters of anisotropy vary as the material strain hardens.

If the principal axes of anisotropy do not coincide with the reference axes x, y but are rotated by an angle θ (see Fig. 3.4), the stresses in Eq. (3.5) are obtained using the transformation law

$$\sigma_1 = \sigma_x \cos^2\theta + \sigma_y \sin^2\theta + 2\sigma_{xy} \sin\theta \cos\theta$$

$$\sigma_2 = \sigma_x \sin^2\theta + \sigma_y \cos^2\theta - 2\sigma_{xy} \sin\theta \cos\theta$$

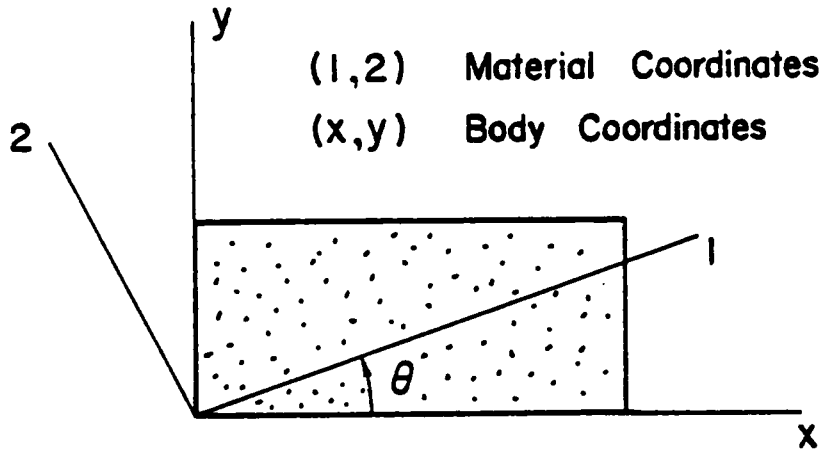

Fig. 3·4 Transformation between Material Axes and Body Coordinates

$$\sigma_{23} - \sigma_{xz} \sin\theta + \sigma_{yz} \cos\theta$$

$$\sigma_{13} = \sigma_{xz} \cos\theta + \sigma_{yz} \sin\theta$$

$$\sigma_{12} = -\sigma_x \sin\theta \cos\theta + \sigma_y \sin\theta \cos\theta + \sigma_{xy}(\cos^2\theta - \sin^2\theta)$$

It is informative to note that the current model, which is based on Hill's anisotropic yield criterion for metals, excludes the hyrostatic effect. It has been argued [61] that, unlike metals, for fibrous composites the neglect of hydrostatic pressure is unjustified. However, there is no evidence that the hydrostatic pressure has significant effect on yielding. Also, the present work is based on the macroscopic approach and thus cannot handle the complex fiber-matrix interactions which are responsible for the yield surface translation in the composite lamina, called constrained hardening [62].

3.4 Elastic-Plastic Constitutive Equation

Yielding can occur if the stress $\{\sigma\}$, satisfies the general yield criterion

$$f(\{\sigma\},\kappa) = 0$$

where κ is the hardening parameter.

In order to justify the validity of plasticity theory, Fig. 3.5 shows the loading/unloading curve for metal matrix composites, namely, Boron/Aluminum and Graphite/Aluminum, which exhibits a permanent set.

In the incremental theory of plasticity, the total strain increment is the sum of the elastic and plastic components:

$$d\{\varepsilon\} = d\{\varepsilon^e\} + d\{\varepsilon^p\}$$

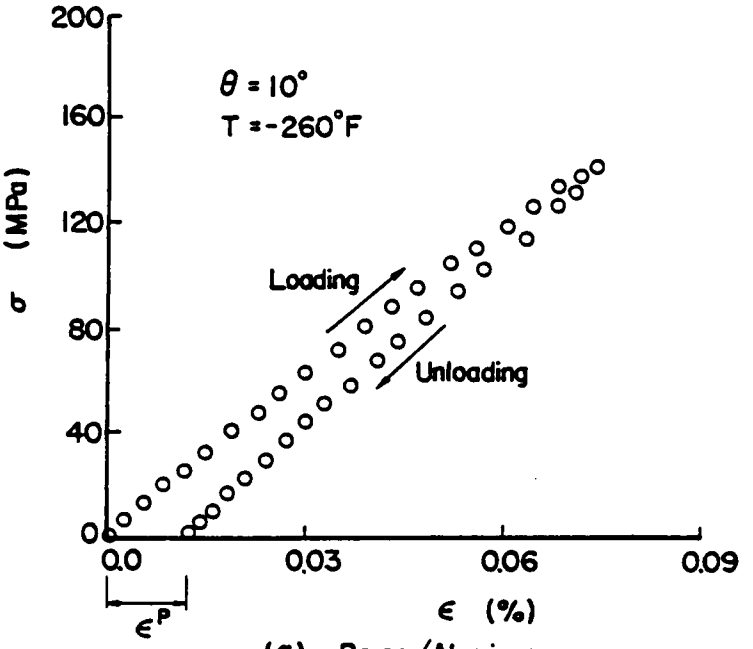

(a) Boron/Aluminum

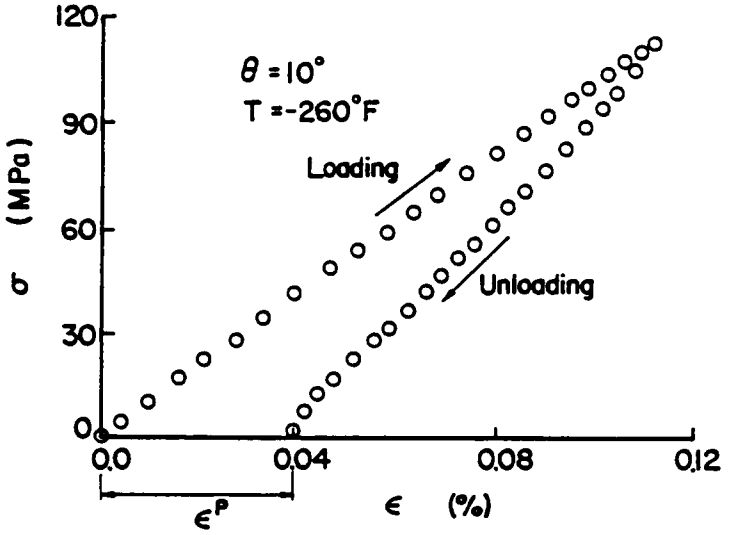

(b) Graphite/Aluminum

Fig. 3-5 Loading-Unloading Curves for Metal Matrix Composite

The elastic strain increment is related to the stress increment by Hooke's law as

$$d\{\varepsilon^e\} = [D^e]^{-1} d\{\sigma\} \tag{3.13}$$

where $[D^e]$ is the elastic modulus matrix, which for orthotropic material takes the form

$$[D^e] = \begin{bmatrix} \frac{E_1}{1-\nu_{12}\nu_{21}} & \frac{\nu_{12}E_2}{1-\nu_{12}\nu_{21}} & 0 & 0 & 0 \\ \frac{\nu_{12}E_2}{1-\nu_{12}\nu_{21}} & \frac{E_2}{1-\nu_{12}\nu_{21}} & 0 & 0 & 0 \\ 0 & 0 & G_{23} & 0 & 0 \\ 0 & 0 & 0 & G_{13} & 0 \\ 0 & 0 & 0 & 0 & G_{12} \end{bmatrix}$$

The normality rule for an associated flow is

$$d\{\varepsilon\}^P = d\lambda \frac{df}{d\{\sigma\}}$$

where $d\lambda$ is the proportionality constant evaluated using the condition that during the plastic deformation the stresses remain on the yield surface, so that

$$df = \frac{\partial f}{\partial \{\sigma\}} d\{\sigma\} - A d\lambda$$

$$0 = \frac{\partial f}{\partial \sigma_1} d\sigma_1 + \frac{\partial f}{\partial \sigma_2} d\sigma_2 + \frac{\partial f}{\partial \sigma_{23}} d\sigma_{23} + \frac{\partial f}{\partial \sigma_{13}} d\sigma_{13} + \frac{\partial f}{\partial \sigma_{12}} d\sigma_{12} - A d\lambda$$

or

$$0 = \left\{\frac{\partial f}{\partial \{\sigma\}}\right\}^T \{d\{\sigma\}\} - A d\lambda \tag{3.14}$$

From Eqs. (3.13) and (3.14)

$$d\{\sigma\} = [D^e](d\{\varepsilon\} - d\lambda \frac{\partial f}{\partial \{\sigma\}}) \tag{3.15}$$

Evaluating $d\lambda$ from Eq. (3.14) and Eq. (3.15)

$$0 = \{\frac{\partial f}{\partial \{\sigma\}}\}^T [D^e](d\{\varepsilon\} - \lambda \frac{\partial f}{\partial \{\sigma\}}) - A d\lambda$$

or

$$d\lambda = \frac{\{\frac{\partial f}{\partial \{\sigma\}}\}^T [D^e] d\{\varepsilon\}}{A + \{\frac{\partial f}{\partial \{\sigma\}}\}^T [D^e] \{\frac{\partial f}{\partial \{\sigma\}}\}} \tag{3.16}$$

If the yield surface is defined in terms of the uniaxial stress, A is equal to the slope H of the uniaxial stress-plastic strain curve (see Fig. 3.6), given by

$$A = H = \frac{d\bar{\sigma}}{d\bar{\varepsilon}^P} = \frac{E_T}{1 - E_T/E}$$

where E and E_T are the elastic and tangent moduli of the material for uniaxial test. Note that as E_T approaches zero, the problem reduces to the elastic-perfectly plastic one.

Substituting Eq. (3.16) into Eq. (3.15), we get the stress-strain relation in the plastic range

$$d\{\sigma\} = [D^{eP}] d\{\varepsilon\}$$

where

$$[D^{eP}] = [D^e] - \frac{[D^e] \frac{\partial f}{\partial \{\sigma\}} \{\frac{\partial f}{\partial \{\sigma\}}\}^T [D^e]}{H + \{\frac{\partial f}{\partial \{\sigma\}}\}^T [D^e] \{\frac{\partial f}{\partial \{\sigma\}}\}} \tag{3.17}$$

For elastic-perfectly plastic material, obviously H = 0. Hence the modification called for in the elastic-plastic analysis would be solely

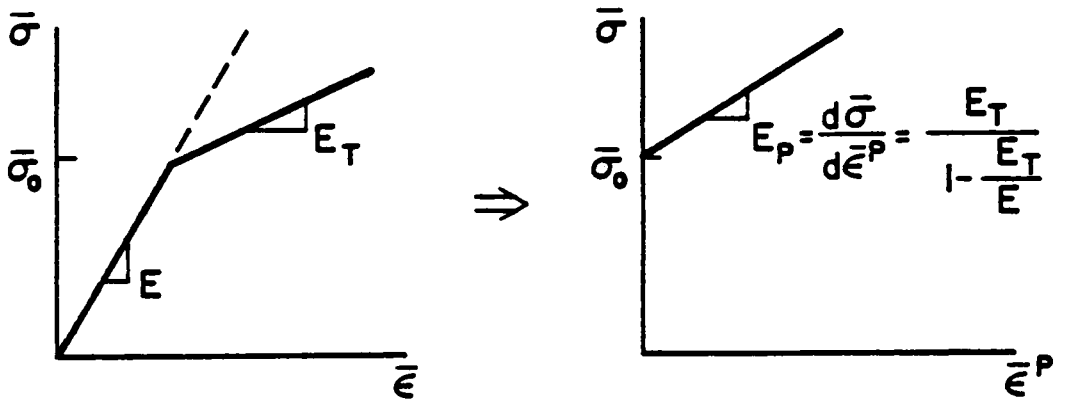

Fig. 3-6 Equivalent Stress-Strain Curve

the replacement of $[D^e]$ by $[D^{eP}]$ for the yielded elements at the successive stages of calculation.

The explicit form of $[D^{eP}]$ for laminated composite plates and shells is given in Appendix A.

The stress-strain relations for the k^{th} lamina, transformed to the laminate coordinate xy (see Fig. 3.4) are of the form

$$\{d\sigma\}^k = [Q^{(k)}]\{d\varepsilon\}^k$$

where $[Q^{(k)}]$ are the material properties of the k^{th} layer. Accordingly, the populated stress-strain matrix $[D^{eP}]$ is transformed from the material axes to the shell reference axes (see Reddy [63]). The transformed coordinates are shown in Appendix B.

CHAPTER 4

COMBINED GEOMETRIC AND MATERIAL NONLINEARITY

In the preceding sections, the treatment of geometric nonlinear analysis and elasto-plastic analysis of laminated composite plates and shells acting separately have been considered. Which of these two main sources of nonlinearities is most important depends, of course, on the geometry and material properties themselves. In general, the geometric effects are most important for "thin" structures, whereas for "thick" structures the latter group ofeffects is prevailing.

It is desirable, under these circumstances, to extend the methodology to include both types of nonlinearities acting in combination. In the present work simultaneous treatment of plasticity and geometric nonlinearity is accomplished by means of the constitutive relation and changing geometry. Consequently, a primary consideration in choosing a method for the analysis of geometric nonlinearity from among the several currently available is the ease with which it can be combined with methods of plastic analysis. For this reason, though the solution ofgeometric nonlinearity when considered separately is reached by either the direct iteration method or Newton-Raphson method (as explained in the subsequent sections), for the treatment of material nonlinearity and combined nonlinearity only the latter method is adopted due to the incremental nature of the plasticity relations. Thus, the modification necessary toincorporate both the nonlinearities acting in combination is minimal.

The counterbalancing effect ofgeometric and material nonlinearity is demonstrated with a variety of examples for both static and dynamic

analysis. The prsent study constitutes the first one to consider the combined nonlinearity of laminated composite plates and shells.

CHAPTER 5

FINITE ELEMENT FORMULATION

In the development of the finite element model for nonlinear analysis, emphasis is based on the deformation theory, choice of the element and the solution iteration. The present work is based onan extension of the Sanders shell theory and accounts for the large deformation in the von Karman sense. The effect of plastic deformation is incorporated using a modified version of Hill's yield criterion in which anisotropic parameters are introduced. A doubly curved isoparametric element is used for the analysis and the nonlinear solution is reached by an iterative technique.

5.1 Equations of Motion

The dynamic version of the principle of virtual work for the present problem is given by

$$
\begin{aligned}
0 = \sum_{k=1}^{L} \int_{\zeta_k}^{\zeta_{k-1}} \Big[\int_{\Omega} \{ & \sigma_1^{(k)} \delta\varepsilon_1 + \sigma_2^{(k)} \delta\varepsilon_2 + \sigma_6^{(k)} \delta\varepsilon_6 + \sigma_4^{(k)} \delta\varepsilon_4 \\
& + \sigma_5^{(k)} \delta\varepsilon_5 - \zeta^{(k)} [(1 + \tfrac{\zeta}{R_1})\dot{u}_1 + \zeta\delta\dot{\phi}_1][(1 + \tfrac{\zeta}{R_1})\delta\dot{u}_1 + \zeta\delta\dot{\phi}_1] \\
& - \zeta^{(k)} [(1 + \tfrac{\zeta}{R_1})\dot{u}_1 + \zeta\dot{\phi}_1][(1 + \tfrac{\zeta}{R_1})\delta\dot{u}_1 + \zeta\delta\dot{\phi}_1] \\
& - \zeta^{(k)} [(1 + \tfrac{\zeta}{R_2})\dot{u}_2 + \zeta\dot{\phi}_2][(1 + \tfrac{\zeta}{R_2})\delta\dot{u}_2 + \zeta\dot{\phi}_2] \\
& - \zeta^{(k)} u_3 \delta\dot{u}_3 \} \alpha_1 \alpha_2 d\xi_1 d\xi_2 \Big] d\zeta - \int_{\Omega} q \delta u_3 \alpha_1 \alpha_2 d\xi_1 d\xi_2
\end{aligned}
\tag{5.1}
$$

Here (ζ_{k-1}, ζ_k) are the ζ-coordinates of the k^{th} layer, L is the total number of layers in the laminated shell and q is the distributed

transverse load. Equation (5.1) can be written as

$$0 = \int_{\Omega} [N_1\delta\varepsilon_1^o + N_2\delta\varepsilon_2^o + N_6\delta\varepsilon_6^o + M_1\delta\kappa_1 + M_2\delta\kappa_2 + M_6\delta\kappa_6$$
$$+ Q_1\delta\varepsilon_5^o + Q_2\delta\varepsilon_4^o + (P_1\ddot{u}_1 + P_2\ddot{\phi}_1)\delta u_1 + (\bar{P}_1\ddot{u}_2 + \bar{P}_2\ddot{\phi}_2)\delta u_2$$
$$+ I_1\ddot{u}_3\delta u_3 + (I_3\ddot{\phi}_1 + P_2\ddot{u}_1)\delta\phi_1 + (I_3\ddot{\phi}_2 + \bar{P}_2\ddot{u}_2)\delta\phi_2$$
$$- q\delta u_3]\alpha_1\alpha_2 d\xi_1 d\xi_2 \tag{5.2}$$

where N_i and M_i are the stress and moment resultants, and Q_i are the shear force resultants:

$$(N_i, M_i) = \sum_{k=1}^{L} \int_{\zeta_{k-1}}^{\zeta_k} \sigma_i(1,\zeta)d\zeta \quad , \quad i = 1,2,6$$
$$(Q_1, Q_2) = \sum_{k=1}^{L} \int_{\zeta_{k-1}}^{\zeta_k} (K_1^2\sigma_5,\ K_2^2\sigma_4)d\zeta \tag{5.3}$$

Here K_i $(i = 1,2)$ are the shear correction factors and P_i are the inertias:

$$P_1 = I_1 + \frac{2I_2}{R_1} \quad , \quad P_2 = I_2 + \frac{I_3}{R_1}$$
$$\bar{P}_1 = I_1 + \frac{2I_2}{R_2} \quad , \quad \bar{P}_2 = I_2 + \frac{I_3}{R_2} \tag{5.4}$$

where

$$(I_1, I_2, I_3) = \sum_{k=1}^{L} \int_{\zeta_{k-1}}^{\zeta_k} \zeta^{(k)}(1,\zeta,\zeta^2)d\zeta$$

It is informative to note that the governing equations of motion can be derived from Eq. (5.2) by integrating the displacement gradients in ε_i^o by parts and setting the coefficients of δu_i $(i = 1,2,3)$ and $\delta\phi_i$

(i = 1,2) to zero separately. We obtain [with $C_o = \frac{1}{2}\left(\frac{1}{R_1} - \frac{1}{R_2}\right)$ and $dx_i = \alpha_i d\xi_i$]

$$\frac{\partial N_1}{\partial x_1} + \frac{\partial}{\partial x_2}(N_6 - C_o M_6) + \frac{Q_1}{R_1} = P_1 \frac{\partial^2 u_1}{\partial t^2} + P_2 \frac{\partial^2 \phi_1}{\partial t^2}$$

$$\frac{\partial}{\partial x_1}(N_6 + C_o M_6) + \frac{\partial N_2}{\partial x_2} + \frac{Q_2}{R_2} = \bar{P}_1 \frac{\partial^2 u_1}{\partial t^2} + \bar{P}_2 \frac{\partial^2 \phi_2}{\partial t^2}$$

$$\frac{\partial \phi_1}{\partial x_1} + \frac{\partial \phi_2}{\partial x_2} - \left(\frac{N_1}{R_1} + \frac{N_2}{R_2} - q\right) + N(u_3) = I_1 \frac{\partial^2 u_3}{\partial t^2}$$

$$\frac{\partial M_1}{\partial x_1} + \frac{\partial M_6}{\partial x_2} - Q_1 = I_3 \frac{\partial^2 \phi_1}{\partial t^2} + P_2 \frac{\partial^2 u_1}{\partial t^2}$$

$$\frac{\partial M_6}{\partial x_1} + \frac{\partial M_2}{\partial x_2} - Q_2 = I_3 \frac{\partial^2 \phi_2}{\partial t^2} + \bar{P}_2 \frac{\partial^2 u_2}{\partial t^2} \qquad (5.5)$$

where

$$N(u_3) = \frac{\partial}{\partial x_1}\left(N_1 \frac{\partial u_3}{\partial x_1} + N_6 \frac{\partial u_3}{\partial x_2}\right) + \frac{\partial}{\partial x_2}\left(N_6 \frac{\partial u_3}{\partial x_1} + N_2 \frac{\partial u_3}{\partial x_2}\right)$$

The resultants (N_i, M_i, Q_i) are related to $(\varepsilon_i^o, \kappa_i)$ (i,j = 1,2,6) by

$$N_i = A_{ij}\varepsilon_j^o + B_{\ell p}\kappa_p \quad i,j = 1,2,6,4,5$$

$$M_\ell = B_{\ell j}\varepsilon_j^o + D_{\ell p}\kappa_p \quad \ell,p = 1,2,6 \text{ (with } \ell = i \text{ for } i = 1,2,6) \qquad (5.6)$$

Here A_{ij}, B_{ij} and D_{ij} denote the extensional, flexural-extensional coupling and flexural stiffnesses of the laminate:

$$(A_{ij}, B_{ij}, D_{ij}) = \sum_{k=1}^{L} \int_{\zeta_{k-1}}^{\zeta_k} Q_{ij}^{(k)} (1, \zeta, \zeta^2) d\zeta$$

$$(A_{44}, A_{45}, A_{55}) = \sum_{k=1}^{L} \int_{\zeta_{k-1}}^{\zeta_k} (K_1^2 Q_{44}^{(k)}, K_1 K_2 Q_{45}^{(k)}, K_2^2 Q_{55}^{(k)}) d\zeta \qquad (5.7)$$

In the unabridged notation Eq. (5.6) takes the form

$$\begin{Bmatrix} N_1 \\ N_2 \\ N_6 \\ N_4 \\ N_5 \\ M_1 \\ M_2 \\ M_6 \end{Bmatrix} = \begin{bmatrix} A_{11} & A_{12} & A_{16} & \underline{A_{14}} & \underline{A_{15}} & B_{11} & B_{12} & B_{16} \\ A_{12} & A_{22} & A_{26} & \underline{A_{24}} & \underline{A_{25}} & B_{12} & B_{22} & B_{26} \\ A_{16} & A_{26} & A_{66} & \underline{A_{46}} & \underline{A_{56}} & B_{16} & B_{26} & B_{66} \\ \underline{A_{14}} & \underline{A_{24}} & \underline{A_{46}} & A_{44} & A_{45} & \underline{B_{14}} & \underline{B_{24}} & \underline{B_{46}} \\ \underline{A_{15}} & \underline{A_{25}} & \underline{A_{56}} & A_{45} & A_{55} & \underline{B_{15}} & \underline{B_{25}} & \underline{B_{56}} \\ B_{11} & B_{12} & B_{16} & \underline{B_{14}} & \underline{B_{15}} & D_{11} & D_{12} & D_{16} \\ B_{12} & B_{22} & B_{26} & \underline{B_{24}} & \underline{B_{25}} & D_{12} & D_{22} & D_{26} \\ B_{16} & B_{26} & B_{66} & \underline{B_{46}} & \underline{B_{56}} & D_{16} & D_{26} & D_{66} \end{bmatrix} \begin{Bmatrix} \varepsilon_1^o \\ \varepsilon_2^o \\ \varepsilon_6^o \\ \varepsilon_4^o \\ \varepsilon_5^o \\ \kappa_1 \\ \kappa_2 \\ \kappa_6 \end{Bmatrix} \tag{5.8}$$

The underscored coefficients are due to the material nonlinear stress-strain relationship.

5.2 Finite Element Model

A typical finite element is a doubly curved shell element whose projection on the $\xi_1\xi_2$-plane is an isoparametric quadrilateral element. Over the typical shell element $\Omega^{(e)}$, the displacements (u_1, u_2, u_3, ϕ_1, ϕ_2) are interpolated by expressions of the form

$$\begin{aligned} u_i &= \sum_{j=1}^{N} u_i^j \psi_j(\xi_1,\xi_2) \quad i = 1,2,3 \\ \phi_i &= \sum_{j=1}^{N} \phi_i^j \psi_j(\xi_1,\xi_2) \quad i = 1,2 \end{aligned} \tag{5.9}$$

in which ψ_j are the interpolation functions, and u_i^j and ϕ_i^j are the nodal values of u_i and ϕ_i, respectively.

Substitution of q. (5.9) into the variational form, Eq. (5.2) gives

$$[K(\Delta)]\{\Delta\} + [M]\{\ddot{\Delta}\} = \{F\} \tag{5.10}$$

where $\{\Delta\} = \{\{u_1\},\{u_2\},\{u_3\},\{\phi_1\},\{\phi_2\}\}^T$, $[K]$ and $[M]$ are the element stiffness and mass matrices, respectively, and $\{F\}$ is the force vector.

The element stiffness matrix contains nonlinear coefficients in addition to the usual linear terms. In general, the element stiffness matrix takes the form

$$[K] = [K]_L + [K]_G + [K]_M + [K]_{GM} \tag{5.11}$$

where

$[K]_L$ = linear stiffness originating from linear displacement theory,

$[K]_G$ = geometric stiffness accounting for the additional stiffness due to changed geometry,

$[K]_M$ = combined stiffness due to plastic deformation,

and

$[K]_{GM}$ = combined stiffness considering both types of nonlinearities.

In the interest of brevity, the stiffness and mass matrices are included in Appendix C.

To complete the approximation, we should approximate the time derivatives in Eq. (5.10). Here we use the Newmark direct integration scheme (the constant-average-acceleration method). Use of the Newmark method with Eq. (5.10) yields

$$[\hat{K}]\{\Delta\}_{n+1} = \{\hat{F}\}_{n,n+1} \tag{5.12}$$

where

$$[\hat{K}] = [K] + a_o[M]$$

$$\{\hat{F}\} = \{F\}_{n+1} + [M](a_o\{\Delta\}_n + a_1\{\dot{\Delta}\}_n + a_2\{\ddot{\Delta}\}_n),$$

$$a_o = \frac{1}{(\beta\Delta t)^2} \quad , \quad a_1 = a_o\Delta t \quad , \quad a_2 = \frac{1}{2\beta} - 1 \tag{5.13}$$

Once the solution $\{\Delta\}$ is known at $t_{n+1} = (n + 1)\Delta t$, the first and second derivatives (velocity and accelerations) of $\{\Delta\}$ at t_{n+1} can be computed from

$$\{\ddot{\Delta}\}_{n+1} = a_o(\{\Delta\}_{n+1} - \{\Delta\}_n) - a_1\{\dot{\Delta}\}_n - a_2\{\ddot{\Delta}\}_n$$

$$\{\dot{\Delta}\}_{n+1} = \{\dot{\Delta}\}_n + a_3\{\ddot{\Delta}\}_n + a_4\{\ddot{\Delta}\}_{n+1} \tag{5.14}$$

where $a_3 = (1 - \alpha)\Delta t$ and $a_4 = \alpha\Delta t$.

For a nine noded quadratic element, the element stiffness matrix is of order 45 x 45. The evaluation of the element matrices requires numerical integration. Reduced integration is used to evluate the coefficients associated with the shear energy terms to avoid the so called locking effect. More specifically, the 2 x 2 Gauss rule must be used for shear terms and the standard 3 x 3 Gauss rule is used for the bending terms when the nine noded quadratic isoparametric element is considered.

It should be noted that the underscored coefficients in Eq. (5.8) are also redefined like the shear coefficients in Eq. (5.7) and reduced integration is used for the terms arising in the stiffness matrices due to the presence of these coefficients.

The element equations (5.10) can be assembled, bundary conditions can be imposed, and the resulting equations can be solved (as explained in the subsequent section) at each time step using the information known from the preceding time step solution. A time t = 0, the initial values of $\{\Delta\}$, $\{\dot{\Delta}\}$, and $\{\ddot{\Delta}\}$, obtained by solving Eq. (5.10) at t = 0, are used

to initiate the time marching scheme. An iterative technique is used to solve the nonlinear algebraic equations.

5.3 Solution Procedure

The solution of the nonlinear problem is reached by an incremental and iterative procedure. In the present work, the direct iteration and Newton-Raphson method are used for the numerical computation. The two methods are described below for the basic, equation

$$[K(\Delta)]\{\Delta\} = \{F\}$$

5.3.1 Direct Iteration

In the direct iteration, also known as the Picard method, the basic equation is solved according to the equation

$$[K(\{\Delta\}^r)]\{\Delta\}^{r+1} = \{F\} \tag{5.15}$$

where $\{\Delta^r\}$ denotes the solution vector obtained in the rth iteration (at any given load step).

At the beginning of the first load step, we assume that $\{\Delta\}^0 = \{0\}$ and obtain the linear solution. The linear solution is used to compute the stiffness matrix for the second iteration. The solution at the end of r^{th} iteration is used to compute the stiffness matrix for the (r + 1)-th iteration. At the end of each iteration (for any load step), the solution is compared with that obtained in the previous iteration to see if they are close enough to terminate the iteration and to move on to the next load step. The following convergence criterion is used in the present study:

$$\left[\sum_{i=1}^{N} |\Delta_i^r - \Delta_i^{r+1}|^2 \Big/ \sum_{i=1}^{N} |\Delta_i^r|^2\right]^{1/2} \leq 0.01 \tag{5.16}$$

To accelerate the convergence, a weighted average of the solution from the last two iterations are used to compute the stiffness matrix:

$$[K(\gamma\{\Delta\}^{r-1} + (1 - \gamma)\{\Delta\}^{r})]\{\Delta\}^{r+1} = \{F\} \tag{5.17}$$

where γ is the acceleration parameter, $0 \leq \gamma \leq 1$. In the present study a value of 0.25-0.35 was used for the acceleration parameter.

5.3.2 The Newton-Raphson Method

In the Newton-Raphson iteration technique, the basic equation is expressed in the form

$$\{R\} \equiv [R(\Delta)]\{\Delta\} - \{F\} = 0 \tag{5.18}$$

Assuming that the solution is known at the r-th iteration, for any given load step, the vector $\{R\}$ is expanded in Taylor's series about $\{\Delta^r\}$:

$$0 = \{R\}_r + \frac{\partial\{R\}}{\partial\{\Delta\}}\{\delta\Delta\}^r + \ldots$$

$$= ([K(\Delta^r)]\{\Delta^r\} - [F]) + K_T(\Delta^R)\delta\Delta^r$$

where

$$[K_T] = [\frac{\partial\{R\}}{\partial\{\Delta\}}]_r$$

The increment of the solution $\{\delta\Delta^r\}$ is obtained from

$$\{\delta\Delta^r\} = - [K_T(\Delta^r)]^{-1}\{R\} \tag{5.19}$$

The total displacement at the $(r + 1)$th iteration becomes,

$$\{\Delta^{r+1}\} = \{\Delta^r\} + \{\delta\Delta^r\} \tag{5.20}$$

The iteration is stopped when Eq. (5.16), with $\{\delta\Delta^r\} = \{\Delta^r\} - \{\Delta^{r+1}\}$ is satisfied.

Figure 5.1 shows the flow chart for the Newton-Raphson method. The coefficients of the tangent stiffness matrix $[K_T]$, which contains

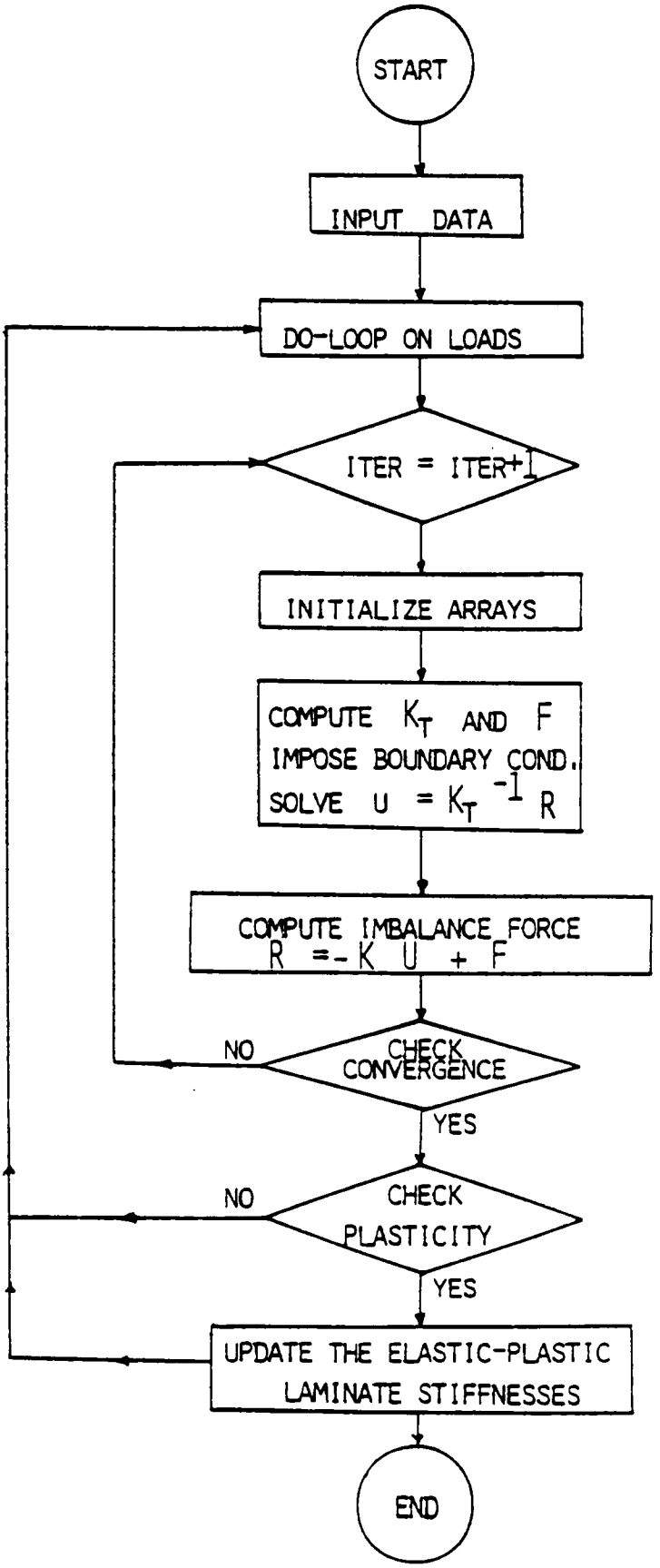
START
INPUT DATA
DO-LOOP ON LOADS
ITER = ITER+1
INITIALIZE ARRAYS
COMPUTE K_T AND F
IMPOSE BOUNDARY COND.
SOLVE $U = K_T^{-1} R$
COMPUTE IMBALANCE FORCE
$R = -K U + F$
CHECK CONVERGENCE
NO
YES
CHECK PLASTICITY
NO
YES
UPDATE THE ELASTIC-PLASTIC LAMINATE STIFFNESSES
END

Fig. 5·1

additional terms compared to the initial nonlinear stiffness matrix $K(\Delta)$, are given in Appendix D.

In the direct iteration, the problem is solved for the total solution at every iteration and therefore the vector of prescribed unknowns must be introduced unchanged into the solution subroutines at each stage. However, for the Newton-Raphson method, the process is essentially accumulative with the value of the unknown being totalled from the incremental values obtained for each iteration. Consequently, both the methods are applicable to the solution of geometric nonlinear analysis while only the Newton-Raphson method is adopted for the solution of elasto-plastic and/or combined nonlinear problems due to the incremental nature of the constitutive equation.

Once the displacement is obtained, the state of stress and the value of $f(\sigma_{ij})$ are calculated for each element at the Gauss points. If $f < 0$, the process is elastic. For the yielded Gauss points, $f > 0$ and the elasticity matrix has to be replaced by the elasto-plastic matrix. Before updating the stress-strain matrix, the stresses are reduced to the yield surface $f = 0$ using plastic correction (as explained in the subsequent section). Once the convergence is achieved, the next load increment is applied and the iteration procedure is repeated.

If the application of a small load increment causes very large deflection, the calculation is stopped and the limit load is considered to be found.

5.4 Layered Model Approach

The concept of a layered model is introduced in order to handle the plasticity in the cross-section of the element in which progressive yielding through the shell thickness is accounted for by depicting it as a collection of thin layers. Accurate representation of the stress is particularly important in the plasticity analysis and the variation of properties from layer to layer must be considered in the elasto-plastic stiffness.

The layers are numbered sequentially starting at the lower surface of the shell (see Fig. 5.2a). Each layer contains the stress points on its mid surface. The stresses of the layers are computed at these stress points by taking the average values of the top and bottom surfaces of the individual layers. For a nine noded quadratic element, the stresses are computed at 3 x 3 full integration points and 2 x 2 reduced integration points (see Fig. 5.2b,c). For yielded Gauss points the elasticity matrix is replaced by the plasticity matrix.

It is informative to note that the layered model only influences the calculation of the stresses which are required for updating the stiffness matrices.

5.5 Plastic Correction

For the yielded Gauss points, the stresses are calculated so that the yield criterion is satisfied. Consequently, the actual stress is greater than this permissible value, then the portion of the stress greater than the yield value must be reduced to the yield surface.

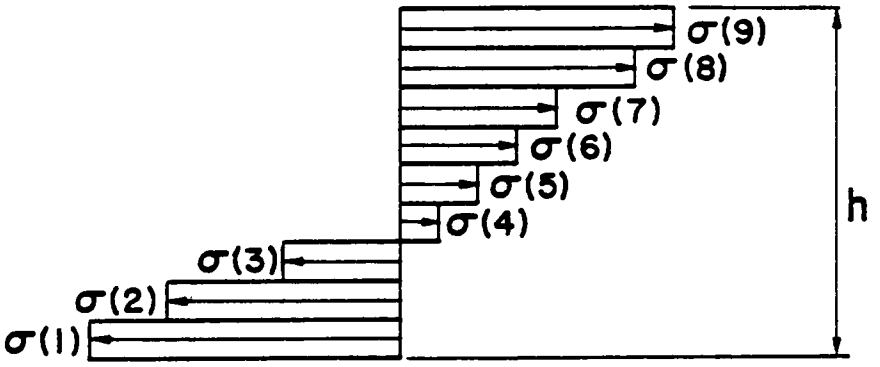

(a) Stress Profile

● – Full Integration

* – Reduced Integration

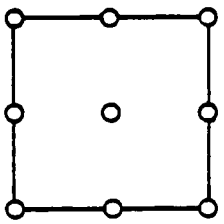

(b) 9-Noded Isoparametric Element

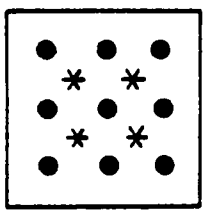

(c) Stress Points

Fig. 5·2 Computation of Stress at Each Layer

Consider the situation for the rth iteration of any particular load increment (see Fig. 5.3). On loading from point C, the stress point moves elastically until the yield surface is met at B. Elastic behavior beyond this point will result in a final stress state defined by point A. However, in order to satisfy the yield criterion, the stress point cannot move outside the yield surface and thus can only traverse the surface until the yield criterion and the constitutive equations are satisfied.

To reduce the stresses to the yield surface, for the yielded Gauss points, the following steps are considered.

Step a

Compute the incremental changes, $d\sigma_e^r$, where subscript 'e' denotes that we are assuming elastic behavior.

Step b

Accumulate the total stress for each element Gauss point as

$$\sigma_e^r = \sigma_e^{r-1} + d\sigma_e^r$$

Step c

Calculate the effective stresses $\bar{\sigma}_e^{r-1}$ and $\bar{\sigma}_e^r$ and check for the following cases:

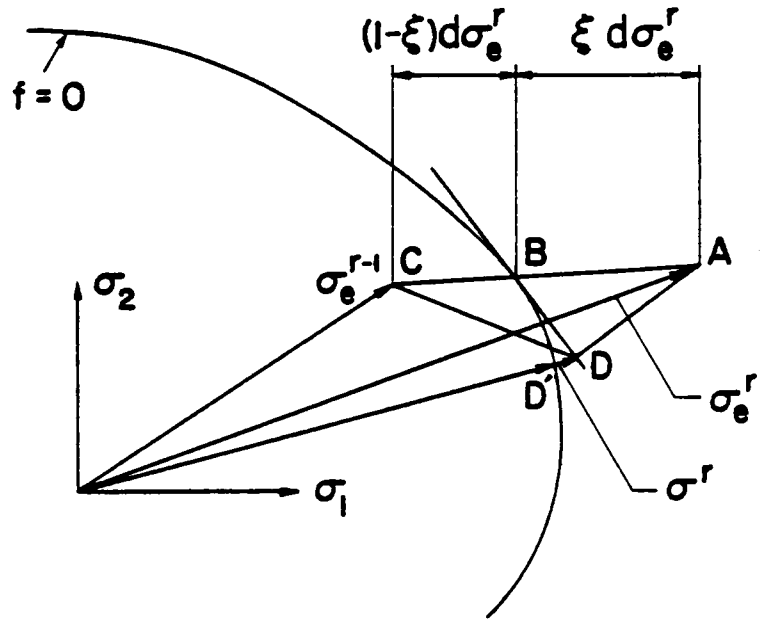

Fig. 5·3 Reducing a Stress Point to the Yield Surface

Case (i)	Case (ii)	Case (iii)	Case (iv)
$\bar{\sigma}_e^{r-1} < \sigma_y$	$\bar{\sigma}_e^{r-1} > \sigma_y$	$\bar{\sigma}_e^{r-1} < \sigma_y$	$\bar{\sigma}_e^{r-1} > \sigma_y$
$\bar{\sigma}_e^{r} < \sigma_y$	$\bar{\sigma}_e^{r} < \sigma_y$	$\bar{\sigma}_e^{r} > \sigma_y$	$\bar{\sigma}_e^{r} > \sigma_y$
Elastic point is still elastic. No reduction of stress is required.	Elastic point now unloading. No reduction of stress is required.	Elastic point becomes plastic. The portion of the stress greater than the yield value must be reduced to the yield surface.	Plastic point goes further plastic. Reduce the entire increase in stress to remain on the yield surface.

Step d

For the yielded Gauss point only, namely for cases (iii) and (iv), compute the portion of the total sress which satisfies the yield criterion as

$$\sigma^r = \sigma_e^{r-1} + (1 - \xi)d\sigma_e^r$$

where

$$\xi = \frac{\bar{\sigma}_e^r - \sigma_y}{\bar{\sigma}_e^r - \bar{\sigma}_e^{r-1}} \text{ for case (iii) and } \xi = 1 \text{ for case (iv).}$$

5.6 Parameters of Anisotropy

When considering the modeling of a material system, one must always survey the availability of material property data.

Advanced fibrous composites materials can be divided into two classes, those being composites with resin matrix and those with metal matrix. Metal matrix composites, specifically Boron/Aluminum, have a large operating temperature range, higher strength, better transverse properties, and can be braze welded to other parts of the structure.

Also, the potential problem of moisture absorption into the matrix is not present in the metal matrix system as it is in the resin matrix. But the applications of metal matrix composite materials has not been as numerous as their counterpart resin matrix composites primarily due to cost considerations.

For typical resin matrix and metal matrix composites, the paramaters of anisotropy are obtained from the unidirectional experimental curves. Figure 5.4 shows the stress-strain curves for Boron/Epoxy with 0°, 90° and ±45 fiber orientation. Also, the shear curve is shown. These curves are obtained at room temperature with fiber volume fraction v_f = 0.5. Figures 5.5 and 5.6 are for Graphite/Epoxy and Boron/Aluminum respectively. All the curves shown in Figs. 5.4-5.6 are taken from the existing literature.

These stress-strain curves indicate that the nonlinearity in ± 45° plies and shear is severe for all three materials in comparison to 0°, and 90° plies. Also, elasto-plastic analysis is crucial for metal matrix composites since the onset of plastic yielding starts very early in the loading process as compared to the ultimate strength.

The elastic constants for typical composite materials considered are shown in Table 5.1. Depending on the hardening model under consideration, the initial and subsequent parameters of anisotropy can be obtained from the stress-strain curves.

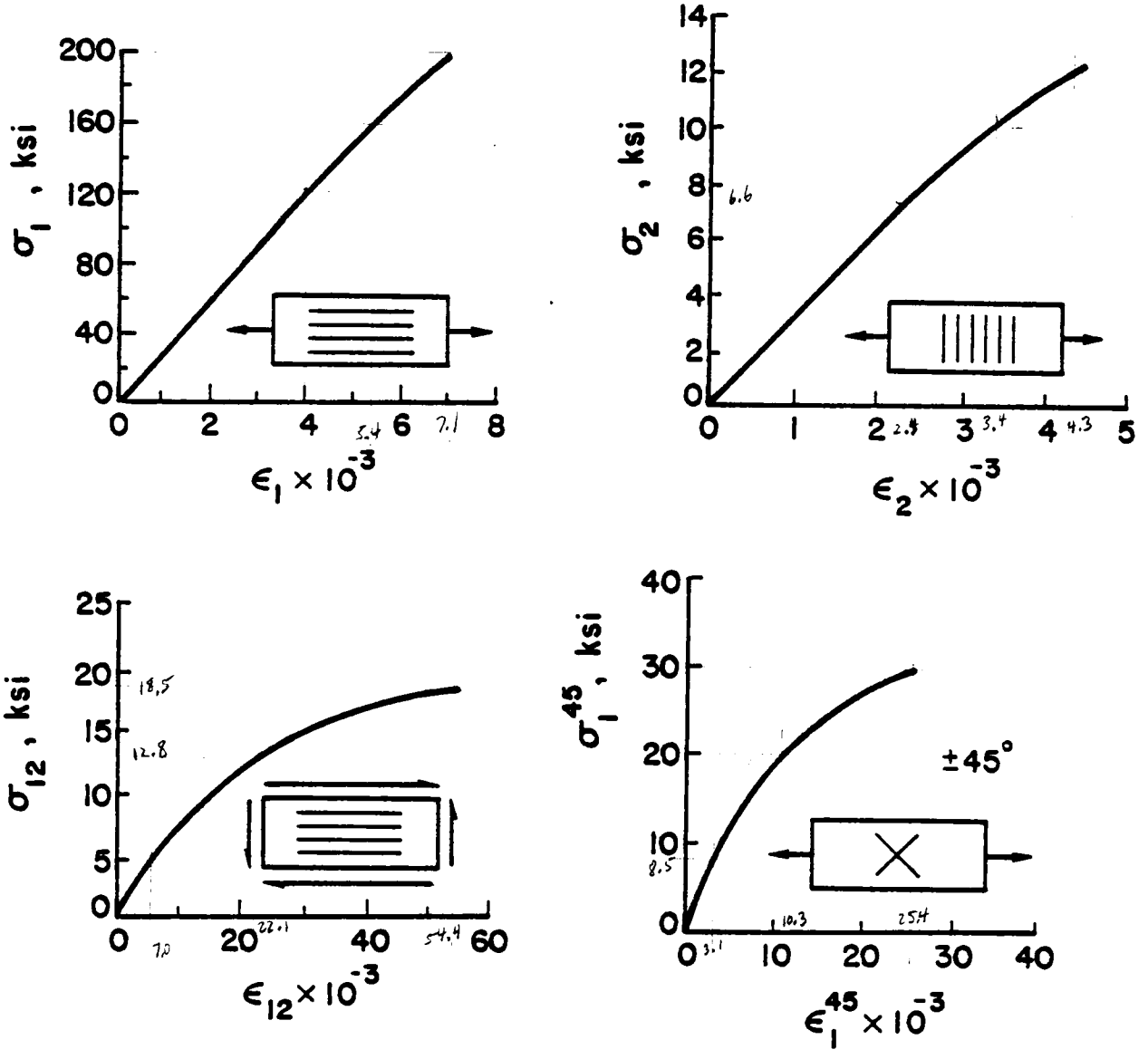

Fig. 5·4 Stress-Strain Curves for Boron/Epoxy (RT ; $V_f = 0.5$)

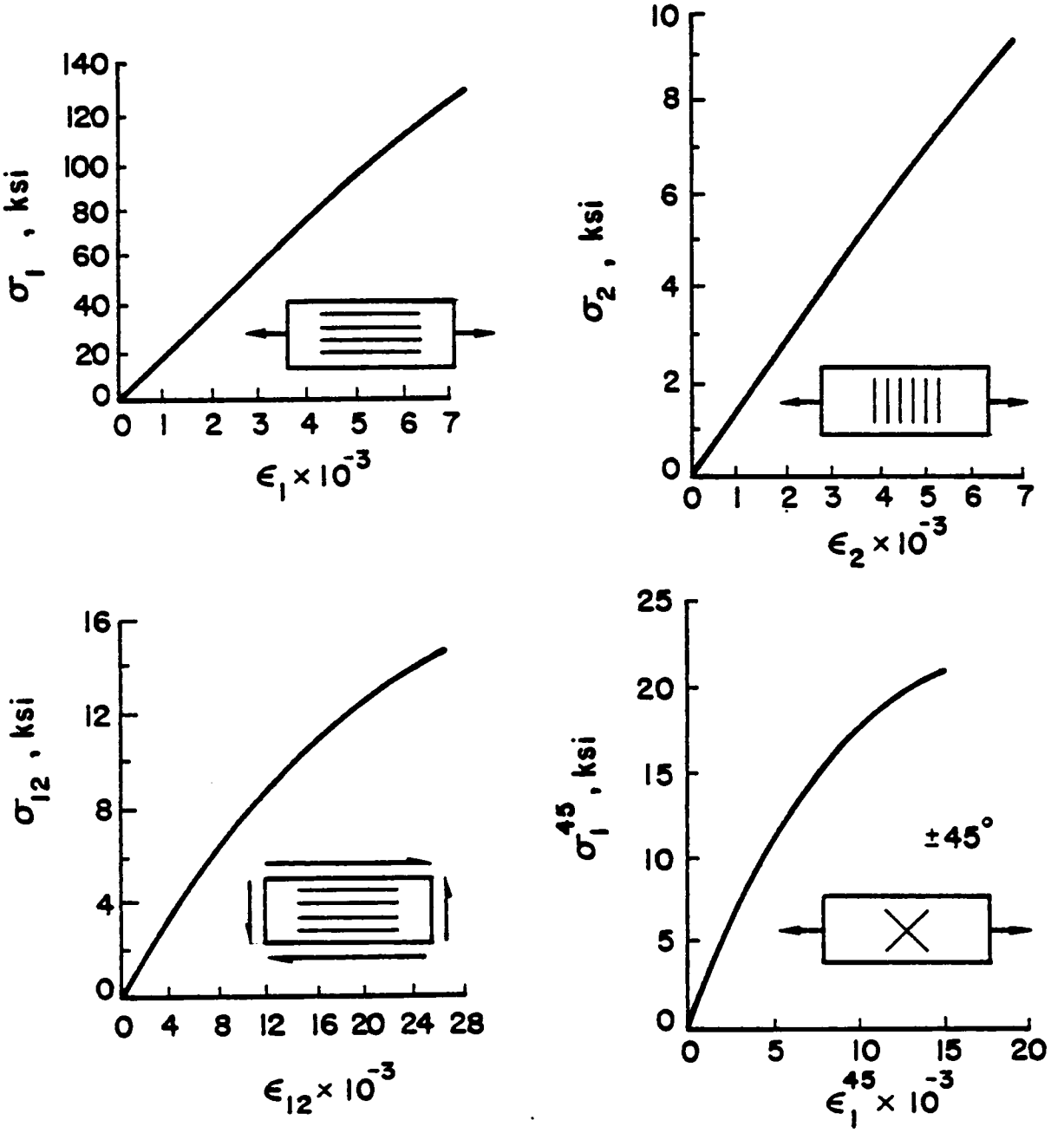

Fig. 5·5 Stress-Strain Curves for Graphite/Epoxy (RT ; $V_f = 0.5$)

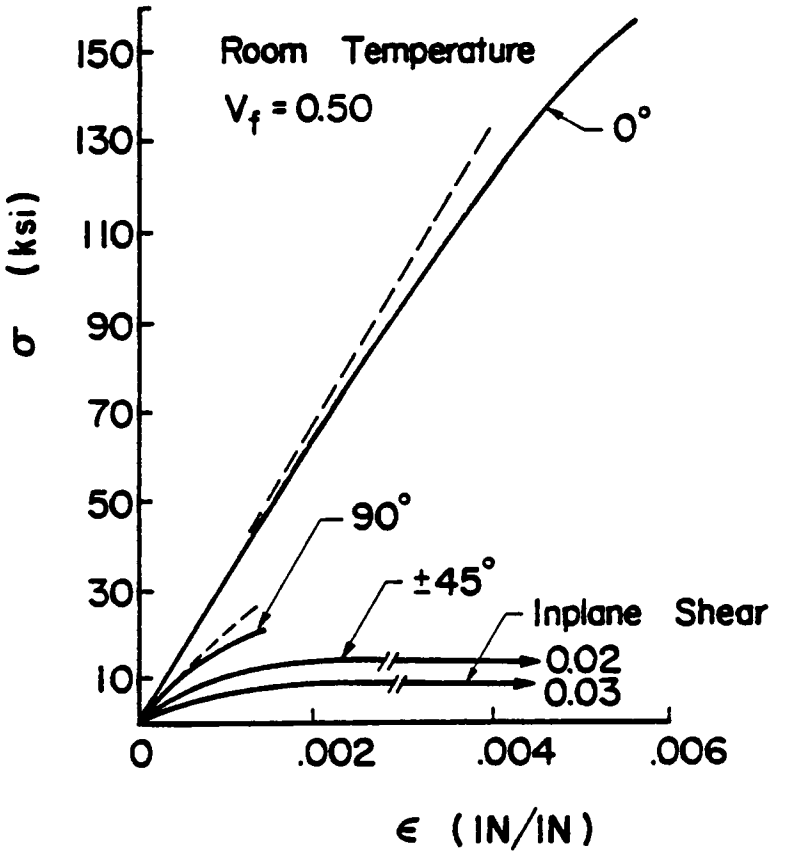

Fig. 5-6 Stress-Strain Curves for Boron/Aluminum

TABLE 5.1

Typical Material Properties for Resin-Matrix and Metal-Matrix Composites

Property	Boron/Epoxy	Graphite/Epxoy	Boron/Aluminum
E_1(psi)	30.0×10^6	21.0×10^6	34.0×10^6
E_2(psi)	2.7×10^6	1.7×10^6	20.0×10^6
G_{12}(psi)	0.7×10^6	0.65×10^6	9.5×10^6
ν_{12}	0.21	0.22	0.25

CHAPTER 6

NUMERICAL RESULTS

To evaluate the efficiency and validity of the present nonlinear material model and the finite-element formulation, a variety of bending problems were considered. Most of the problems were analyzed using a 2 x 2 uniform mesh of nine-node quadratic elements. The shear correction factors $K_1^2 = K_2^2$ were taken to be 5/6. All computations were carried out using an IBM 3081 processor with double precision arithmetic.

Although a number of problems were analyzed, the results of only few sample problems are presented here. The intensity of the distributed load is denoted by p_o. The results of linear, geometrically nonlinear, materially nonlinear and cobined nonlinear problems are discussed. To illustrate the validity and accuracy of the present formulation and the finite element model, example problems that have known, often numerical, solutions are presented.

6.1 Static Bending Analysis

6.1.1 Linear Analysis

Pinched cylindrical shell. An isotropic cylindrical shell shown in Fig. 6.1 was analyzed to test the performance of the shell element for linear analysis. The boundary conditions and material properties are shown in the figure. Due to the biaxial symmetry only a quadrant of the shell is modeled. The linear radial displacement obtained is found to be $w_A = 0.039$ in., which agrees favorably with 0.0405 of Yang [65], who used finite element based on the classical (i.e. Love's) shell theory.

Spherical shell under point load. The next example deals with the bending of an isotropic doubly curved shell. The geometry and loading of the shell are shown in Fig. 6.2. The static deflection under the concentrated load is found to be 0.037258 in. as compared with 0.038661 in. of Rao [66]. The latter solution is based on the classical shell theory.

6.1.2 Geometric Nonlinearity

A convergence study of the direct and Newton-Raphson iterative procedures is carried out to determine the relative accuracy and computational effort. Table 6.1 contains the center deflections obtained using both techniques for a simply-supported, two-layer cross-ply (0/90°) spherical shell under uniform load. The shell dimensions are: R = 1000 in., a = b = 50 in., h = 1 in. Here 2a and 2b are the dimensions of the shell. The material parameters used are

$$E_1 = 25 \times 10^6 \text{ psi}, \; E_2 = 10^6 \text{ psi}, \; G_{12} = G_{13} = 0.5 \times 10^6 \text{ psi}$$

$$G_{23} = 0.2 \times 10^6 \text{ psi}, \; \nu_{12} = 0.25$$

It is clear from the table 6.1 that the solution took fewer iterations to converge in the case of the Newton-Raphson method as compared with the direct iteration technique.

Simply supported beam under uniform load. Consider the simply supported plate strip shown in Fig. 6.3. The problem is mathematically one-dimensional and an analytical solution of the problem, based on the classical theory, can be found in Timoshenko and Woinowsky-Krieger [67]. The plate length along the y-coordinate is assumed to belarge compared to the width, and it is simply supported on edges parallel to

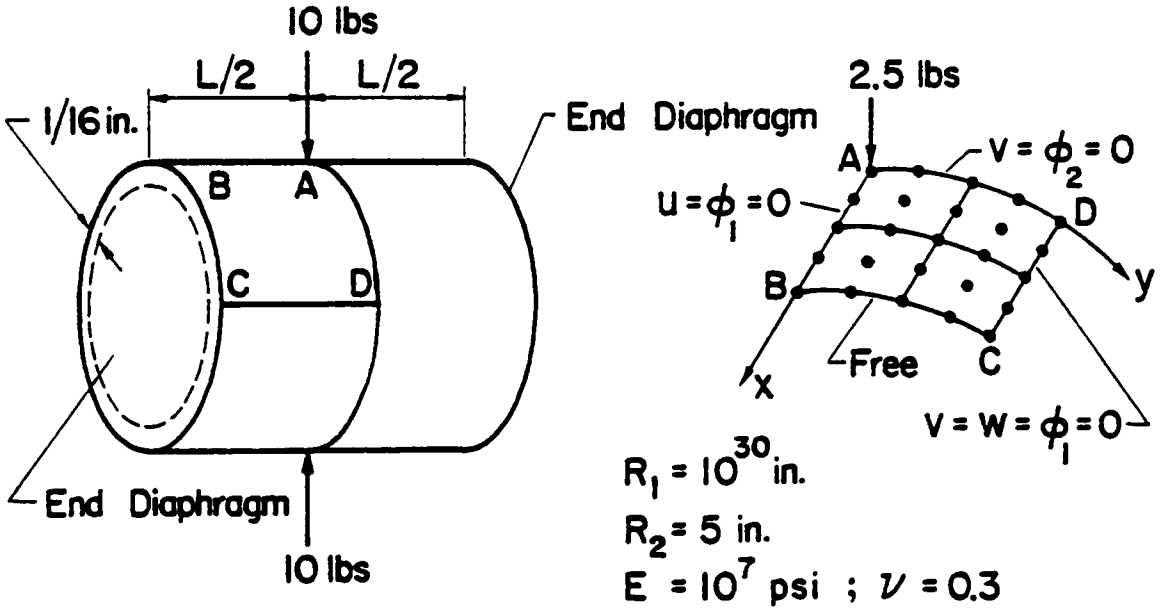

Fig. 6.1 Linear Analysis of a Pinched Cylinder

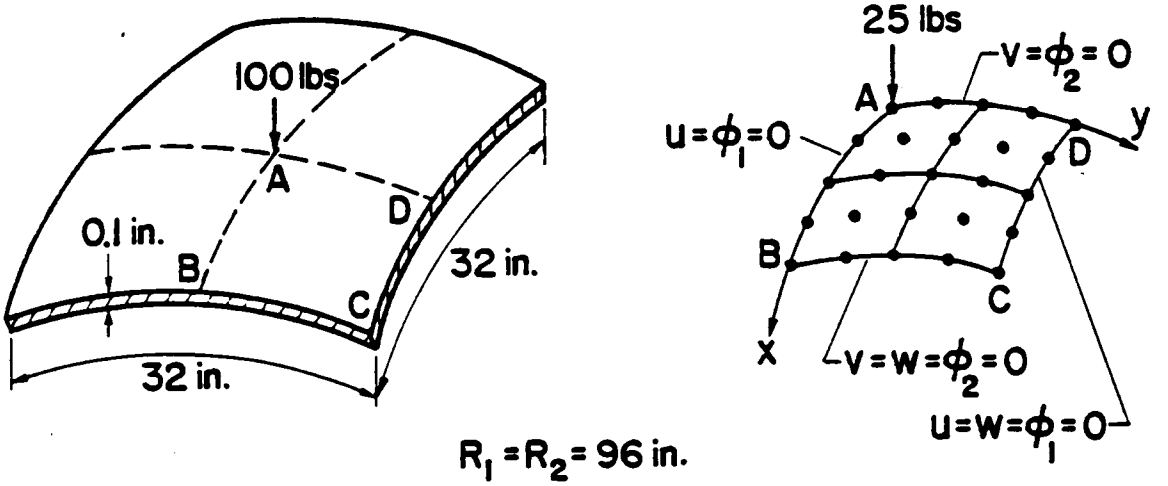

Fig. 6·2 Linear Analysis of a Spherical Shell under Point Load

TABLE 6.1

Convergence Study - A comparison of direct iteration and Newton-Raphson method for a simply-supported‡ two-layer cross-ply (0/90°) under uniform load.

Load p_o (psi)	Direct Iteration		New-Raphson	
	No. of Iterations	W_c(in.)	No. of Iterations	W_c(in.)
0.50	4	0.04257	3	0.04260
0.75	4	0.06617	3	0.066224
1.00	4	0.09171	3	0.09284
1.25	4	0.11966	2	0.11994
1.50	4	0.15063	2	0.15121
1.75	4	0.18556	3	0.18673
2.00	4	0.22584	3	0.22822
2.25	5	0.27593	3	0.27887
2.50	5	0.33795	3	0.34576
2.75	7	0.43487	3	0.45296

‡$v = w = \phi_1 = 0$ at $y = b$

$u = w = \phi_2 = 0$ at $x = a$

$v = \phi_2 = 0$ along $y = 0$

$u = \phi_1 = 0$ along $x = 0$

the y-axis. The following siply supported boundary conditions are used:

$$w = \phi_2 = 0 \text{ along edges } x = \pm 127 \text{ mm}$$

All inplane displacement degrees of freedom are restrained. A 5 x 1 mesh of four-node rectangular elements in the half plate is used to analyze the problem. Figure 6.3 contains a plot of the center deflection versus the load. The present solution is in close agreement with the analytical solution.

Clamped square plate under uniform load. Due to the biaxial symmetry, only one quadrant of the plate is modeled with the 2 x 2 mesh of nine-node elements (4 x 4 mesh of linear elements give almost the same result). Pertinent data and results are presented in Fig. 6.4 for side to thickness ratios a/h = 10 and 500. The result for a/h = 500 is in agreement with the results of Way [68]. The difference is attributed to the fact that the present model includes the inplane displacement degrees of freedom and transverse shear deformation.

Clamped cylindrical shell under uniform load. Figure 6.5 contains the pertinent data and the load-deflection curve for a clamped cylindrical shell (isotropic) subjected to uniform load. The results are compared with those obtained by Dhatt [69]. The agreement is very good.

Clamped orthotropic and laminated square plate under uniform load. Figure 6.6 contains the transverse deflection versus load for clamped orthotropic, cross-ply and angle-ply plates. The geometry and lamina properties are also shown in the figure. From the results one can observe that for the same total thickness the clamped orthotropic

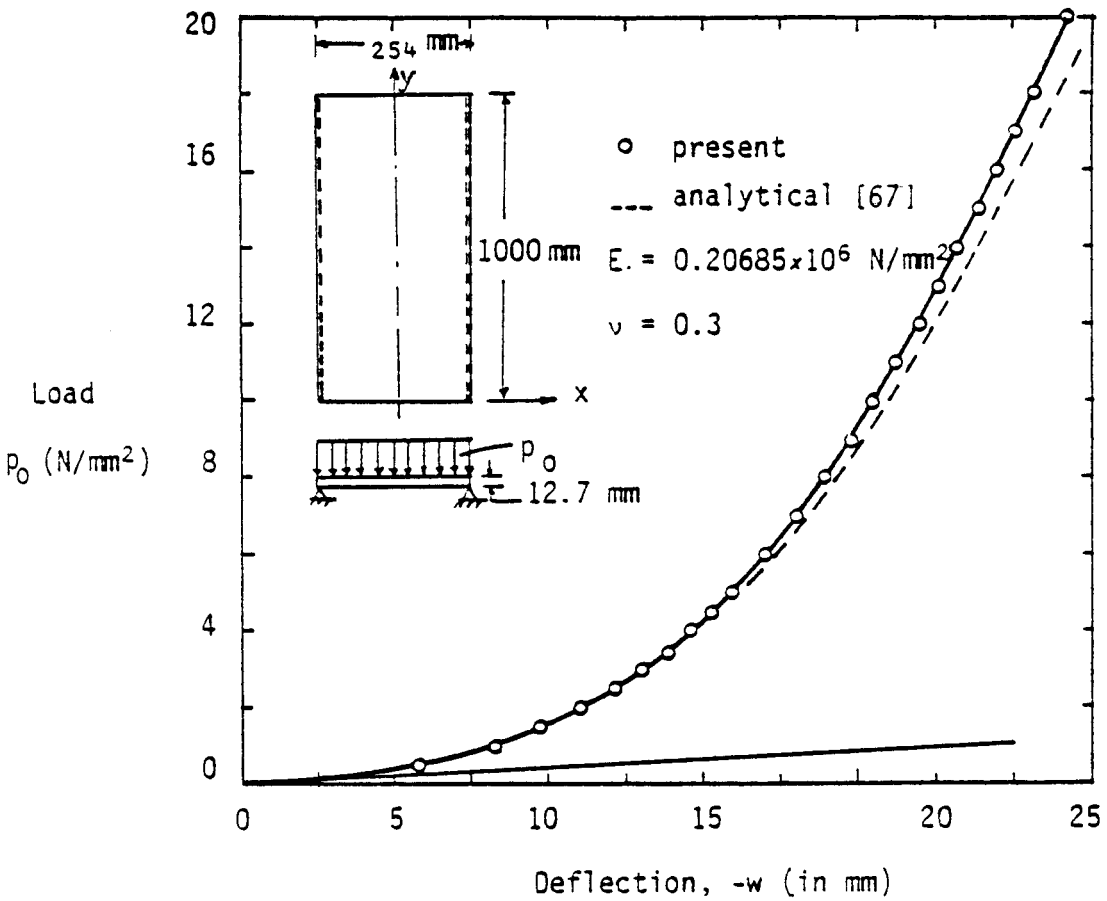

Figure 6.3. Bending of an isotropic simply supported plate strip under uniform load.

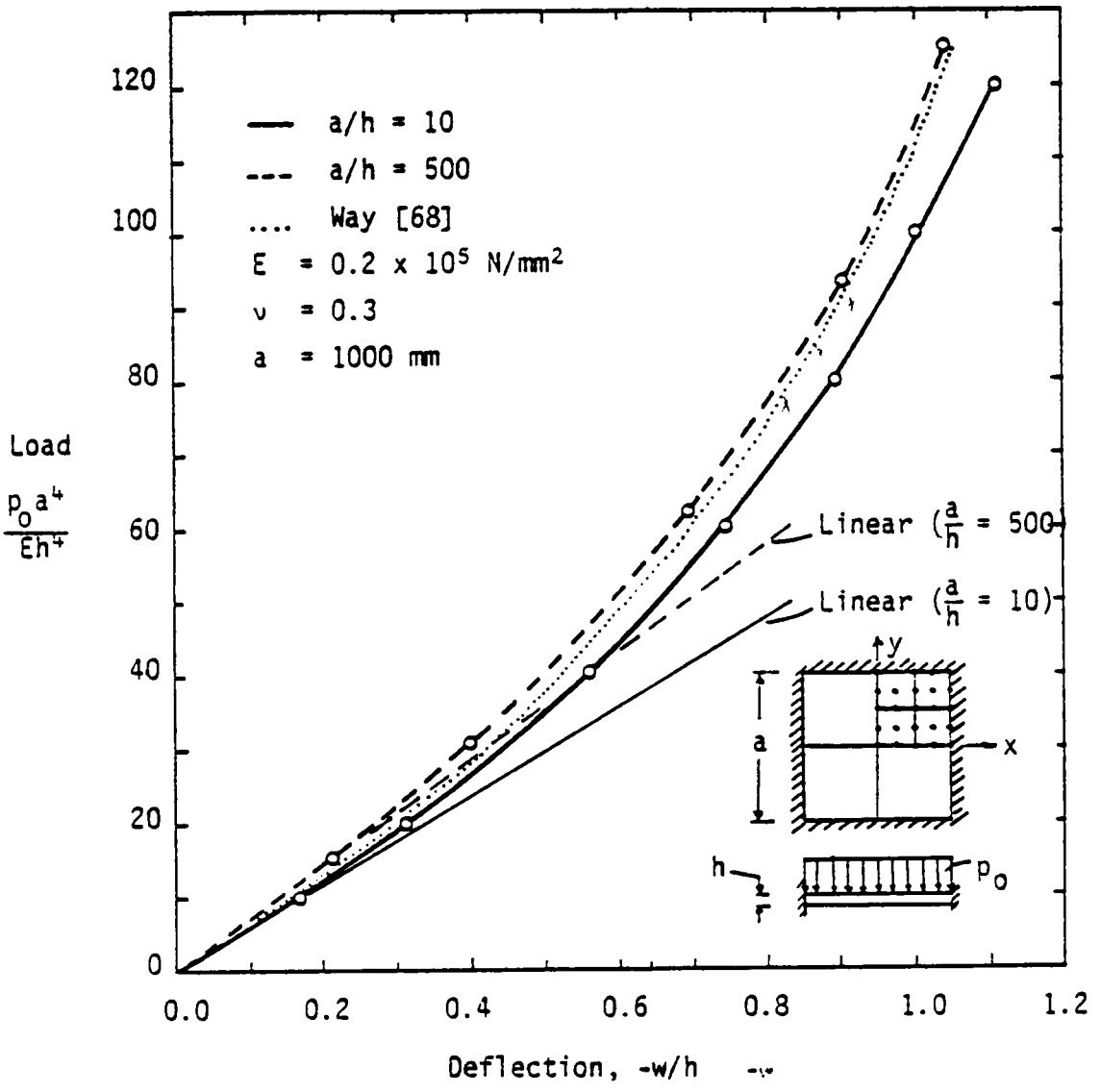

Figure 6.4. Bending of clamped isotropic square plate under uniform load.

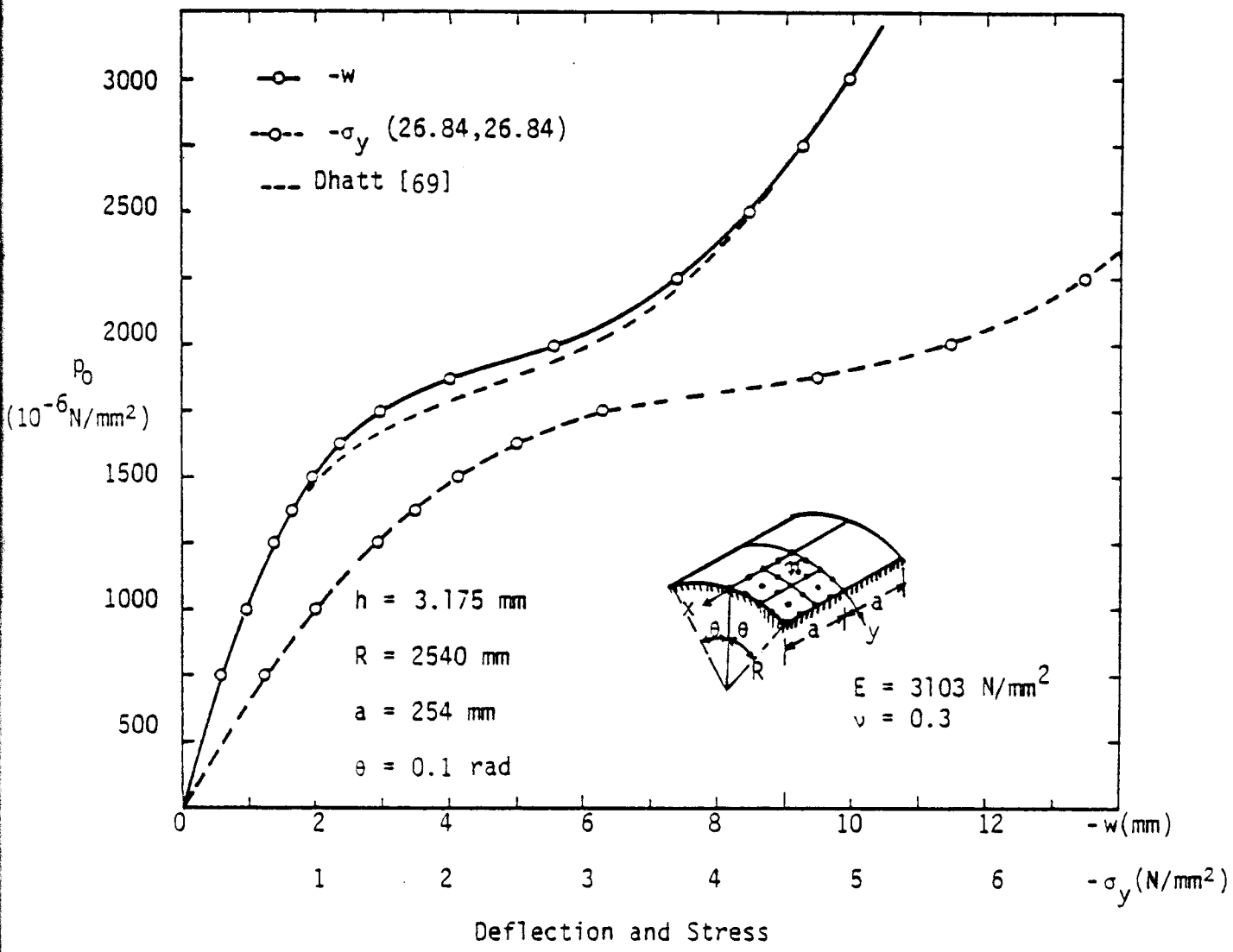

Figure 6.5. Bending of a clamped, isotropic, cylindrical shell under uniform load.

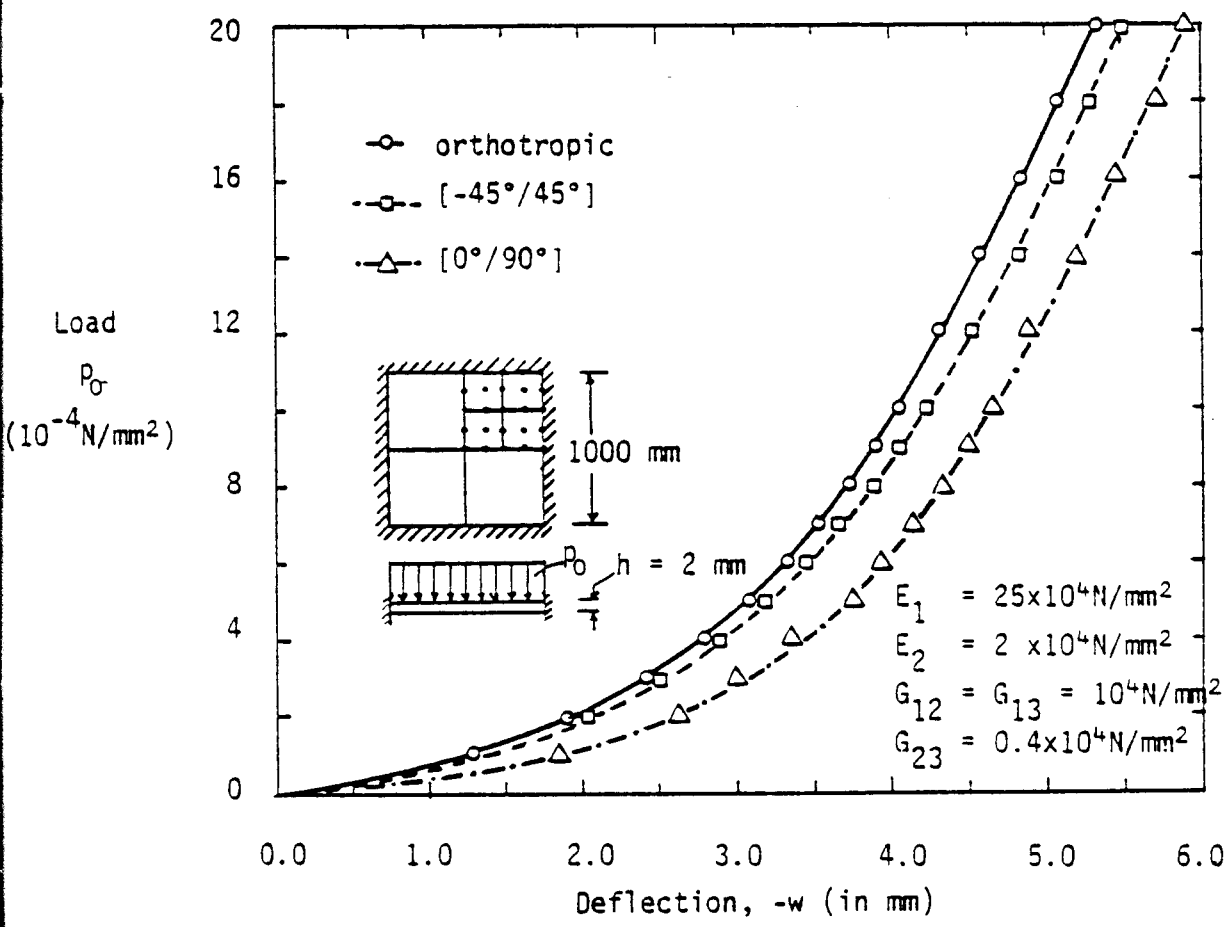

Figure 6.6. Bending of clamped orthotropic and laminated square plates under uniform load.

square plate is stiffer than both wo-layer angle-ply and cross-ply plates.

Effect of inplane boundary conditions on deflections. It should be noted that, unlike the case of isotropic plates and shells, the type of boundary conditions on the inplane displacements for laminated composite shells have a significant effect on the deflections. To investigate this effect, four types of simply supported condisions on the center deflection are investigated:

SS-1: $u = w = \phi_1 = 0$ at $y = b$; $v = w = \phi_2 = 0$ at $x = a$

SS-2: $u = v = w = \phi_1 = 0$ at $y = b$; $u = v = w = \phi_2 = 0$ at $x = a$

SS-3: $v = w = \phi_1 = 0$ at $y = b$; $u = w = \phi_2 = 0$ at $x = a$

SS-4: $w = \phi_2 = 0$ at $y = b$; $w = \phi_1 = 0$ at $x = a$

and

$$\left.\begin{aligned} v = \phi_2 = 0 \text{ along } y = 0 \\ u = \phi_1 = 0 \text{ along } x = 0 \end{aligned}\right\} \quad \text{(symmetry lines)}$$

The geometry of the shell is shown in Fig. 6.7. The shell dimensions and material parameters used are

$$R = 1000 \text{ in.}, \; a = b = 50 \text{ in.}, \; h = 1 \text{ in.}$$

$$E_1 = 25 \times 10^6 \text{ psi}, \; E_2 = 10^6 \text{ psi}, \; G_{12} = G_{13} = 0.5 \times 10^6 \text{ psi}$$

$$G_{23} = 0.2 \times 10^6 \text{ psi}, \; \nu_{12} = 0.25$$

Table 6.2 contains the results for the four boundary conditions. It is clear from the results that the transverse deflection is sensitive to the boundary conditions on the inplane displacements of simply supported shells. SS-2 and SS-3 give almost the same deflections. Boundary conditons SS-1 and SS-4 give deflections an order of magnitude higher

TABLE 6.2

Effect of various simply-supported boundary conditions on the transverse deflections of cross-ply [0°/90°] spherical shells under uniform load

q_o (psi)	- w (in.)			
	SS-1	SS-2	SS-3	SS-4
0.50	0.3344	0.04246	0.04257	0.4692
0.75	0.5757	0.06599	0.06617	0.8255
1.00	0.9485	0.09144	0.09171	1.3845
1.25	1.6529	0.11926	0.11966	1.9589
1.50	2.2826	0.15008	0.15063	2.3597
1.75	2.6421	0.18478	0.18556	2.5951
2.00	2.8499	0.22473	0.22584	2.8074
2.25	3.0764	0.27425	0.27593	3.0284
2.50	3.2432	0.33534	0.33795	3.1948
2.75	3.4214	0.42970	0.43487	3.3719

than those given by SS-2 and SS-3. Thus, boundary conditions SS-2 and SS-3 make the shell quite stiffer.

Two layer cross-ply [0/90°] and angle-ply [-45°/45°], simply-supported (SS-3) spherical shells. Figure 6.8 contains the prtinent data and the load-deflection curves (with different scales) for the cross-ply and angle ply cases. The material parameters used are

$$E_1 = 40 \times 10^6 \text{ psi}, \; E_2 = 10^6 \text{ psi}, \; G_{12} = G_{13} = 0.6 \times 10^6 \text{ psi}$$

$$G_{23} = 0.5 \times 10^6 \text{ psi}, \; \nu_{12} = 0.25$$

It is interesting to note that the type of nonlinearity exhibited by the tuso shells is quite different; the cross-ply shell gets softer whereas the angle-ply shell gets stiffer withan increase in the applied load. While both shells have bending-stretching coupling due to the lamination scheme ($B_{22} = -B_{11}$ nonzero for the cross-ply shell and B_{16} and B_{26} are non-zero for the angle-ply shell), the angle-ply experiences shear coupling that stiffens the spherical shell relatively more than the normal coupling (note that, in general, shells get stiffer under externally applied pressure loads).

6.1.3 Material Nonlinearity

Simply-supported square plate under uniform load. The geometry of the plate is shown in Fig. 6.9. Due to symmetry only a quadrant of the plate is modeled. For the elastic-perfectly plastic material considered, the following properties were used:

$$E_1 = E_2 = 10 \times 10^6 \text{ psi}, \; \nu = 0.3$$

$$G_{12} = 3.486 \times 10^6 \text{ psi}, \; G_{23} = G_{13} = G_{12}$$

$$\sigma_{01} = \sigma_{02} = \sigma_{045} = 144{,}000 \text{ psi}$$

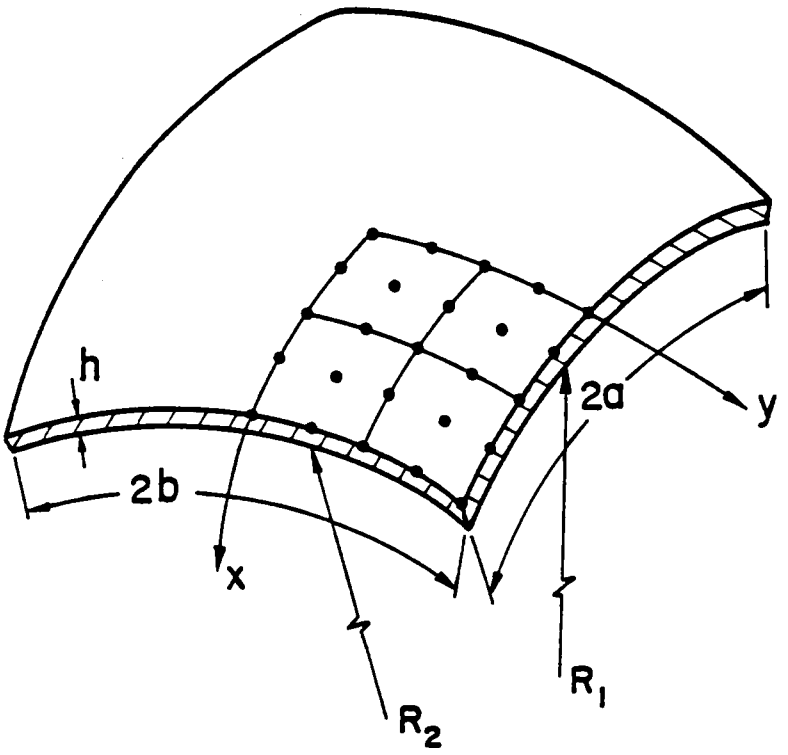

Fig.6·7 Geometry of a Doubly Curved Shell

$$\sigma_{012} = \sigma_{023} = \sigma_{013} = 83{,}138.4 \text{ psi}$$

A non-dimensionalized plot of the center deflection versus load is shown in Fig. 6.9. The results are compared with those presented by Armen et al. [34]. The agreement between the two solutions, is good for most of the load range considered, with the greatest discrepancy occurring as the magnitude of the load approaches the collapse value. The difference can be attributed to the difference in the element type used in the two investigations. In the present study a shear deformable element is used whereas Armen used a classical plate element.

Figure 6.10 contains pictures showing the development of the plastic zone for the same problem. Yielding starts at the corners of the plate due to the twisting moments. Next the center of the plate yields. Beyond this value of the load, the plastic regions propagate from the vicinity of the corners and the center of the plate until a collapse mechanism forms. Figure 6.10d represents the plastic zone just before the collapse load. The approximate representation of the plastic zone is obtained by simply connecting the yielded Gauss points by straight lines. The plastic zone obtained is in good agreement with the results reported in [34].

Clamped circular plate of strain hardening material. A clamped isotropic circular plate subjected to uniform load was analyzed. Due to the biaxial symmetry only a quadrant of the plate was modeled. Figure 6.11 contains the finite element mesh and the uniaxial stress-strain diagram for the plate material. The nondimensionalized center deflection obtained was compared with that of Popov [32]. Once again the present results exhibit the more flexible character of the finite

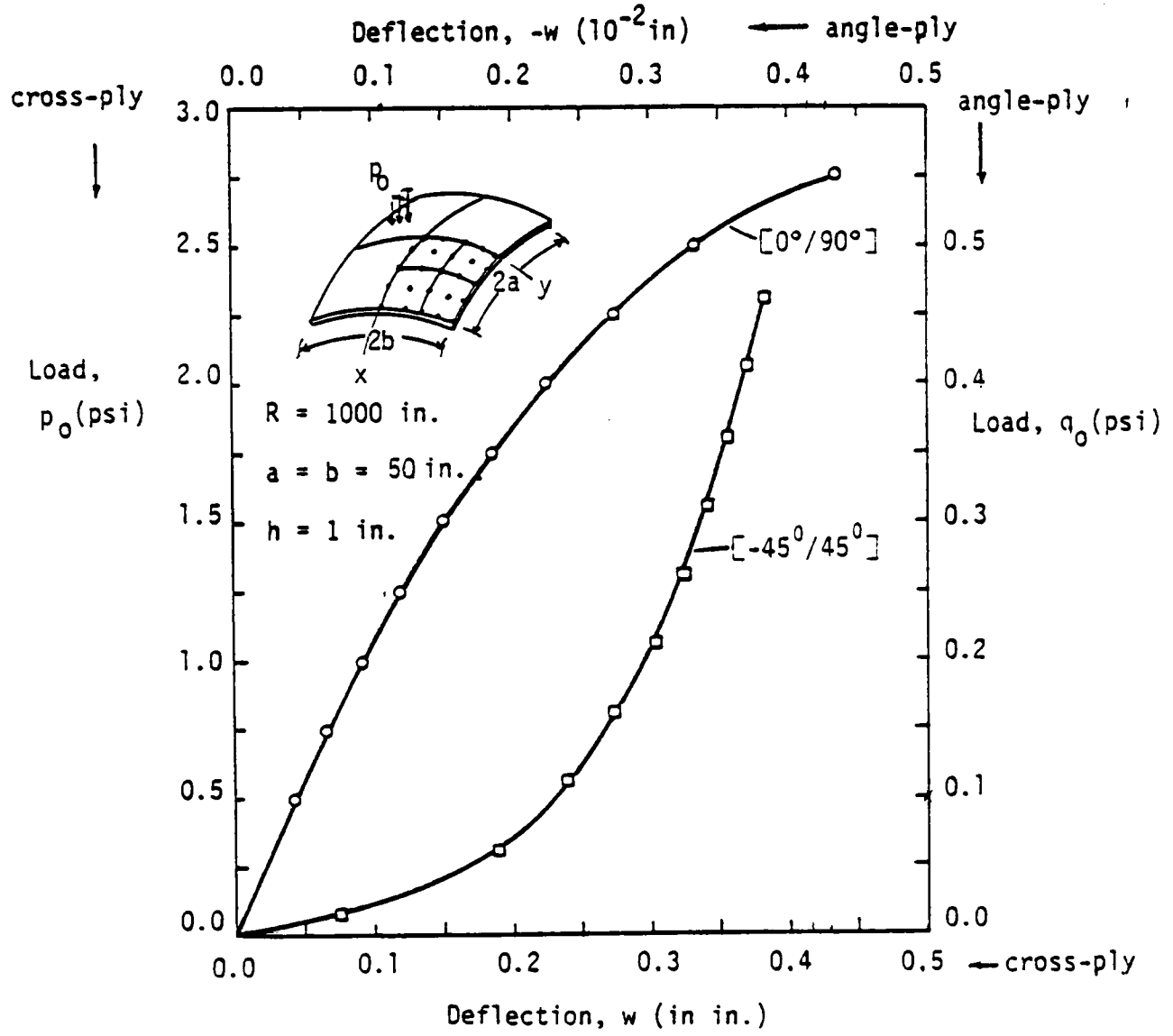

Figure 6.8. Bending of two-layer cross-ply and angle-ply, simply supported (SS-3) spherical shells under uniform load.

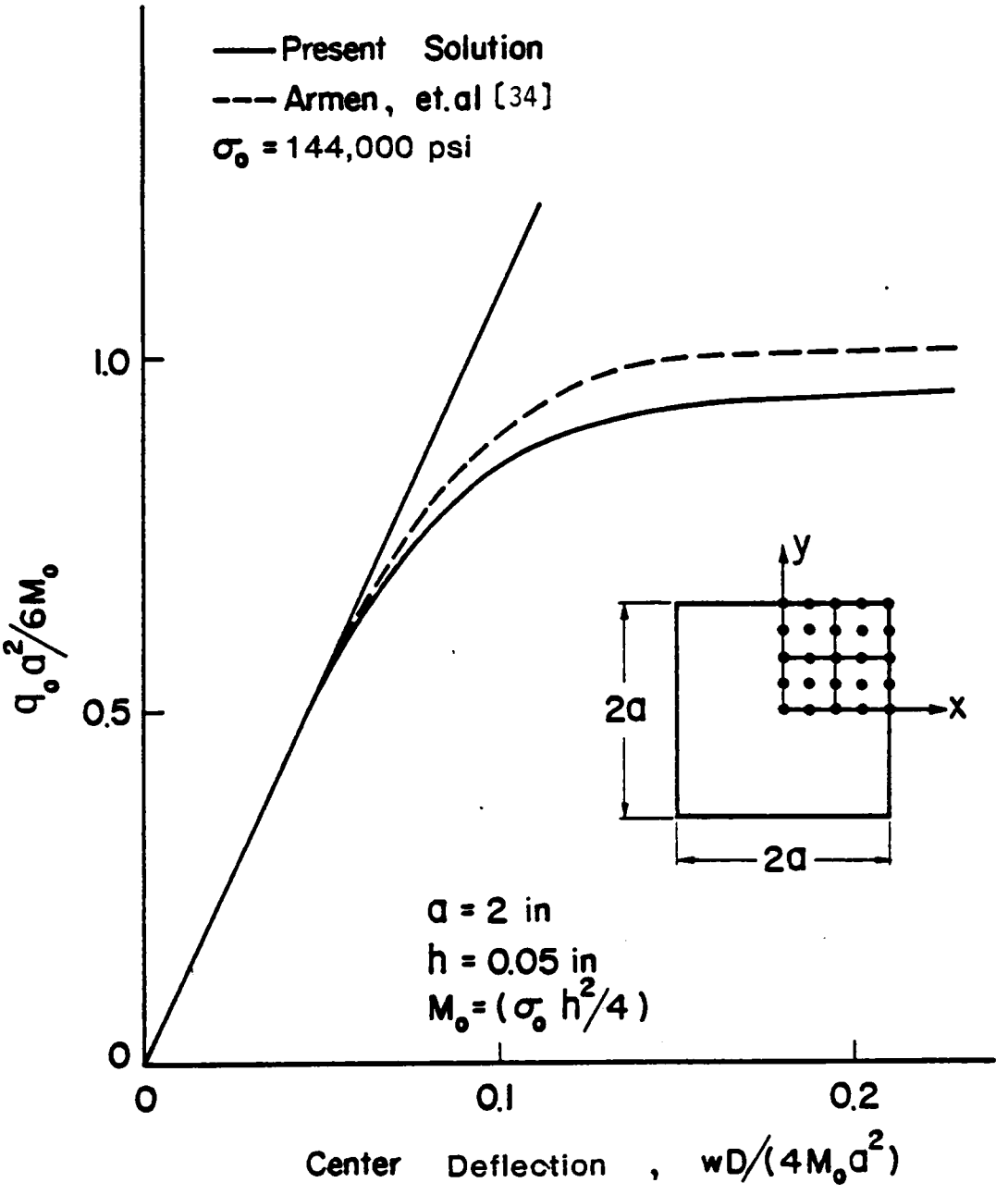

Fig.6·9 Response of Elastic-perfectly Plastic Simply-Supported Plate under Uniform Load

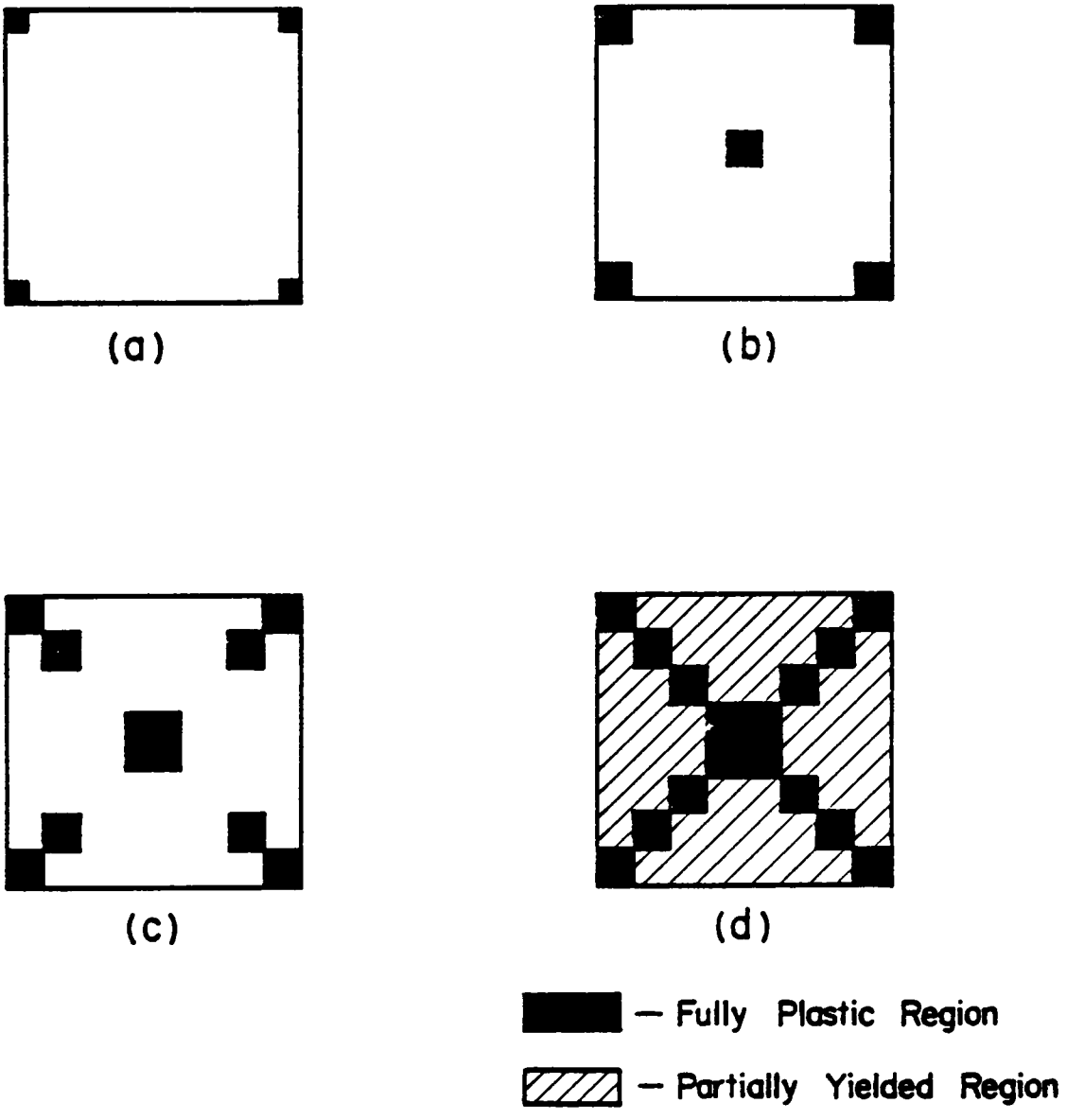

Fig.6-10 Development of Plastic Region for a Simply-supported Plate under Uniform Load

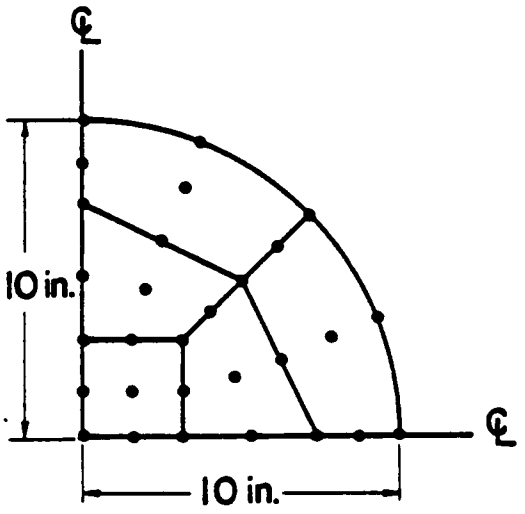

(a) 9-Node Plate Model

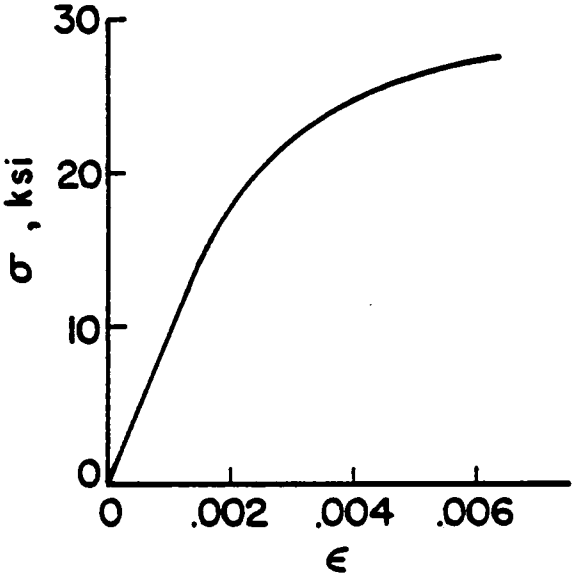

(b) Uniaxial Stress-strain Diagram of Plate Material

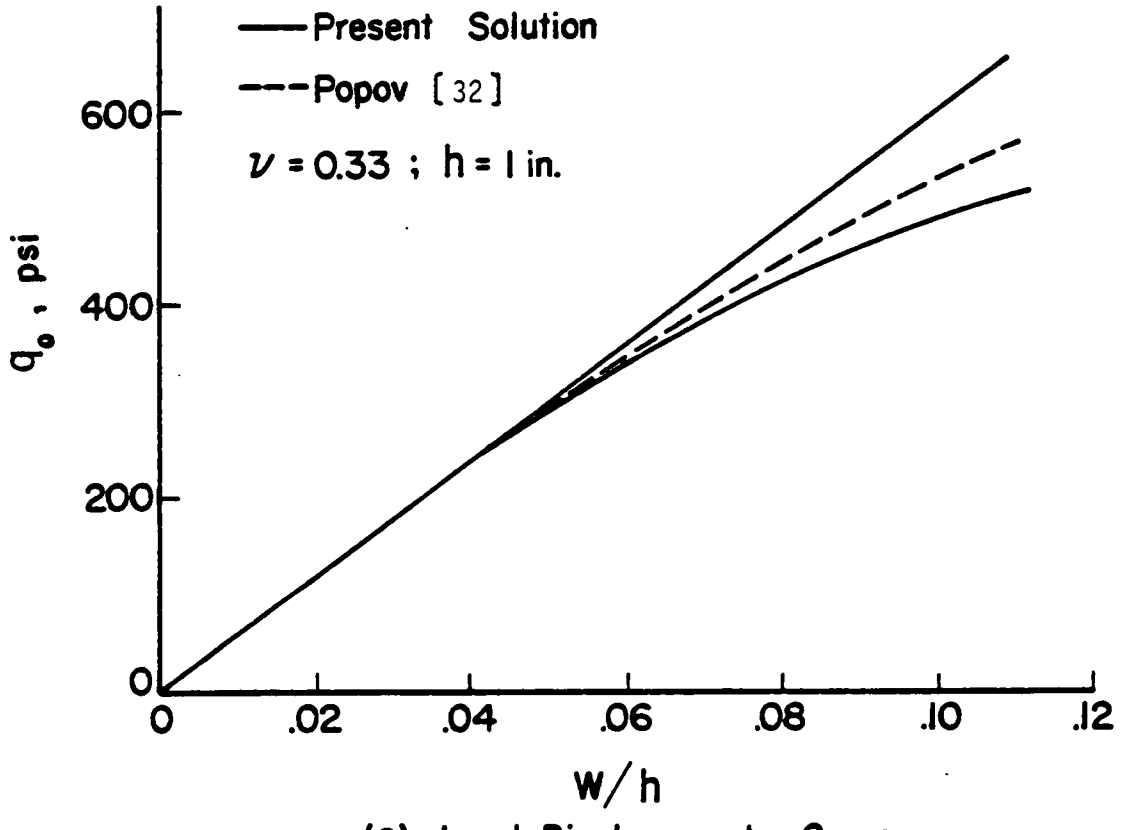

(c) Load-Displacement Curve

Fig.6-11 Analysis of Isotropic Circular Plate of Hardening Material

element model, which is due to the accommodation of the transverse shear strains in the model.

Two-layer cross-ply [0/90°] simply supported (SS-3) spherical shells under uniform load. The material parameters for the boron/epoxy and graphite/epoxy shells ued here were obtained from Fig. 5.4 and 5.5 repsectively. Figure 6.12 shows that for a given load, the shell made of graphite/epoxy deflects more than the shell made of boron/epoxy which is stiffer, but experiences a smaller degree of nonlinearity.

Two-layer cross-ply [0/90°] and angle-ply [-45°/45°] simply supported (SS-3) spherical shells under uniform load. Figure 6.13 contains the load-deflection curves for the graphite/epoxy cross-ply and angle-ply shells under uniform load. Clearly, the angle-ply shell shows greater displacement and nonlinearity than the cross-ply shell for the same load.

6.1.4 Combined Nonlinearity

Two-layer cross-ply [0/90] simply supported (SS-3) spherical shell under uniform load. The boron/epoxy cross-ply spherical shell which was previously studied for the effects of material nonlinearity only, was analyzed to include the effects of geometric nonlinearity. Figure 6.14 contains the load deflection curves, which exhibit the stiffening effect due to combined nonlinearity.

6.2 Dynamic Analysis

6.2.1 Geometric Nonlinearity

Cantilever beam under uniform load. A cantilever beam of length 10 (in.), width 1 (in.), height 1 (in.), modulus of elasticity 1.2×10^4

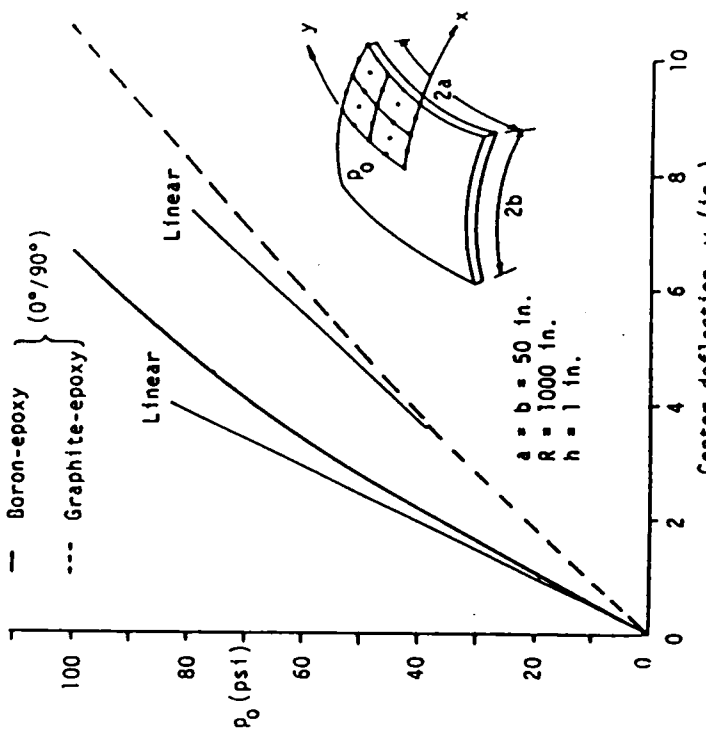

Figure 6.12 Load-deflection curves for a simply supported spherical shell under uniform transverse load.

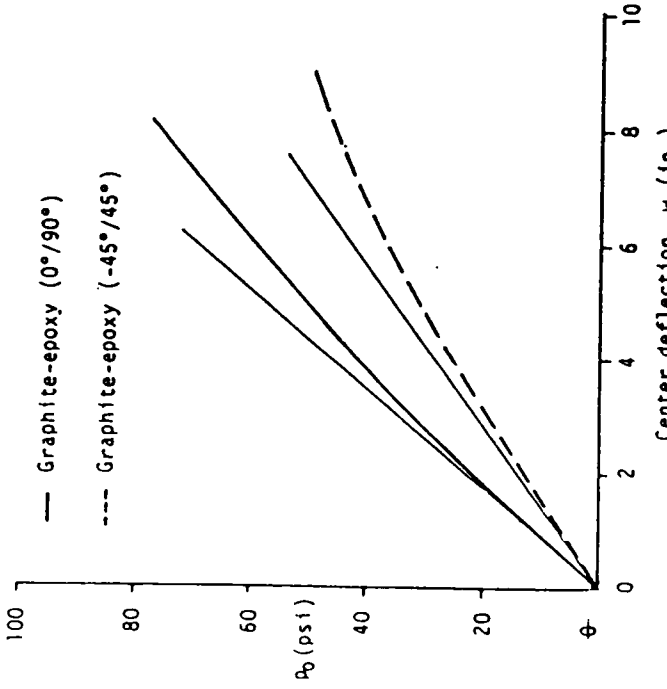

Figure 6.13 Load-deflection curves for a simply supported spherical shell (see Fig. 6.12 for the geometry).

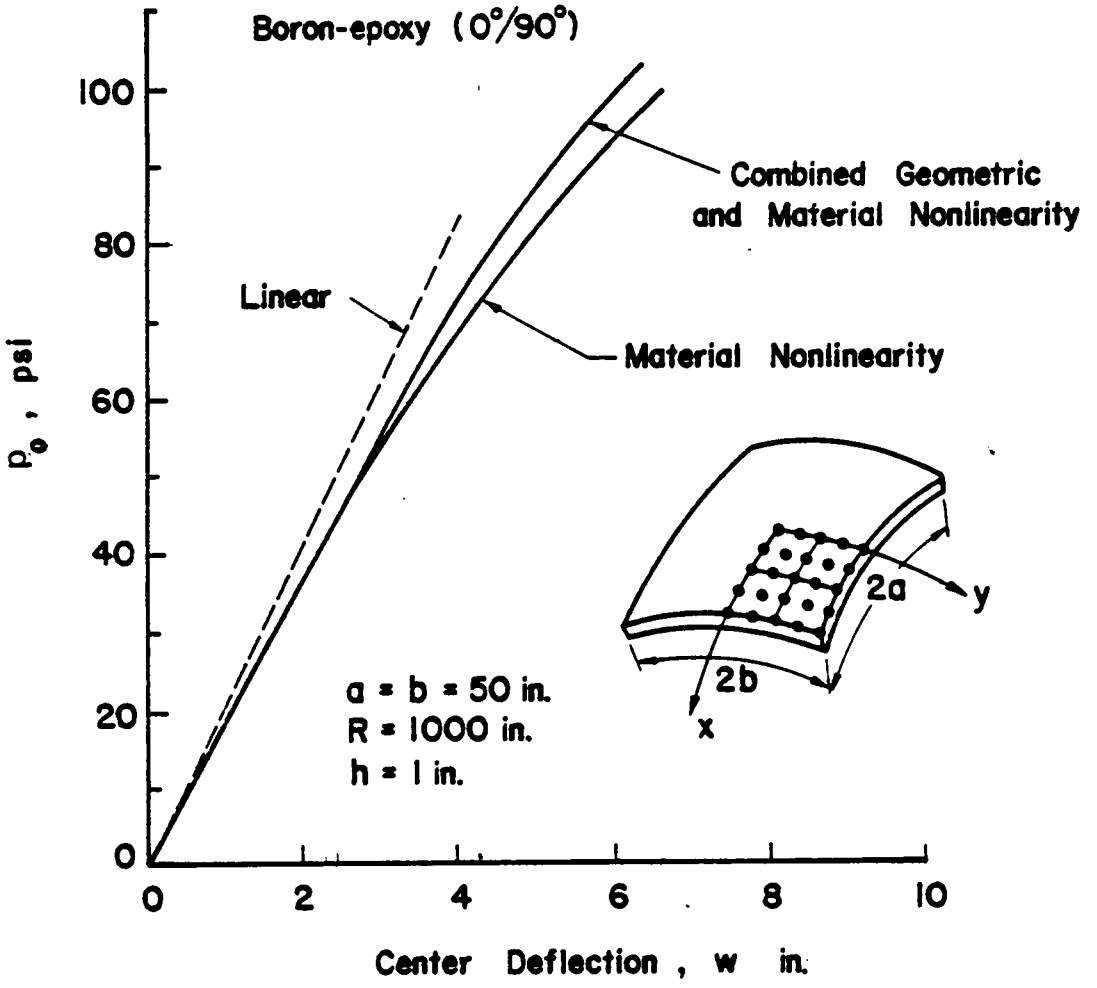

Fig.6·14 Load-deflection Curves for a Simply Supported Spherical Shell under Uniform Transverse Load

(psi), Poisson's ratio 0.2, and density 10^{-6} ($lb\text{-}s^2/in^4$.) is analyzed using a 2 x 2 mesh of nine-node quadratic elements in the half width of the beam. The load is assumed to be a step load (i.e., applied at time t = 0 and kept indefinitely). Figure 6.15 contains a plot of the transverse deflection of the tip versus time for time step $\Delta t = 1.35 \times 10^{-3}$ sec. The results are compared with tose of Bathe, et al. [56], who used a fully nonlinear model derived from three-dimensional elasticity theory. The difference in the result is partly due to the fact that the loading is treated as conservative in the present analysis, whereas it is treated as nonconservative by Bathe, et al. [56].

Clamped spherical cap under external pressure loading. The following geometric and material parameters are used:

$$R = 22.27 \text{ in.}, \; h = 0.41 \text{ in.}, \; \theta = 26.67^{\circ}$$

$$E = 10.5 \times 10^6 \text{ psi}, \; \nu = 0.3, \; \rho = 0.0002465 \text{ lb-s}^2/\text{in}^4$$

Five nine-node elements were used to model one quadrant of the shell. The results of the present study are compared in Fig. 6.16 with those obtained by Stricklin, et al. [70]. The results are in good agreement except in the regions of local maxima and minima.

Two layer cross-ply [0/90°] clamped cylindrical shell under internal pressure. The following geometric and material (for individual lamina) parameters are used:

$$wR = 20 \text{ in.}, \; h = 1 \text{ in.}$$

$$E_1 = 7.5 \times 10^6 \text{psi}, \; E_2 = 2.0 \times 10^6 \text{psi}, \; G_{12} = G_{13} = G_{23} = 1.25 \times 10^6 \text{psi}$$

$$\nu = 0.25, \; \rho = 1 \text{ lb-s}^2/\text{in}^4$$

One quadrant of the shell was modelled using a 2 x 2 mesh of nine-node

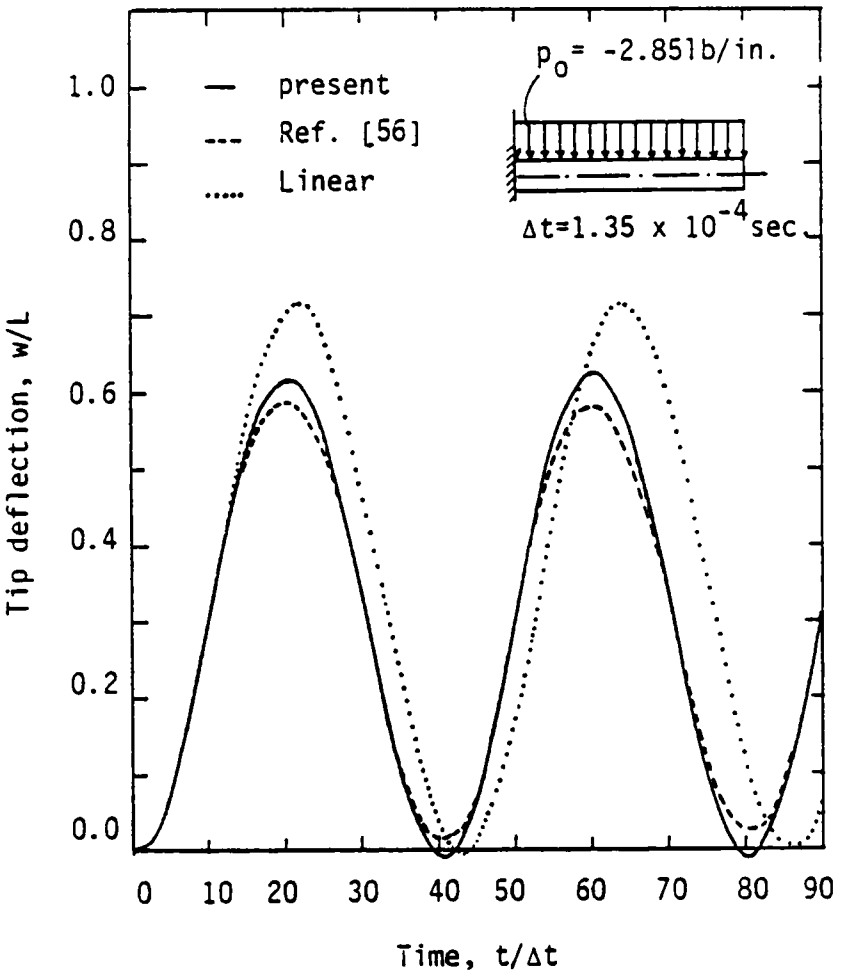

Figure 6.15. Transient response of an isotropic cantilever problem under uniform load.

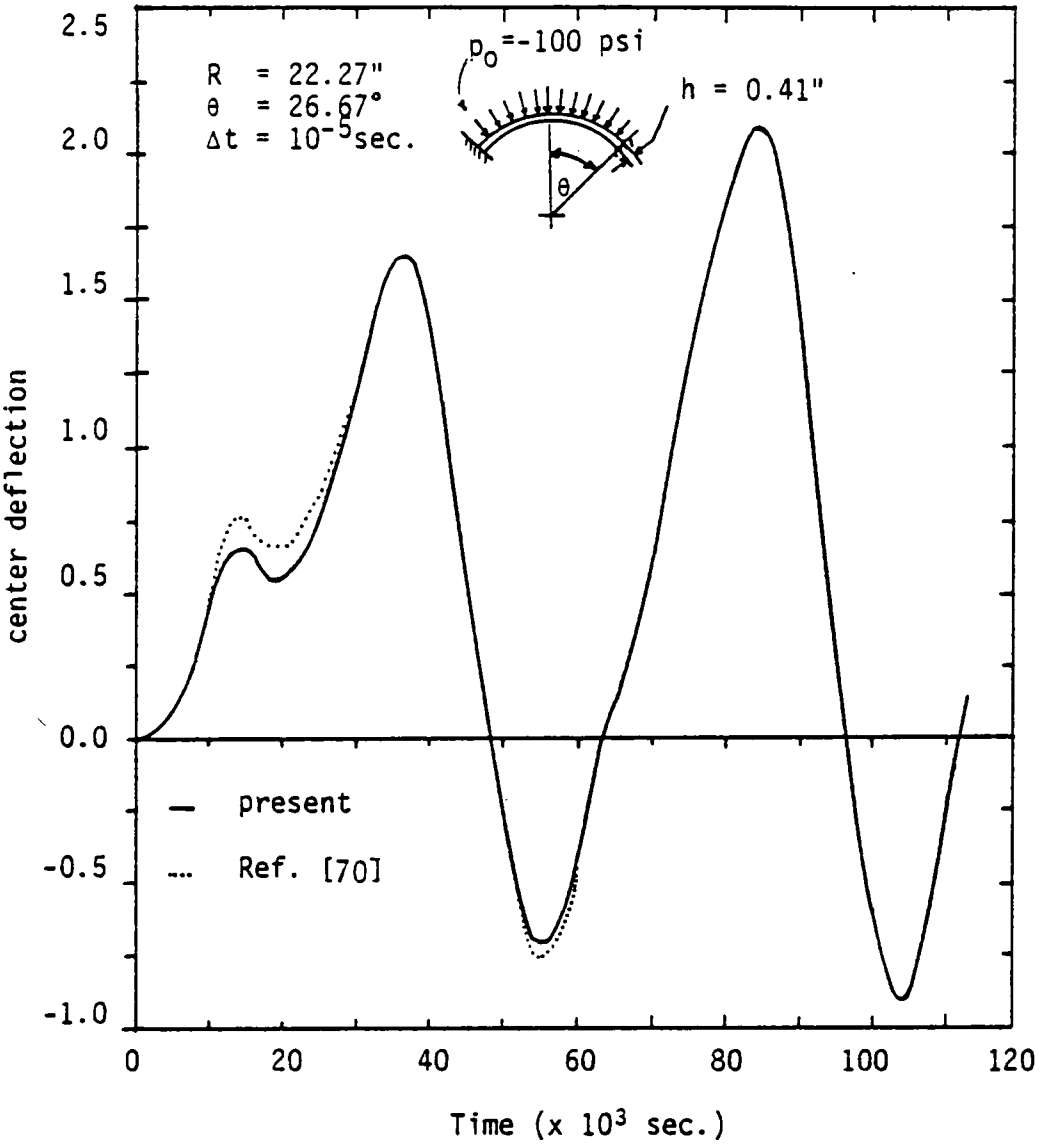

Figure 6.16. Center deflection versus time for a clamped spherical cap under external pressure loading.

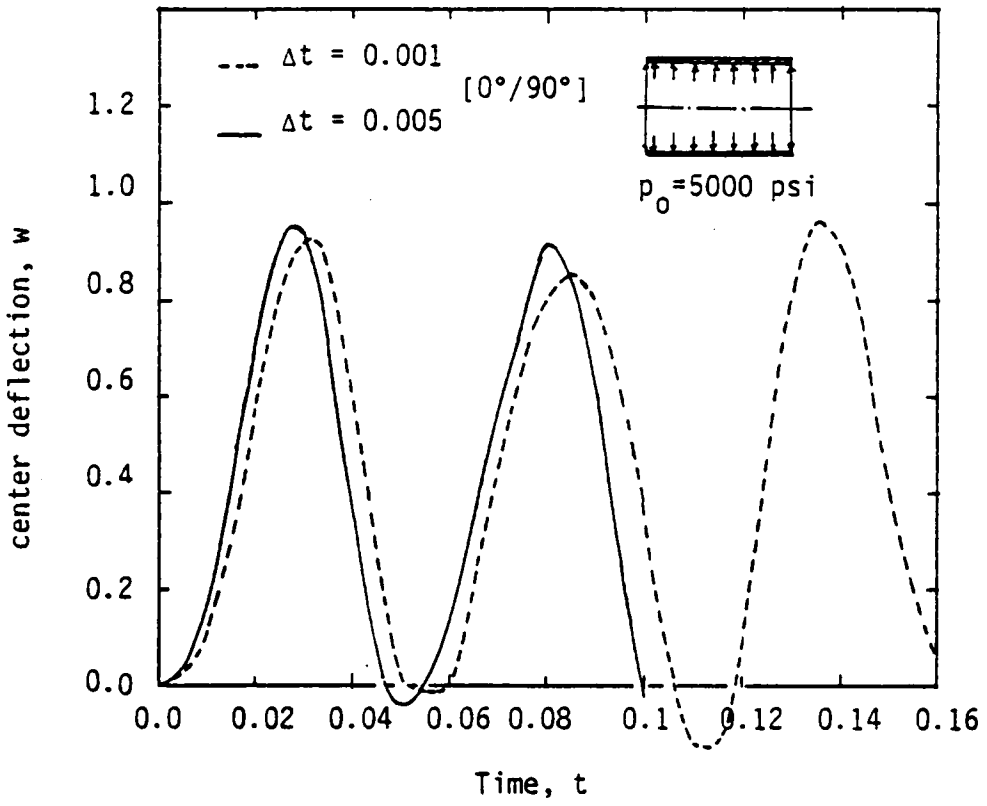

Figure 6.17. Transient response of two-layer cross-ply [0°/90°] clamped cylindrical shell under internal pressure

elements. Figure 6.17 contain the plots of the center deflection versus time for cross ply shell.

Two layer cross-ply [0/90°] and angle-ply [-45°/45°] laminated, simply supported (SS-3), spherical panels under external pressure loads. The geometric and material properties are

$$R = 1000 \text{ cm}, \; a = b = 50 \text{ cm}, \; h = 1 \text{ cm}$$

$$E_1 = 25 \times 10^6 \text{ N/cm}^2, \; E_2 = 10^6 \text{ N/cm}^2, \; G_{12} = G_{13} = 0.5 \times 10^6 \text{ N/cm}^2$$

$$G_{23} = 0.2 \times 10^6 \text{ N/cm}^2, \; \nu = 0.25, \; \rho = 1 \text{ N-s}^2/\text{cm}^4$$

A 2 x 2 mesh of nine-node elements was used to model a quadrant of the panel. Figures 6.18 and 6.19 contain plots of center deflection versus time for the cross-ply and angle-ply laminates, respectively. For comparison purposes, the linear solution is also included.

6.2.2 Material Nonlinearity

Simply supported isotropic plate under uniform load. The elastic-perfectly plastic plate shown in Fig. 6.20 was analyzed for the lateral loading of 300 psi uniform pressure. The following material properties were used

$$E_1 = E_2 = 10 \times 10^6 \text{ psi}, \; \nu = 0.3$$

$$G_{12} = 3.846 \times 10^6 \text{ psi}, \; G_{12} = G_{23} = G_{13}$$

$$\sigma_{01} = \sigma_{02} = \sigma_{045} = 3.0 \times 10^4 \text{ psi}$$

$$\sigma_{012} = \sigma_{023} = \sigma_{013} = 1.372 \times 10^4 \text{ psi}$$

$$\rho = 0.000259 \text{ lb-s}^2/\text{in}^4$$

Due to symmetry, only a quadrant of the plate was analyzed using a 2 x 2 quadratic mesh. It is seen that the effect of material nonlinearity results in softening of the plate and therefore the

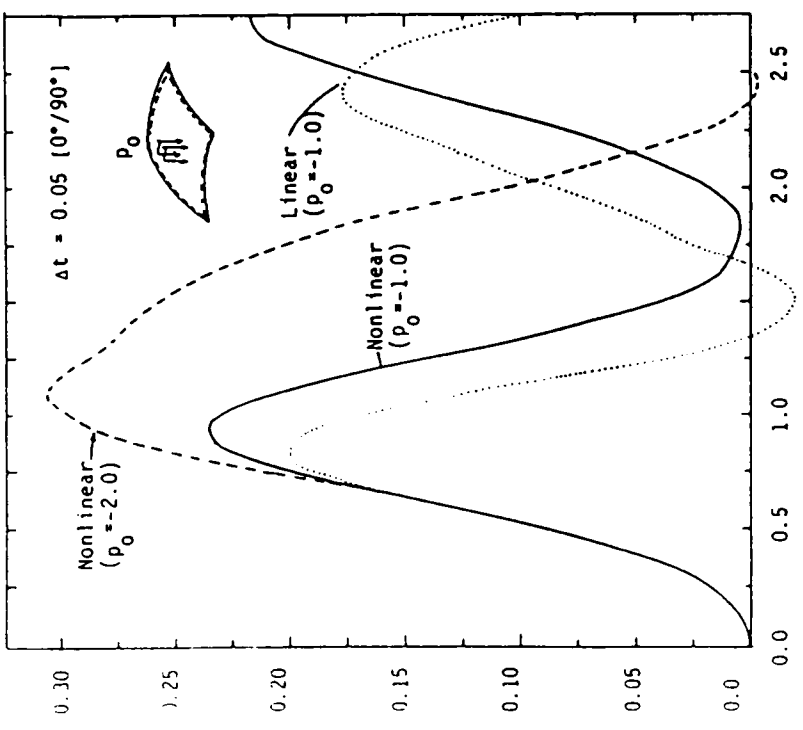

Figure 6.18 Center deflection versus time for a two-layer cross-ply [0°/90°] spherical shell under uniformly distributed load.

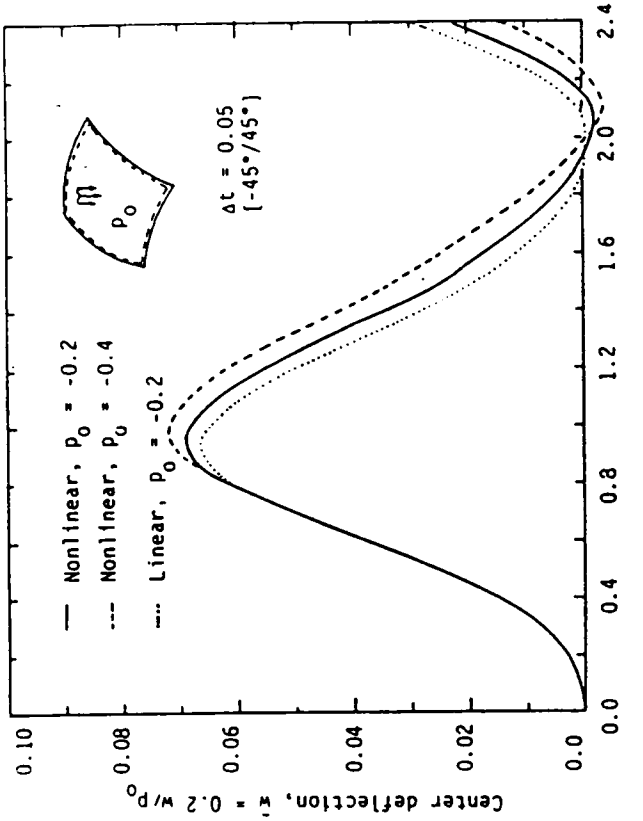

Figure 6.19 Center deflection versus time for a simply supported angle-ply [-45°/45°] spherical shell under uniformly distributed load.

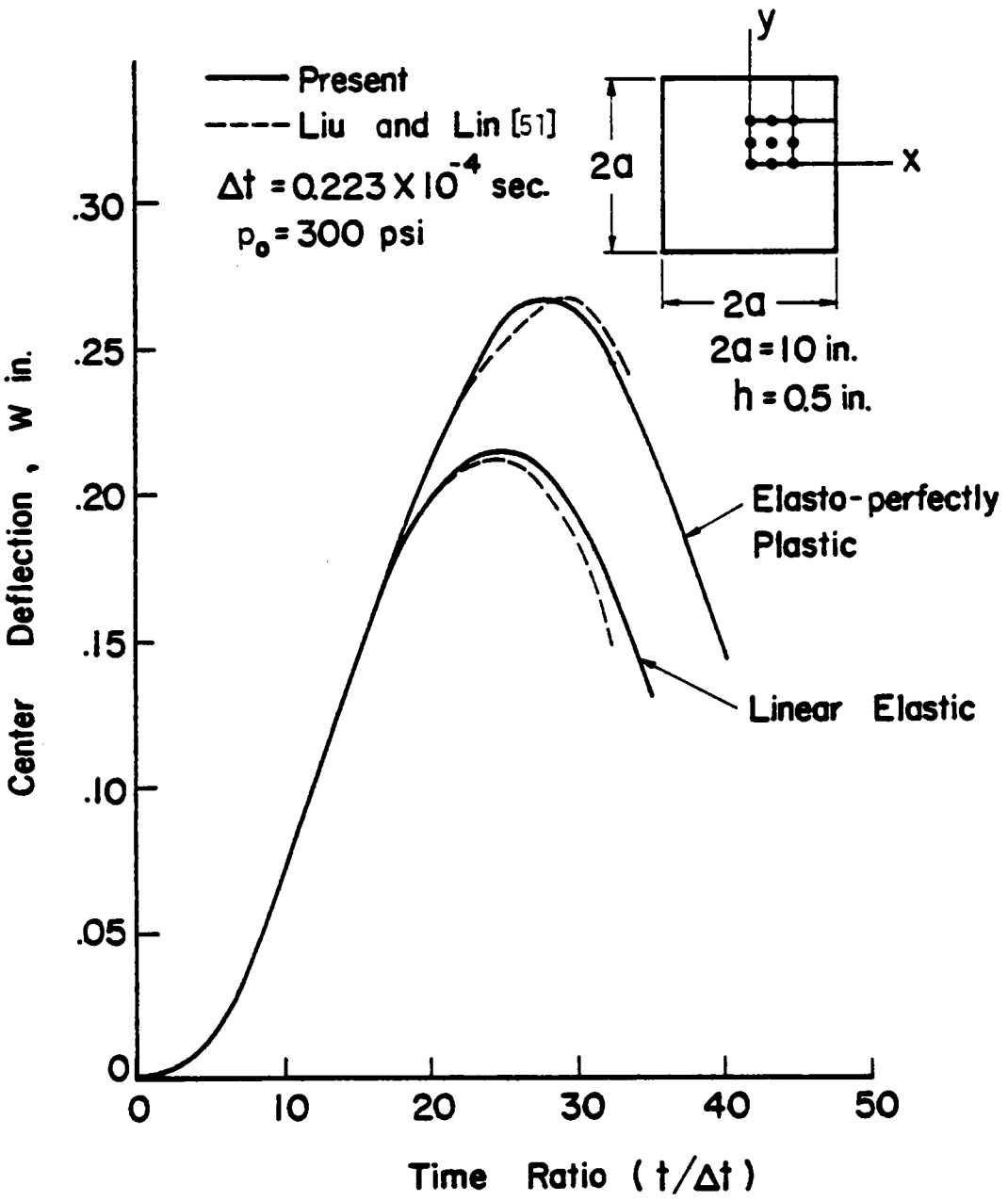

Fig.6.20 Elastic-perfectly Plastic Dynamic Response of Simply-supported Isotropic Square Plate

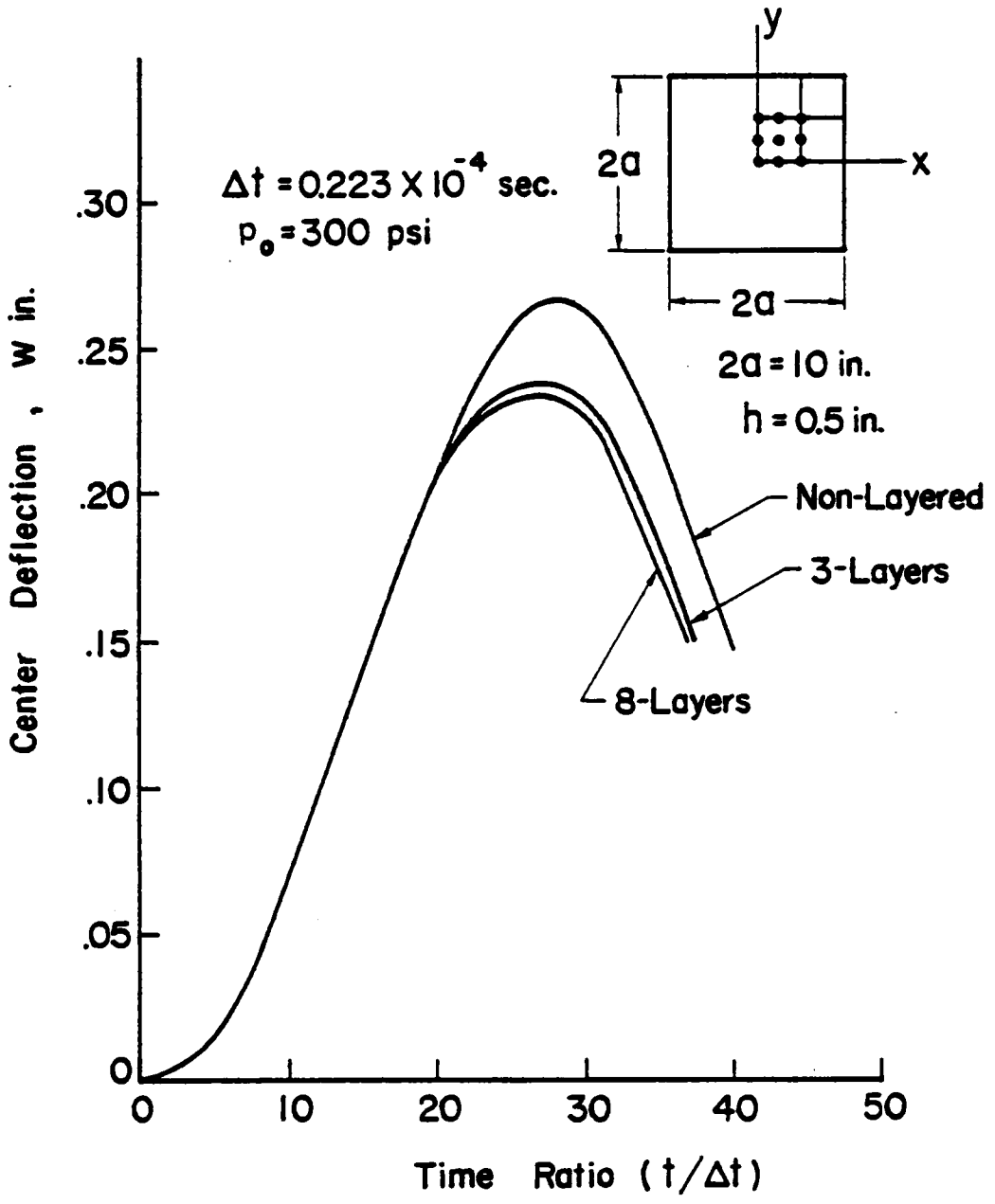

Fig. 6.21 Effect of Layered Approach on the Elasto-plastic Dynamic Response of a Square Plate

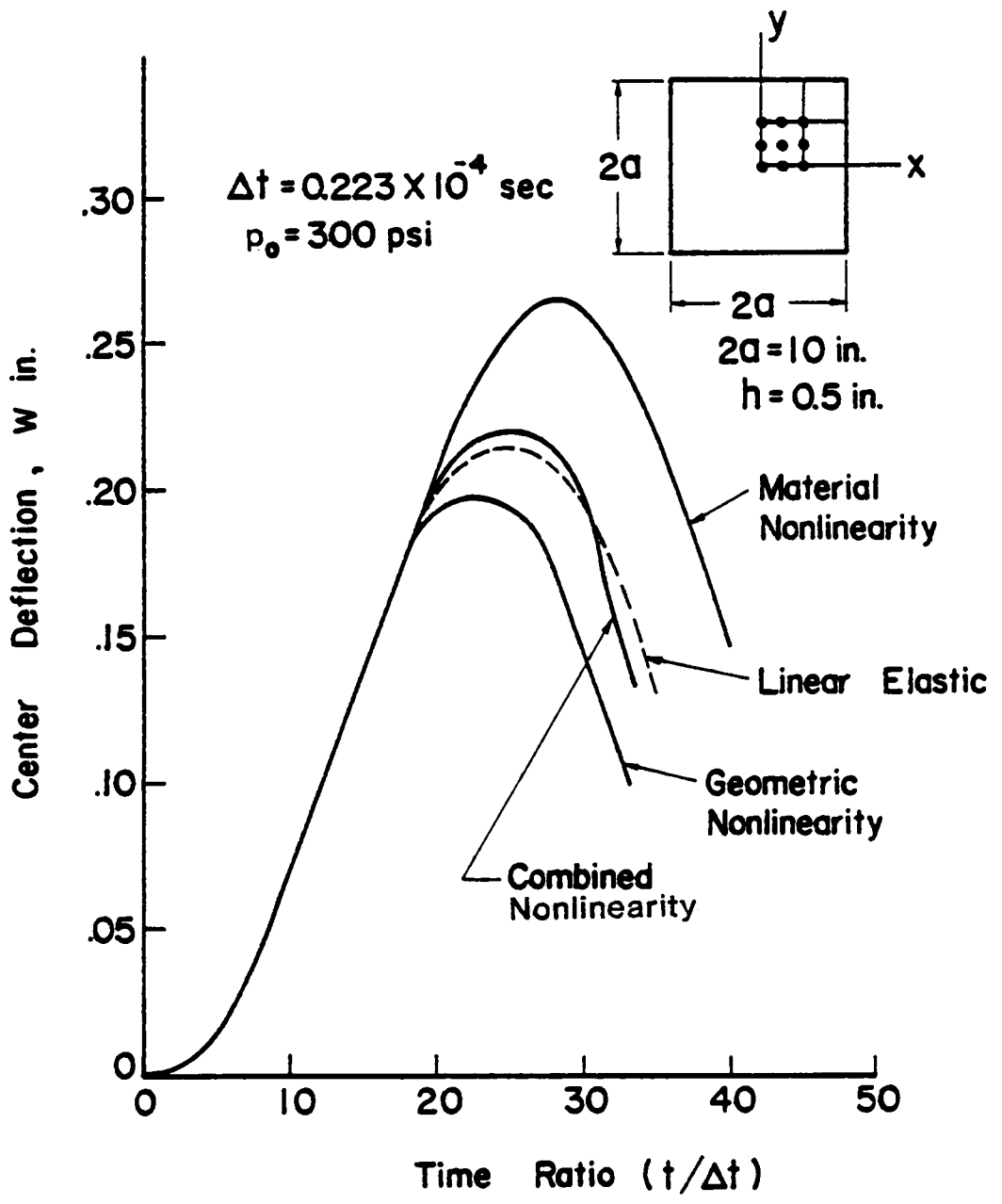

Fig. 6.22 Combined Geometric and Material Nonlinear Analysis of a Simply-supported Square Plate

amplitude of displacement is larger than the linear elastic behavior. The results were compared with those obtained by Liu andLin [56] and are in good agreement.

Effect of layered model on the deflection of simply supported plate. For the plate considered inthe prvious example, the results are based on the nonlayered approach. Figure 6.21 shows the results using the layered model. It is seen that both 3-layers and 8-layers give almost the same results.

6.2.3 Combined Nonlinearity

Simply supported plate under uniform load. The square plate which was studied for the effects of material nonlinearity only, was analyzed to include the effects of geometric nonlinearity also. Figure 6.22 contains plots of deflection versus load for linear, material nonlinear only, geometric nonlinear only, and the combined material and geometric nonlinear analysis. From the results presented in Fig. 6.22, it is clear that the two nonlinearities have opposing effects, and therefore the results of the combined nonlinearity are closer to the linear solution. Such a behavior should be considered as incidental rather than typical of all problems.

CHAPTER 7

CONCLUSIONS AND RECOMMENDATIONS

7.1 Conclusions

A displacement finite element formulation for general nonlinear analysis of laminated composite plates and shells is presented. The element modeled is capable of solving geometrically and materially nonlinear problems, either acting separately or in combination.

The element is based on an extension of the Sanders shell theory that accounts for shear deformation. Geometric nonlinearity is incorporated using the von Karman strains. Material nonlinearity is introduced using a modified version of Hill's initial yield criterion by considering the anisotropic parameter of plasticity. The material model is applicable for both elastic - perfectly plastic and strain hardening behaviors. Through-the-thickness plasticity is accounted for using a layered approach. The assumption of constant shear strain is modified by the application of shear correction factors, and reduced integration is adopted to account for the locking phenomenon when dealing with thin structures.

Numerical examples, for both static and dynamic bending analysis, demonstrate the validity of the formulation and solution procedure. The results obtained are in good agreement with those availble in the literature. The variety of case studies performed aid in identifying the effect of boundary conditions, number of layers through the thickness, anisotropic parameters and iteration scheme on the solution. The present work is the first one to consider the simultaneous treatment of geometric and material nonlinearity of fiber

reinforced composites and the results presented here should serve as references for future investigations.

7.2 Recommendations

One obvious extension would be to use the presently developed finite element formulation for the vibration and buckling analysis of laminated composite plates and shells. The inlastic anisotropic material model developed here could be used to solve fracture or viscoplastic problems.

Another logical extension of the prsent line of research is to include laminated stiffeners. Stiffened laminated plates and shells constitute a frequently occurring type of structure. Also, the present doubly curved shell element could be easily extended to deal with the analysis of arbitrarily shaped shell structures.

Accurate representation of the stress is particularly important in plasticity analysis. In the displacement method the stresses are computed by taking the derivatives of the displacement. The stresses obtained thus are not usually accurate, even though the displacements are accurate. As an alternative, a mixed finite element formulation could be used to improve the accuracy of prediciton of the stresses.

Another area which needs further study is the constitutive relation for anisotropic materials. Although a basic understanding of the macroscopic behavior of simple structures in the plastic range has been attained by the application of available plasticity theories, these theories are rather crude and limited in their applicability. Hence, one of the fundamental problems in the theory of layered composites is

the description of macroscopic behavior of the material knowing the mechanical properties of constituents and the internal geometry of the structure.

These deficiencies in the anisotropic material model inevitably raise questions conerning the accuracy of the results obtained by finite element plastic analysis. However, as improved constitutive relations become available, it should be possible to incorporate them readily in the present formulation.

REFERENCES

1. A. E. H. Love, "On the Small Free Vibrations and Deformations of the Elastic Shells," Phil. Trans. Roy. Soc., (London), Ser. A., Vol. 17, pp. 401-546, 1888.

2. E. Reissner, "A New Derivation of the Equations for the Deformation of Elastic Shells," Am. Jour. Math., Vol. 63, No. 1, pp. 177-184, 1941.

3. E. Reissner, "On Some Problems in Shell Theory," Structural Mechanics, (Proceedings of the First Symposium on Naval Structural Mechanics), J. N. Goodier and N. J. Hoff (eds.), Pergamon Press, New York, pp. 76-114, 1960.

4. E. Reissner, "A Note on Generating Generalized Two-Dimensional Plate and Shell Theories," J. Appl. Math. Physics, (ZAMP), Vol. 28, pp. 633-642, 1977.

5. J. L. Sanders, "An Improved First-Approximation Theory for Thin Shells," NASA Technical Report, R-24, 1959.

6. S. A. Ambartsumyan, "Calculation of Laminated Anisotropic Shells," Izvestiia Akademiia Nauk Armenskoi SSR, Ser. Fiz. Mat. Est. Tekh. Nauk., Vol. 6, No. 3, p. 15, 1953.

7. S. A. Ambartsumyan, Theory of Anisotropic Shells, Moscow, 1961; English translation, NASA TT F-118, May 1964.

8. S. B. Dong, K. S. Pister and R. L. Taylor, "On the Theory of Laminated Anisotropic Shells and Plates," Journal of Aerospace Sceicnes, Vol. 29, pp. 969-975, 1962.

9. L. H. Donnell, "Stability of Thin Walled Tubes in Torsion," NACA Report 479, 1933.

10. G. E. O. Widera, and S. W. Chung, "A Theory of Non-Homogeneous Anisotropic Cylindrical Shells," Journal of Applied Mechanics, (ZAMP), Vol. 21, pp. 378-399, 1970.

11. J. A. Zukas, and J. R. Vinson, "Laminated Transversely Isotropic Cylindrical Shells," Journal of Applied Mechanics, pp. 400-407, 1971.

12. S. B. Dong, and F. K. W. Tso, "On a Laminated Orthotropic Shell Theory Including Transverse Shear Deformation," Journal of Applied Mechanics, Vol. 39, pp. 1091-1097, 1972.

13. J. M. Whitney, and C. T. Sun, "A Refined Theory for Laminated Anisotropic, Cylindrical Shells," Journal of Applied Mechanics, Vol. 41, pp. 471-476, 1974.

14. G. E. O. Widera and D. L. Logan, "Refined Theories for Nonhomogeneous Anisotropic Cylindrical Shells: Part I-Derivation," Journal of the Engineering Mechanics Division, Vol. 106, No. EM6, pp. 1053-1074, 1980.

15. D. L. Logan, and G. E. O. Widera, "Refined Theories for Nonhomogeneous Aniostropic Cylindrical Shells: Part II-Application, "Journal of the Engineering Mechanics Division, Vol. 106, No. EM6, pp. 1075-1090, 1980.

16. L. A. Schmit, and G. R. Monforton, "Finite Element Analysis of Sandwich Plate and Laminated Shells with Laminated Faces," American Institute of Aeronautics and Astronautics Journal, Vol. 8, pp. 1454-1461,1970.

17. S. C. Panda, and R. Natarajan, "Finite Element Analysis of Laminated Shells of Revolution," Computers and Structures, Vol. 6, pp. 61-64, 1976.

18. K. N. Shivakumar, and A. V. Krishna Murty, "A High Precision Ring Element for Vibrations of Laminated Shells," Journal of Sound and Vibration, Vol. 58, No. 3, pp. 311-318, 1978.

19. K. P. Rao, "A Rectangular Laminated Anisotropic Shallow Thin Shell Finite Element," Computer Methods in Applied Mechanics and Engineering, Vol. 15, pp. 13-33, 1978.

20. P. Seide, and P. H. H. Chang, "Finite Element Analysis of Laminated Plates and Shells," NASA CR-157106, 1978.

21. Y. S. Hsu, J. N. Reddy, and C. W. Bert, "Thermoelasticity of Circular Cylindrical Shells Laminated of Bimodulus Composite Materials," Jounal of Thermal Stresses, Vol. 4, No. 2, pp. 115-177, 1981.

22. J. N. Reddy, "Bending of Laminated Anisotropic Shells by a Shear Deformable Finite Element," Fiber Science and Technology, Vol. 17, pp. 2-24, 1982.

23. A. Venkatesh and K. P. Rao, "A Doubly Curved Quarilateral Finite Element for the Analysis of Laminated Anisotropic Thin Shells of Revolution," Computers and Structures, Vol. 12, pp. 825-832, 1980.

24. A. Venkatesh and K. P. Rao, "Analysis of Laminated Shells with Laminated Stiffners Using Rectangular Shell Finite Elements," Computer MetHods in Appl. Mech. Engng., Vol. 38, pp. 255-272, 1983.

25. J. N. Reddy, "Exact Solutions of Moderately Thick Laminated Shells," J. Engng. Mechanics, ASCE, Vol. 110, pp. 794-809, 1984.

26. F. C. Moon, "Wave Surfaces due to Impact on Anisotropic Plates," J. Comp. Mat., Vol. 6, pp. 62-79, 1972.

27. T. S. Chow, "On the Propagation of Flexural Waves in an Orthotropic Laminated Plate and its Response to an Impulsive Load," J. Comp. Mat., Vol. 5, pp. 306-319, 1971.

28. A. S. D. Wang, P. C. Chou and J. L. Rose, "Strongly Coupled Stress Waves in Heterogeneous Plates," AIAA Journal, pp. 1088-1090, 1972.

29. A. L. Dobyns, "Analysis of Simply-Supported Orthotropic Plates Subject to Static and Dynamic Loads," AIAA Journal, Vol. 19, pp. 642-650, 1981.

30. P. V. Marcal and I. P. King, "Elastic-Plastic Analysis of Two Dimensional Stress Systems by the Finite Element Method," Int. J. Mech. Sci., Vol. 9 No. 3, pp. 143-155, 1967.

31. E. P. Popov, M. Khojesteh-Bakht, and S. Yaghmai, "Analysis of Elastic-Plastic Circular Plates," J. Engng. Mech. Div., ASCE, Vol. 93, pp. 49-65, 1967.

32. E. P. Popov, M. Khojesteh-Bakht, and S. Yaghmai, "Bending of Circular Plates of Hardening Material," Int. J. Solids Struct., Vol. 3, pp. 975-988, 1967.

33. Y. Yamada, N. Yoshimura and T. Sakurai, "Plastic Stress-Strain Matrix and its Application for the Solution of Elastic-Elastic Problems by the Finite Element Method," Int. J. Mech. Sci., Vol. 10, pp. 343-354, 1968.

34. H. Armen, Jr., A. Pifko, and H. S. Levine, "Finite Element Method for the Plastic Bending Analysis of Structures," Proc. 2nd Conf. on Matrix Methods in Struct. Mechanics, AFFDL-TR-68-150, Oct. 1968.

35. J. Backlund and H. Wennerstrom, "Finite Element Analysis of Elasto-Plastic Shells," Int. J. Num. Methods in Engng, Vol. 8, pp. 415-424, 1974.

36. R. Hill, "A Theory of Yielding and Plastic Flow of Anisotropic Metals," Proc. Roy. Soc. Lond., Ser 193, 1948.

37. L. W. Hu, "Studies on Plastic Flow of Anisotropic Metals," J. Appl. Mech., pp. 444-450, Sept. 1956.

38. Jensen, W. R., W. E. Falby, and N. Prince, "Matrix Analysis for Anisotropic Inelastic Structures," AFFDL-TR-65-220, 1966.

39. B. Whang, "Elasto-plastic Orthotropic Plates and Shells," Proc. Symp. on Application of F.E.M. in Civil Eng., Vanderbilt University, Tennessee, pp. 481-515, 1969.

40. S. Valliappan, "Elasto-plastic Analysis of Anisotropic Work-hardening Materials," Arch. Mech., Vol. 24 No. 3, pp. 465-481, 1972.

41. D. R. J. Owen and Figueiras, J. A., "Anisotropic Elasto-plastic Finite Element Analysis of Thick and Thin Plates and Shells," Int. J. Num. Methods in Engng., Vol. 19, pp. 551-566, 1983.

42. Lin, T. H., Salinas, D., and Ito, Y. N., "Initial Yield Surface of a Unidirectionally Reinforced Composite," Journal of Applied Mechanics, Vol. 39, No. 2; Trans. ASME, Vol. 94, Series E, pp. 321-326, 1972.

43. Foye, R. L., "Theoretical Post Buckling Yielding Behavior of Composite Laminates, Part I - Inelastic Micromechanics," Journal of Composite Materials, Vol. 7, p. 48, 1973.

44. A. Sawicki, "Yield Conditions for Layered Composites," Int. J. Solids Struct., Vol. 7, No. 10, pp. 969-979, 1981.

45. Y. A. Bahei-El-Din, Dvorak, G. J., and Utku, S., "Finite Element Analysis of Elastic-plastic Fibrous Composite Structures," Computers and Structures, Vol. 13, pp. 321-330, 1981.

46. J. Aboudi and Benveniste, "Constitutive Relation for Fiber-reinforced Elastic-Viscoplastic Composites," Int. J. Eng. Sci., Vol. 20, pp. 605-621, 1982.

47. G. J. Dvorak and Bahei-El-Din, Y. A., "Plasticity Analysis of Fibrous Composites," Journal of Applied Mechanics, Vol. 49, pp. 327-335, 1982.

48. H. S. Levine, H. Armen, Jr., R. Winter and A. Pifko, "Nonlinear Behavior of Shells of Revolution Under Cyclic Loading," Computers and Structures, Vol. 3, pp. 589-617, 1973.

49. S. Nagarajan and E. P. Popov, "Elastoplastic Dynamic Analysis of Axisymmetric Solids," Computers and STructures, Vol. 4, pp. 1117-1134, 1974.

50. K. J. Bathe and S. Bolourchi, "A Geometric and Material Nonlinear Plate and Shell Element," Computers and Structures, Vol. 11, pp. 23-48, 1980.

51. S. C. Liu and T. H. Lin, "Elastic-plastic Dynamic Analysis of Structures Using Known Elastic Solutions," Earthquake Engng. and Struct. Dynamics, Vol. 7, pp. 147-159, 1979.

52. H. Javahevian, P. J. Dowling and L. P. R. Lyons, "Nonlinear Finite Element Analysis of Shell Structures using the Semi-Loof Element," Computers and Structures, Vol. 12, pp. 147-159, 1980.

53. D. N. Herting and R. Norayona Swami, "Efficient Methods for Static Nonlinear Analysis of Large Order Problems," In Nonlinear Finite Element Analysis of Plates and Shells, edited by T. J. R. Hughes, A. Pifko and A. Jay, AMD-48, ASME, pp. 35-45, 1981.

54. H. Parisch, "Large Displacements of Shells Including Material Nonlinearities," Computer Methods in Applied Mechanics and Engineering, Vol. 27, pp. 183-214, 1981.

55. E. N. Dvorkin and K. J. Bathe, "A Continuum Mechanics Based Four-Node Shell Element for General Nonlinear Analysis," Eng. Comput., Vol. 1, pp. 77-88, 1984.

56. K. J. Bathe, E. Ramm and E. L. Wilson, "Finite Element Formulations for Large Deformation Dynamic Analysis," Int. J. Num. Methods in Engng., Vol. 19, pp. 353-386, 1975.

57. D. P. Mondkar and G. H. Powell, "Finite Element Analysis of Nonlinear Static and Dynamic Response," Int. J. Num. Methods in Engng., Vol. 11, pp. 499-520, 1977.

58. T. von Karman, "Festigkeitsprobleme in Maschinenbau," Encyklopaedie der Mathematischen Wissenschafter, Vol. 4, pp. 348-351, 1910.

59. R. von Mises, "Gottingen Nachnichten," Math. Phy. Klasse, p. 382, 1913.

60. A. Mendelson, Pasticity: Theory and Application, The MacMillan Company, New York, 1968.

61. T. H. Lin, D. Salinos and Y. M. Ito, "Effects of Hydrostatic Stress on the Yielding of Cold Rolled Metals and Fiber-reinforced Composites," J. Comp. Materials, Vol. 6, p. 409, 1972.

62. A. A. Baker and D. Cratchley, "Stress-Strain Behavior and Toughness of a Fiber-Reinforced Metal," Applied Materials Research, Vol. 5, pp. 92-103, 1966.

63. J. N. Reddy, Energy and Variational Methods in Applied Mechanics, John Wiley, New York, 1984.

64. W. Prager, "The Theory of Plasticity: A Survey of Recent Achievements, (James Clayton Lecture) Proc. Instn, Mech. Engrs., Vol. 169, pp. 41-57, 1955.

65. T. Y. Tang, "High Order Rectangular Shallow Shell Finite Element," J. Eng. Mech. Div., ASCE 99, pp. 157-181, 1973.

66. K. P. Rao, "A Rectangular Laminated Anisotropic Shallow Thin Shell Finite Element," Computer Methods in Applied Mechanics and Engineering, Vol. 15, pp. 13-33, 1978.

67. S. Timoshenko and S. Woinowsky-Krieger, Theory of Plates and Shells, 2nd Ed., McGraw-Hill, New York, 1959.

68. S. Way, "Uniformly Loaded, Clamped, Rectangular Plates with Large Deformation," Proc. 5th Inter. Congr. of Appl. Mech., Cambridge, MA, 1938.

69. G. S. Dhatt, "Instability of Thin Shells by the Finite Element Method," IASS Symposium for Folded Plates and Prismatic Structures, Vienna, 1970.

70. J. A. Stricklin et al., "Nonlinear Dynamic Analysis of Shells of Revolution by Matrix Displacement Method," Am. Int. Aeronaut. Astronaut. J., Vol. 9, pp. 629-636 1971.

APPENDIX A

ELASTIC-PLASTIC MATRIX

$$[D^{eP}]_{5x5} = [D^{e}]_{5x5} - \frac{[D^{e}]_{5x5}\left\{\frac{\partial f}{\partial\{\sigma\}}\right\}_{5x1}\left\{\frac{\partial f}{\partial\{\sigma\}}\right\}^{T}_{1x5}[D^{e}]_{5x5}}{H + \left\{\frac{\partial f}{\partial\{\sigma\}}\right\}^{T}_{1x5}[D^{e}]_{5x5}\left\{\frac{\partial f}{\partial\{\sigma\}}\right\}_{5x1}} \qquad (A1)$$

We have the yield function

$$f(\sigma_{ij}) = \bar{\sigma}^2 = \beta_{11}\sigma_1^2 - \beta_{12}\sigma_1\sigma_2 + \beta_{22}\sigma_2^2 + 3\beta_{44}\sigma_{23}^2 + 3\beta_{55}\sigma_{13}^2 + 3\beta_{66}\sigma_{12}^2$$

$$\left\{\frac{\partial f}{\partial\{\sigma\}}\right\} = \begin{Bmatrix} \frac{\partial f}{\partial\sigma_1} \\ \frac{\partial f}{\partial\sigma_2} \\ \frac{\partial f}{\partial\sigma_{12}} \\ \frac{\partial f}{\partial\sigma_{23}} \\ \frac{\partial f}{\partial\sigma_{13}} \end{Bmatrix} = \begin{Bmatrix} F_{11} \\ F_{22} \\ F_{12} \\ F_{23} \\ F_{13} \end{Bmatrix} = \begin{Bmatrix} 2\beta_{11}\sigma_1 - \beta_{12}\sigma_2 \\ 2\beta_{22}\sigma_2 - \beta_{12}\sigma_1 \\ 6\beta_{66}\sigma_{12} \\ 6\beta_{44}\sigma_{23} \\ 6\beta_{55}\sigma_{13} \end{Bmatrix}$$

$$[D^{e}]\left\{\frac{\partial f}{\partial\{\sigma\}}\right\} = \begin{bmatrix} C_{11} & C_{12} & 0 & 0 & 0 \\ C_{12} & C_{22} & 0 & 0 & 0 \\ 0 & 0 & C_{33} & 0 & 0 \\ 0 & 0 & 0 & C_{44} & 0 \\ 0 & 0 & 0 & 0 & C_{55} \end{bmatrix} \begin{Bmatrix} F_{11} \\ F_{22} \\ F_{12} \\ F_{23} \\ F_{13} \end{Bmatrix} = \begin{Bmatrix} F_{11}C_{11}+F_{22}C_{12} \\ F_{11}C_{12}+F_{22}C_{22} \\ F_{12}C_{33} \\ F_{23}C_{44} \\ F_{13}C_{55} \end{Bmatrix} = \begin{Bmatrix} \bar{C}_{11} \\ \bar{C}_{22} \\ \bar{C}_{12} \\ \bar{C}_{23} \\ \bar{C}_{13} \end{Bmatrix}$$

The numerator of Eq. (1) becomes

$$NR = [D^e]\left\{\frac{\partial f}{\partial\{\sigma\}}\right\}\left\{\frac{\partial f}{\partial\{\sigma\}}\right\}^T[D^e] = \begin{Bmatrix} \bar{C}_{11} \\ \bar{C}_{22} \\ \bar{C}_{12} \\ \bar{C}_{23} \\ \bar{C}_{13} \end{Bmatrix} [\bar{C}_{11}\bar{C}_{22}\bar{C}_{12}\bar{C}_{23}\bar{C}_{13}]$$

$$= \begin{bmatrix} C_{11} & \bar{C}_{11}\bar{C}_{22} & \bar{C}_{11}\bar{C}_{12} & \bar{C}_{11}\bar{C}_{23} & \bar{C}_{11}\bar{C}_{13} \\ C_{22}C_{11} & \bar{C}_{22}^2 & \bar{C}_{22}\bar{C}_{12} & \bar{C}_{22}\bar{C}_{23} & \bar{C}_{22}\bar{C}_{13} \\ C_{12}C_{11} & \bar{C}_{12}\bar{C}_{22} & \bar{C}_{12}^2 & \bar{C}_{12}\bar{C}_{23} & \bar{C}_{12}\bar{C}_{13} \\ C_{23}C_{11} & \bar{C}_{23}\bar{C}_{22} & \bar{C}_{23}\bar{C}_{12} & \bar{C}_{23}^2 & \bar{C}_{23}\bar{C}_{13} \\ C_{13}C_{11} & \bar{C}_{13}\bar{C}_{22} & \bar{C}_{13}\bar{C}_{12} & \bar{C}_{13}\bar{C}_{23} & \bar{C}_{13}^2 \end{bmatrix} \qquad \text{(A2)}$$

The denominator of Eq. (1) becomes

$$DR = H + \left\{\frac{\partial f}{\partial\{\sigma\}}\right\}^T[D^e]\left\{\frac{\partial f}{\partial\{\sigma\}}\right\}$$

$$= H + [F_{11}F_{22}F_{12}F_{23}F_{13}]\begin{Bmatrix} \bar{C}_{11} \\ \bar{C}_{22} \\ \bar{C}_{12} \\ \bar{C}_{23} \\ \bar{C}_{13} \end{Bmatrix}$$

$$= H + F_{11}\bar{C}_{11} + F_{22}\bar{C}_{22} + F_{12}\bar{C}_{12} + F_{23}\bar{C}_{23} + F_{13}\bar{C}_{13} \qquad \text{(A3)}$$

Substituting Eqs. (A2) and (A3) in Eq. (A1)

$$[D^{eP}] = [D^{e}] - [D]$$

$$= \begin{bmatrix} C_{11} & C_{12} & 0 & 0 & 0 \\ C_{12} & C_{22} & 0 & 0 & 0 \\ 0 & 0 & C_{33} & 0 & 0 \\ 0 & 0 & 0 & C_{44} & 0 \\ 0 & 0 & 0 & 0 & C_{55} \end{bmatrix}$$

$$- \frac{1}{DR} \begin{bmatrix} \overline{C}_{11}^2 & \overline{C}_{11}\overline{C}_{22} & \overline{C}_{11}\overline{C}_{12} & \overline{C}_{11}\overline{C}_{23} & \overline{C}_{11}\overline{C}_{13} \\ \overline{C}_{22}\overline{C}_{11} & \overline{C}_{22}^2 & \overline{C}_{22}\overline{C}_{12} & \overline{C}_{22}\overline{C}_{23} & \overline{C}_{22}\overline{C}_{13} \\ \overline{C}_{12}\overline{C}_{11} & \overline{C}_{12}\overline{C}_{22} & \overline{C}_{12}^2 & \overline{C}_{12}\overline{C}_{23} & \overline{C}_{12}\overline{C}_{13} \\ \overline{C}_{23}\overline{C}_{11} & \overline{C}_{23}\overline{C}_{22} & \overline{C}_{23}\overline{C}_{12} & \overline{C}_{23}^2 & \overline{C}_{23}\overline{C}_{13} \\ \overline{C}_{13}\overline{C}_{11} & \overline{C}_{13}\overline{C}_{22} & \overline{C}_{13}\overline{C}_{12} & \overline{C}_{13}\overline{C}_{23} & \overline{C}_{13}^2 \end{bmatrix}$$

$$[D^{eP}] = \begin{bmatrix} \overline{D}_{11} & \overline{D}_{12} & \overline{D}_{13} & \overline{D}_{14} & \overline{D}_{15} \\ \overline{D}_{12} & \overline{D}_{22} & \overline{D}_{23} & \overline{D}_{24} & \overline{D}_{25} \\ \overline{D}_{13} & \overline{D}_{23} & \overline{D}_{33} & \overline{D}_{34} & \overline{D}_{35} \\ \overline{D}_{14} & \overline{D}_{24} & \overline{D}_{34} & \overline{D}_{44} & \overline{D}_{45} \\ \overline{D}_{15} & \overline{D}_{25} & \overline{D}_{35} & \overline{D}_{45} & \overline{D}_{55} \end{bmatrix}$$

where

$$\bar{D}_{11}=C_{11}-\frac{\bar{C}_{11}^2}{DR} \qquad \bar{D}_{22}=C_{22}-\frac{\bar{C}_{22}^2}{DR} \qquad \bar{D}_{33}=C_{33}-\frac{\bar{C}_{12}^2}{DR} \qquad \bar{D}_{44}=C_{44}-\frac{\bar{C}_{23}^2}{DR}$$

$$\bar{D}_{12}=C_{12}-\frac{\bar{C}_{11}\bar{C}_{22}}{DR} \qquad \bar{D}_{23}=-\frac{\bar{C}_{12}\bar{C}_{22}}{DR} \qquad \bar{D}_{34}=-\frac{\bar{C}_{23}\bar{C}_{12}}{DR} \qquad \bar{D}_{45}=-\frac{\bar{C}_{23}\bar{C}_{13}}{DR}$$

$$\bar{D}_{13}=-\frac{\bar{C}_{11}\bar{C}_{12}}{DR} \qquad \bar{D}_{24}=-\frac{\bar{C}_{23}\bar{C}_{22}}{DR} \qquad \bar{D}_{35}=-\frac{\bar{C}_{13}\bar{C}_{12}}{DR} \qquad \bar{D}_{55}=C_{55}-\frac{\bar{C}_{13}^2}{DR}$$

$$\bar{D}_{14}=-\frac{\bar{C}_{23}\bar{C}_{11}}{DR} \qquad \bar{D}_{25}=-\frac{\bar{C}_{13}\bar{C}_{22}}{DR}$$

$$\bar{D}_{15}=-\frac{\bar{C}_{13}\bar{C}_{11}}{DR}$$

APPENDIX B

TRANSFORMATION OF THE STRESS-STRAIN MATRIX

Let the elastic-plastic matrix in the material axes (1,2) be $[D^{eP}]_{12}$ and in the body axes be $[D^{eP}]_{xy}$ (see Fig. 3.4).

$$[D^{eP}]_{12} = [C] = \begin{bmatrix} C_{11} & C_{12} & C_{13} & C_{14} & C_{15} \\ & C_{22} & C_{23} & C_{24} & C_{25} \\ & & C_{33} & C_{34} & C_{35} \\ \text{Sym} & & & C_{44} & C_{45} \\ & & & & C_{55} \end{bmatrix}$$

$$[D^{eP}]_{xy} = [Q] = \begin{bmatrix} Q_{11} & Q_{12} & Q_{13} & Q_{14} & Q_{25} \\ & Q_{22} & Q_{23} & Q_{24} & Q_{25} \\ & & Q_{33} & Q_{34} & Q_{35} \\ \text{Sym} & & & Q_{44} & Q_{45} \\ & & & & Q_{55} \end{bmatrix}$$

Then the transformation is given as, (with $m = \cos\theta$, $n = \sin\theta$)

$$Q_{11} = m^4C_{11} + 2m^2n^2(C_{12} + 2C_{33}) - 4mn(m^2C_{13} + n^2C_{23}) + n^4C_{22}$$

$$Q_{12} = m^2n^2(C_{11} + C_{22} - 4C_{33}) - 4mn(m^2C_{13} + n^2C_{23}) + (m^4 + n^4)C_{12}$$

$$Q_{13} = m^2(m^2 - 3n^2)C_{13} + mn[m^2C_{11} - n^2C_{22} - (m^2 - n^2)(C_{12} + 2C_{33})] + n^2(3m^2 - n^2)C_{23}$$

$$Q_{14} = m^3C_{14} - mn[(2C_{34} - C_{15})m - (C_{24} - 2C_{35})n] + C_{25}n^3$$

$$Q_{15} = m^3C_{15} - mn[(C_{14} + 2C_{35})m - (C_{25} + 2C_{34})n] - C_{24}n^3$$

$$Q_{22} = n^4C_{11} + 2m^2n^2(C_{12} + 2C_{33}) + \underline{4mn(m^2C_{23} + n^2C_{13})} + m^4C_{22}$$

$$Q_{23} = \underline{m^2(m^2 - 3n^2)C_{23}} + mn[n^2C_{11} - m^2C_{22} + (m^2 - n^2)(C_{12} + 2C_{33})]$$

$$+ \underline{n^2(3m^2 - n^2)C_{13}}$$

$$Q_{24} = \underline{m^3C_{24} + mn[(C_{25} + 2C_{34})m + (C_{14} + 2C_{35})n] + C_{15}n^3}$$

$$Q_{25} = \underline{m^3C_{25} - mn[(C_{24} - 2C_{35})m - (C_{15} - 2C_{34})n] - C_{14}n^3}$$

$$Q_{33} = m^2n^2(C_{11} + C_{22} - 2C_{12}) - \underline{2mn(m^2 - n^2)(C_{22} - C_{13})} + (m^2 - n^2)^2C_{33}$$

$$Q_{34} = \underline{(mC_{34} + nC_{35})(m^2 - n^2) + m^2n(C_{14} - C_{24}) + mn^2(C_{15} - C_{25})}$$

$$Q_{35} = \underline{(mC_{35} - nC_{34})(m^2 - n^2) + m^2n(C_{15} - C_{25}) + mn^2(C_{24} - C_{14})}$$

$$Q_{44} = m^2C_{44} + \underline{2mnC_{45}} + n^2C_{55}$$

$$Q_{45} = \underline{(m^2 - n^2)C_{45}} - mn(C_{44} - C_{45})$$

$$Q_{55} = m^2C_{55} - \underline{2mnC_{45}} + n^2C_{44}$$

The underscored terms are the additional terms due to material nonlinearity for an orthotropic material. It should be noted that the constitutive matrix is no longer orthotropic.

APPENDIX C

ELEMENT STIFFNESS COEFFICIENTS

(a) Linear Stiffness Coefficients $[K]_L$

$$[K^{11}] = A_{11}[S^{11}] + A_{16}([S^{12}] + [S^{21}]) + A_{66}[S^{22}] + C_o[B_{16}([S_{12}] + [S^{21}]) + B_{66}[S^{22}] + C_o D_{66}[S^{22}]] + \frac{A_{55}}{R_1^2}[S^{oo}]$$

$$[K^{12}] = A_{12}[S^{12}] + A_{16}[S^{11}] + A_{26}[S^{22}] + A_{66}[S^{21}] + C_o(B_{26}[S^{22}] - B_{16}[S^{11}] - C_o D_{66}[S^{21}]) + \frac{A_{45}}{R_1 R_2}[S^{oo}]$$

$$[K^{13}] = \frac{1}{R_1}(A_{11}[S^{10}] + A_{16}[S^{20}]) + \frac{1}{R_2}(A_{12}[S^{10}] + A_{26}[S^{20}]) + C_o(\frac{B_{16}}{R_1}[S^{20}] + \frac{B_{26}}{R_2}[S^{20}]) - \frac{1}{R_1}(A_{45}[S^{02}] + A_{55}[S^{01}])$$

$$[K^{14}] = B_{11}[S^{11}] + B_{16}([S^{12}] + [S^{21}]) + B_{66}[S^{22}] + C_o(D_{16}[S^{21}] + D_{66}[S^{22}]) - \frac{A_{55}}{R_1}[S^{oo}]$$

$$[K^{15}] = B_{12}[S^{12}] + B_{16}[S^{11}] + B_{26}[S^{22}] + B_{66}[S^{21}] + C_o(D_{26}[S^{22}] + D_{66}[S^{21}]) - \frac{A_{45}}{R_1}[S^{oo}]$$

$$[K^{21}] = [K^{12}]^T$$

$$[K^{22}] = A_{22}[S^{22}] + A_{26}([S^{12}] + [S^{21}]) + A_{66}[S^{11}] - 2C_o B_{66}[S^{11}]$$

$$- C_o[B_{26}([S^{12}] + [S^{21}]) - C_o D_{66}[S^{11}]) + \frac{A_{44}}{R_2^2}[S^{oo}]$$

$$[K^{23}] = \frac{1}{R_1}(A_{12}[S^{20}] + A_{16}[S^{10}]) + \frac{1}{R_2}(A_{22}[S^{20}] + A_{26}[S^{10}])$$

$$- C_o(\frac{B_{16}}{R_2} + \frac{B_{26}}{R_2})[S^{10}] - \frac{1}{R_2}(A_{44}[S^{02}] + A_{45}[S^{01}])$$

$$[K^{24}] = B_{12}[S^{21}] + B_{26}[S^{22}] + B_{16}[S^{11}] + B_{66}[S^{12}]$$

$$- C_o(D_{16}[S^{11}] + D_{66}[S^{12}]) - \frac{A_{45}}{R_2}[S^{oo}]$$

$$[K^{25}] = B_{22}[S^{22}] + B_{26}([S^{21}] + [S^{12}]) + B_{66}[S^{11}]$$

$$- C_o(D_{26}[S^{12}] + D_{66}[S^{11}]) - \frac{A_{44}}{R_2}[S^{oo}]$$

$$[K^{31}] = [K^{13}]^T$$

$$[K^{32}] = [K^{23}]^T$$

$$[K^{33}] = A_{45}[S^{12}] + A_{55}[S^{11}] + A_{44}[S^{22}] + A_{45}[S^{21}]$$

$$+ [S^{oo}][\frac{1}{R_1}(\frac{A_{11}}{R_1} + \frac{A_{12}}{R_2}) + \frac{1}{R_2}(\frac{A_{12}}{R_1} + \frac{A_{22}}{R_2})]$$

$$]K^{34}] = A_{55}[S^{10}] + A_{45}[S^{20}] + (\frac{B_{11}}{R_1} + \frac{B_{12}}{R_2})[S^{01}]$$

$$+ (\frac{B_{16}}{R_1} + \frac{B_{26}}{R_2})[S^{02}]$$

$$[K^{35}] = A_{45}[S^{10}] + A_{44}[S^{20}] + (\frac{B_{16}}{R_1} + \frac{B_{26}}{R_2})[S^{01}]$$

$$+ (\frac{B_{12}}{R_1} + \frac{B_{22}}{R_2})[S^{02}]$$

$$[K^{41}] = [K^{14}]^T$$

$$[K^{42}] = [K^{24}]^T$$

$$[K^{43}] = [K^{34}]^T$$

$$[K^{44}] = D_{11}[S^{11}] + D_{16}([S^{12}] + [S^{21}]) + D_{66}[S^{22}] + A_{55}[S^{oo}]$$

$$[K^{45}] = D_{12}[S^{12}] + D_{16}[S^{11}] + D_{26}[S^{22}] + D_{66}[S^{21}] + A_{45}[S^{oo}]$$

$$[K^{51}] = [K^{15}]^T$$

$$[K^{52}] = [K^{25}]^T$$

$$[K^{53}] = [K^{35}]^T$$

$$[K^{54}] = [K^{45}]^T$$

$$[K^{55}] = D_{22}[S^{22}] + D_{26}([S^{12}] + [S^{21}]) + D_{66}[S^{11}] + A_{44}[S^{oo}]$$

where

$$S_{ij}^{\alpha\beta} = \int_{\Omega^e} \frac{\partial \psi_i}{\partial \psi_\alpha} \frac{\partial \psi_j}{\partial x_\beta} \, dx_1 dx_2$$

$$S_{ij}^{oo} = \int_{\Omega^e} \psi_i \psi_j \, dx_1 dx_2$$

and

$$C_o = \frac{1}{2} (\frac{1}{R_1} - \frac{1}{R_2})$$

(b) Geometrical Nonlinear Stiffness Terms $[K]_G$

$$[K^{13}] = f_1[A_{11}[S^{11}] + A_{16}([S^{12}] + [S^{21}]) + A_{66}[S^{22}]]$$

$$+ f_2(A_{12}[S^{12}] + A_{16}[S^{11}] + A_{26}[S^{22}] + A_{66}[S^{21}])$$

$$+ C_o[f_1(B_{16}[S^{21}] + B_{66}[S^{22}]) + f_2(B_{26}[S^{22}] + B_{66}[S^{21}])]$$

$$[K^{23}] = f_1(A_{12}[S^{21}] + A_{26}[S^{22}] + A_{16}[S^{11}] + A_{66}[S^{12}])$$

$$+ f_2[A_{22}[S^{22}] + A_{26}([S^{12}] + [S^{21}]) + A_{66}[S^{11}])$$

$$- C_o[f_1(B_{16}[S^{11}] + B_{66}[S^{12}]) + f_2(B_{26}[S^{12}] + B_{66}[S^{11}])]$$

$$[K^{31}] = [2K^{13}]^T$$

$$[K^{32}] = [2K^{23}]^T$$

$$[K^{33}] = 2[S^{11}](A_{11}f_1^2 + 2A_{16}f_1f_2 + A_{66}f_2^2)$$

$$+ 2[([S^{12}] + [S^{21}])(f_1^2A_{16} + (A_{12} + A_{66})f_1f_2 + f_2^2A_{26})]$$

$$+ 2[S^{22}](A_{66}f_1^2 + 2A_{26}f_1f_2 + A_{22}f_2^2)$$

$$+ ([S^{01}] + 2[S^{10}])[f_1(\frac{A_{11}}{R_1} + \frac{A_{12}}{R_2}) + f_2(\frac{A_{16}}{R_1} + \frac{A_{26}}{R_2})]$$

$$+ ([S^{02}] + 2[S^{20}])[f_1(\frac{A_{16}}{R_1} + \frac{A_{26}}{R_2}) + f_2(\frac{A_{12}}{R_1} + \frac{A_{22}}{R_2})]$$

$$[K^{34}] = 2f_1[B_{11}[S^{11}] + B_{16}([S^{12}] + [S^{21}]) + B_{66}[S^{22}]]$$

$$+ 2f_2(B_{12}[S^{21}] + B_{66}[S^{12}] + B_{26}[S^{22}] + B_{16}[S^{11}])$$

$$[K^{35}] = 2f_1(B_{12}[S^{12}] + B_{66}[S^{21}] + B_{16}[S^{11}] + B_{26}[S^{22}])$$

$$+ 2f_2(B_{22}[S^{22}] + B_{26}([S^{12}] + [S^{21}]) + B_{66}[S^{11}]$$

$$[K^{43}] = \frac{1}{2}\,[K^{34}]^T$$

$$[K^{53}] = \frac{1}{2}\,[K^{35}]^T$$

where

$$f_1 = \frac{1}{2}\frac{\partial u_3}{\partial x_1} \quad ; \quad f_2 = \frac{1}{2}\frac{\partial u_3}{\partial x_2}$$

(c) Material Nonlinear Coefficients $[K]_M$

$$[K^{11}] = -\frac{1}{R_1}\,[A_{15}([S^{10}] + [S^{01}]) + A_{56}([S^{20}] + [S^{02}])$$

$$- C_o B_{56}([S^{20}] + [S^{02}]]$$

$$[K^{12}] = -\frac{1}{R_2}\,(A_{14}[S^{10}] + A_{46}[S^{20}] + C_o B_{46}[S^{20}])$$

$$-\frac{1}{R_1}\,(A_{25}[S^{02}] + A_{56}[S^{01}] - C_o B_{56}[S^{01}])$$

$$[K^{13}] = A_{14}[S^{12}] + A_{15}([S^{11}] - \frac{[S^{00}]}{R_1^2}) + A_{46}[S^{22}] + A_{56}[S^{21}]$$

$$+ C_o(B_{46}[S^{22}] + B_{56}[S^{21}]) - A_{25}\,\frac{[S^{00}]}{R_1 R_2}$$

$$[K^{14}] = A_{15}[S^{10}] + A_{56}[S^{20}] - \frac{1}{R_1}\,(B_{15}[S^{01}] + B_{56}[S^{02}])$$

$$+ C_o B_{46}[S^{20}]$$

$$[K^{21}] = [K^{12}]^T$$

$$[K^{22}] = -\frac{1}{R_2}\,[A_{24}([S^{20}] + [S^{02}]) + A_{46}([S^{10}] + [S^{01}] + C_o[S^{10}]) - C_oB_{46}[S^{10}]]$$

$$[K^{23}] = A_{24}([S^{22}] - \frac{1}{R_2^2}\,[S^{00}]) + A_{25}[S^{21}] + A_{46}[S^{12}] + A_{56}[S^{11}] - C_o(B_{46}[S^{12}] + B_{56}[S^{11}]) - \frac{A_{14}}{R_1R_2}\,[S^{00}]$$

$$[K^{24}] = A_{25}[S^{20}] + A_{56}[S^{10}] - \frac{1}{R_2}\,(B_{14}[S^{01}] + B_{46}[S^{02}]) - C_oB_{56}[S^{10}]$$

$$[K^{25}] = A_{24}[S^{20}] + A_{46}[S^{10}] - \frac{1}{R_2}\,(B_{24}[S^{02}] + B_{46}[S^{01}]) - C_oB_{46}[S^{10}]$$

$$[K^{31}] = [K^{13}]^T$$

$$[K^{32}] = [K^{23}]^T$$

$$[K^{33}] = \frac{1}{R_1}\,[A_{14}([S^{02}] + [S^{20}]) + A_{15}([S^{01}] + [S^{10}])] + \frac{1}{R_2}\,[A_{24}([S^{02}] + [S^{20}]) + A_{25}([S^{01}] + [S^{10}])]$$

$$[K^{34}] = B_{14}[S^{21}] + B_{46}[S^{22}] + B_{15}[S^{11}] + B_{56}[S^{12}] + (\frac{A_{15}}{R_1} + \frac{A_{25}}{R_2})[S^{00}]$$

$$[K^{35}] = B_{24}[S^{22}] + B_{46}[S^{11}] + B_{25}[S^{12}] + B_{56}[S^{11}]$$

$$+ \left(\frac{A_{14}}{R_1} + \frac{A_{24}}{R_2}\right)[S^{00}]$$

$$[K^{41}] = [K^{14}]^T$$

$$[K^{42}] = [K^{24}]^T$$

$$[K^{43}] = [K^{34}]^T$$

$$[K^{44}] = B_{15}([S^{01}] + [S^{10}]) + B_{56}([S^{20}] + [S^{02}])$$

$$[K^{45}] = B_{14}[S^{10}] + B_{46}[S^{20}] + B_{25}[S^{02}] + B_{56}[S^{01}]$$

$$[K^{51}] = [K^{15}]^T$$

$$[K^{52}] = [K^{25}]^T$$

$$[K^{53}] = [K^{35}]^T$$

$$[K^{54}] = [K^{45}]^T$$

$$[K^{55}] = B_{24}([S^{20}] + [S^{02}]) + B_{46}([S^{10}] + [S^{01}])$$

(d) Combined Nonlinear Stiffness Coefficients $[K]_{GM}$

$$[K^{13}] = -\frac{1}{R_1}\left[f_1 A_{15}[S^{01}] + A_{56}(f_2[S^{01}] + f_1[S^{02}]) + f_2 A_{25}[S^{02}]\right]$$

$$[K^{23}] = -\frac{1}{R_2}\left[f_2 A_{24}[S^{02}] + A_{46}(f_1[S^{02}] + f_2[S^{01}]) + f_1 A_{14}[S^{01}]\right]$$

$$[K^{31}] = 2[K^{13}]^T$$

$$[K^{32}] = 2[K^{23}]^T$$

$$[K^{33}] = A_{14}f_1(2[S^{12}] + [S^{21}]) + 3(f_1A_{15}[S^{11}] + f_2A_{24}[S^{22}])$$
$$+ A_{46}[3f_1[S^{22}] + f_2(2[S^{12}] + [S^{21}])$$
$$+ A_{56}[3f_2[S^{11}] + f_1(2[S^{21}] + [S^{12}])$$

$$[K^{34}] = 2(f_1A_{15}[S^{10}] + f_2A_{25}[S^{20}]) + 2A_{56}(f_1[S^{20}] + f_2[S^{10}])$$

$$[K^{35}] = 2(f_1A_{14}[S^{10}] + f_2A_{24}[S^{20}]) + 2A_{46}(f_2[S^{10}] + f_1[S^{20}])$$

$$[K^{43}] = \frac{1}{2}[K^{34}]^T$$

$$[K^{53}] = \frac{1}{2}[K^{35}]^T$$

Mass Coefficients

$$[M^{11}] = P_1[S^{00}],\ [M^{14}] = P_2[S^{00}]$$

$$[M^{22}] = \bar{P}_1[S^{00}],\ [M^{25}] = \bar{P}_2[S^{00}]$$

$$[M^{33}] = I_1[S^{00}],\ [M^{41}] = [M^{14}],\ [M^{52}] = [M^{25}]$$

$$[M^{44}] = [M^{55}] = I_3[S^{00}],\ \text{all other } [M_{\alpha\beta}] = 0$$

It should be noted that although f_1 and f_2 are shown factored outside the matrices, in the evaluation of the coefficients by the Gauss quadrature f_1 and f_2 are considered as parts of the integrals. For example $f_1A_{11}[S_{11}]$ is evaluated by

$$\int_{\Omega^e} f_1A_{11}\psi_i\psi_j dx_1dx_2 \doteq \sum_{I=1}^{N}\sum_{J=1}^{N} A_{11}\left[\left(\frac{\partial u_3}{\partial x_1}\right)\psi_i\psi_j\right]_{x_1=Z_I, x_2=Z_J} W_IW_J \det J_0$$

where N is the number of Gauss points, W_I and W_J are the Gauss weights, Z_I and Z_J are the Gauss points, and J_0 is the Jacobian of the transformation.

APPENDIX D

TANGENT STIFFNESS MATRIX

The original nonlinear stiffness matrix has the form

$$[K(\Delta)] = \begin{bmatrix} [K^{11}] & [K^{12}] & [K^{13}] & [K^{14}] & [K^{15}] \\ [K^{12}] & [K^{22}] & [K^{23}] & [K^{24}] & [K^{25}] \\ 2[K^{13}] & 2[K^{23}] & [K^{33}] & [K^{34}] & [K^{35}] \\ [K^{14}] & [K^{24}] & \frac{1}{2}[K^{34}] & [K^{44}] & [K^{45}] \\ [K^{15}] & [K^{25}] & \frac{1}{2}[K^{35}] & [K^{45}] & [K^{55}] \end{bmatrix} \qquad (D1)$$

and the tangent stiffness matrix can be written as

$$[K_T(\Delta)] = \begin{bmatrix} [K^{11}] & [K^{12}] & 2[K^{13}] & [K^{14}] & [K^{15}] \\ [K^{21}] & [K^{22}] & 2[K^{23}] & [K^{24}] & [K^{25}] \\ 2[K^{13}] & 2[K^{23}] & [\bar{K}^{33}] & [K^{34}] & [K^{35}] \\ [K^{14}] & [K^{24}] & [K^{34}] & [K^{44}] & [K^{45}] \\ [K^{15}] & [K^{25}] & [K^{35}] & [K^{45}] & [K^{55}] \end{bmatrix} \qquad (D2)$$

It should be noted that the tangent stiffness matrix is symmetric and $[\bar{K}^{33}]$ contains additional terms given by

$$[\bar{K}^{33}] = [K^{33}] + [K^{31}]' + [K^{32}]' + [K^{33}]' + [K^{34}]' + [K^{35}]' \qquad (D3)$$

The terms involved in $[K^{33}]$ are given in Appendix C while the rest of the matrices in Eq. (D3) contains terms due to geometric and combined nonlinear effect and are given below.

(a) Geometric Nonlinear Terms

$$[K^{31}]'_G = 2g_x[A_{11}[S^{11}] + A_{12}[S^{22}] + A_{13}^{6}([S^{12}] + [S^{21}])]$$

$$+ 2g_y[A_{13}^{6}[S^{11}] + A_{23}^{6}[S^{22}] + A_{66}([S^{12}] + [S^{21}])]$$

$$+2C_o g_y[B_{16}[S^{11}] + B_{26}[S^{22}] + B_{66}([S^{12}] + [S^{21}])]$$

$$[K^{32}]'_G = 2h_y[A_{12}[S^{11}] + A_{22}[S^{22}] + A_{26}([S^{12}] + [S^{21}])]$$

$$+ 2h_x[A_{16}[S^{11}] + A_{22}^{6}[S^{22}] + A_{66}([S^{12}] + [S^{21}])]$$

$$+ C_o h_x[B_{16}[S^{11}] + B_{26}[S^{22}] - B_{66}([S^{12}] + [S^{21}])]$$

$$[K^{33}]'_G = \frac{1}{R_1}[f_x(A_{11}[S^{01}] + A_{16}[S^{02}]) + f_y(A_{12}[S^{02}] + A_{16}[S^{01}])]$$

$$+ 2f_x[(\frac{A_{11}}{R_1} + \frac{A_{12}}{R_2})[S^{10}] + f_x(A_{11}[S^{11}] + A_{16}[S^{12}])$$

$$+f_y(A_{16}[S^{01}] + A_{12}[S^{12}])]$$

$$+ \frac{1}{R_2}(f_x A_{12}[S^{01}] + f_y A_{22}[S^{02}]) + A_{26}(f_x[S^{02}] + f_y[S^{01}])$$

$$+ 2f_y[(\frac{A_{12}}{R_1} + \frac{A_{22}}{R_2})[S^{20}] + f_x(A_{12}[S^{21}] + A_{26}[S^{22}])$$

$$+f_y(A_{22}[S^{22}] + A_{26}[S^{21}])]$$

$$+ 2f_y[(\frac{A_{16}}{R_1} + \frac{A_{26}}{R_2})[S^{10}] + f_x(A_{16}[S^{11}] + A_{66}[S^{12}])$$

$$+f_y(A_{26}[S^{12}] + A_{66}[S^{11}])]$$

$$+ 2f_x[(\frac{A_{16}}{R_1} + \frac{A_{26}}{R_2})[S^{20}] + f_x(A_{16}[S^{21}] + A_{66}[S^{22}])$$

$$+ f_y(A_{26}[S^{22}] + A_{66}[S^{21}])]$$

$$[K^{34}]'_G = 2q_x[B_{11}[S^{11}] + B_{12}[S^{22}] + B_{16}[(S^{12}] + [S^{21}])]$$

$$+ 2q_y[B_{16}[S^{11}] + B_{26}[S^{22}] + B_{66}([S^{12}] + [S^{21}])]$$

$$[K^{35}]'_G = 2r_x[B_{16}[S^{11}] + B_{26}[S^{22}] + B_{66}([S^{12}] + [S^{21}])]$$

$$+ 2r_y[B_{12}[S^{11}] + B_{22}[S^{22}] + B_{26}([S^{12}] + [S^{21}])]$$

where

$$g_x = \frac{1}{2}\frac{\partial u}{\partial x} \quad ; \quad g_y = \frac{1}{2}\frac{\partial u}{\partial y}$$

$$h_x = \frac{1}{2}\frac{\partial v}{\partial x} \quad ; \quad h_y = \frac{1}{2}\frac{\partial v}{\partial y}$$

$$q_x = \frac{1}{2}\frac{\partial \phi_x}{\partial x} \quad ; \quad q_y = \frac{1}{2}\frac{\partial \phi_x}{\partial y}$$

$$r_x = \frac{1}{2}\frac{\partial \phi_y}{\partial x} \quad ; \quad r_y = \frac{1}{2}\frac{\partial \phi_y}{\partial y}$$

(b) Combined Nonlinear Terms

$$[K^{31}]'_{GM} = -\frac{g_o}{R_1}[A_{15}[S^{11}] + A_{56}([S^{12}] + [S^{21}]) + A_{25}[S^{22}]]$$

$$[K^{32}]'_{GM} = -\frac{h_o}{R_2}\,[A_{24}[S^{22}] + A_{46}([S^{12}] + [S^{21}]) + A_{14}[S^{11}]]$$

$$[K^{33}]'_{GM} = f_x[A_{14}(2[S^{12}] + [S^{21}]) + 3A_{15}[S^{11}]]$$

$$+ f_y[3A_{24}[S^{22}] + A_{25}([S^{12}] + 2[S^{21}])]$$

$$+ A_{46}[3f_x[S^{22}] + f_y([S^{12}] + 2[S^{21}])]$$

$$+ A_{56}[f_x([S^{12}] + 2[S^{21}]) + 3f_y[S^{11}]]$$

$$[K^{34}]'_{GM} = q_o[A_{15}[S^{11}] + A_{25}[S^{22}] + A_{56}([S^{12}] + [S^{21}])]$$

$$[K^{35}]'_{GM} = r_o[A_{14}[S^{11}] + A_{24}[S^{22}] + A_{46}([S^{12}] + [S^{21}])]$$

where

$g_o = u \quad ; \quad h_o = v$

$q_o = \phi_x \quad ; \quad r_o = \phi_y$

The vita has been removed from the scanned document

GEOMETRIC AND MATERIAL NONLINEAR ANALYSIS OF LAMINATED COMPOSITE PLATES AND SHELLS

by

K. Chandrashekhara

ABSTRACT

An inelastic material model for laminated composite plates and shells is formulated and incorporated into a finite element model that accounts for both geometric nonlinearity and transverse shear stresses. The elasto-plastic material behavior is incorporated using the flow theory of plasticity. In particular, the modified version of Hill's initial yield criterion is used in which anisotropic parameters of plasticity are introduced with isotropic strain hardening. The shear deformation is accounted for using an extension of the Sanders shell theory and the geometric nonlinearity is considered in the sense of the von Karman strains. A doubly curved isoparametric rectangular element is used to model the shell equations. The layered element approach is adopted for the treatment of plastic behavior through the thickness. A wide range of numerical examples is presented for both static and dynamic analysis to demonstrate the validity and efficiency of the present approach. The results for combined nonlinearity are also presented. The results for isotropic results are in good agreement with those available in the literature. The variety of results presented here based on realistic material properties of more commonly used advanced laminated composite plates and shells should serve as references for future investigations.